To the Graduate Council:

I am submitting herewith a dissertation written by Robert Ost Johnson entitled "The Stability of Timoshenko Beams Conveying a Compressible Fluid." I have examined the final copy of this dissertation for form and content and recommend that it be accepted in partial fulfillment of the requirements for the degree of Doctor of Philosophy, with a major in Engineering Science.

Jerry E. Stoneking

Jerry E. Stoneking, Major Professor

Thomas G. Carley

Thomas G. Carley, Major Professor

We have read this dissertation
and recommend its acceptance:

William J. Snyder

Richard L. Becker

Accepted for the Council:

C W Minkel

The Graduate School

√

THE STABILITY OF TIMOSHENKO BEAMS CONVEYING A COMPRESSIBLE FLUID

A Dissertation
Presented for the
Doctor of Philosophy
Degree
The University of Tennessee, Knoxville

Robert Ost Johnson

December 1984

to my beloved wife Rexana

and the memory

of my father-in-law

Mr. Rex K. Stephens

ACKNOWLEDGMENTS

Tuitional support has been provided by the Tennessee Valley Authority beginning with the fall quarter of 1975 and ending with the winter quarter of 1979. The Oak Ridge Gaseous Diffusion Plant operated by Union Carbide Corporation - Nuclear Division and subsequently by Martin Marietta Energy Systems, Incorporated, for the U.S. Department of Energy, accepted responsibility for this tuitional support beginning with the spring quarter of 1980 through the fall quarter of 1984. Computer facilities were made available by the University of Tennessee Computing Center and Martin Marietta Energy Systems, Incorporated.

The author would like to take this opportunity to express his sincere thanks and appreciation to Dr. J. E. Stoneking and Dr. T. G. Carley whose support, advice, and encouragement over the past seven years has been invaluable. The University of Tennessee is one of the few institutions where a complete graduate school in engineering is available on a part-time basis. It offers a rare opportunity to those desiring to pursue higher education.

Many people have graciously contributed to this research effort. Ms. J. A. Jordon, Hughes Aircraft Company, Denver, and Mr. G. Sanders, Martin Marietta Energy Systems, Incorporated, provided computer programming assistance. Dr. M. D. Gunzburger, Carnegie-Mellon University, and Dr. W. K. Sartory, Martin Marietta Energy Systems, Incorporated, provided consultation in the areas of numerical analysis and applied mechanics, respectively. The comments supplied by Dr. Sartory greatly affected many aspects of this dissertation.

A very special thanks is extended to my technical supervisor, Dr. W. F. Lawkins, Martin Marietta Energy Systems, Incorporated, whose support and advice made possible the completion of this dissertation.

Finally, a special thanks is extended to my beloved wife, Rexana, whose encouragement, assistance, and patience has remained steadfast ever since the author began the arduous task of graduate school.

The author would like to take this opportunity to express thanks and appreciation to those individuals, the names of whom are too numerous to list, who have provided encouragement, advice, and fellowship during the completition of this task.

This dissertation was prepared by the Technical Publications Department, Oak Ridge National Laboratory, Martin Marietta Energy Systems, Incorporated. The figures were drawn by Graphic Arts, Oak Ridge Gaseous Diffusion Plant, Martin Marietta Energy Systems, Incorporated. The entire document was proofread by Mr. R. A. Hawsey, Martin Marietta Energy Systems, Incorporated.

ABSTRACT

The purpose of this study is to formulate and solve the stability problem associated with the equations of motion of a Timoshenko beam conveying a compressible fluid. The beam is assumed to be either cantilevered or simply supported. Shear deformation and rotary inertia are considered in the Timoshenko beam theory. The beam analysis that is carried out is quite general and allows for viscous damping external to the tube as well as both internal strain rate and hysteretic damping. Interactions between these three damping mechanisms, shear deformation, and rotary inertia also are accounted for. The compressible, isentropic flow through the tube is governed by Euler's equations of motion. Gravitational effects are neglected in the analysis. This is equivalent to assuming that the tube is horizontal. The motion of the fluid is coupled to that of the beam by a compatibility condition at the tube wall which requires that they vibrate together.

The equations of motion of the fluid and the compatibility condition are nonlinear. They are linearized using a perturbation about a reference solution. A velocity potential is introduced and separation of variables is applied to reduce the equation system to two simultaneous partial differential equations. A characteristic equation is derived by assuming harmonic solutions while a frequency equation is developed using the boundary conditions in conjunction with this harmonic solution. Numerical solutions to the resultant pair of coupled transcendental equations are computed using Muller's method.

The compressibility of the fluid is found to affect the stability of the fluid-tube system through the fluid sonic velocity and the tube aspect ratio. In

the cantilevered case increased aspect ratio raises the critical velocity at which flutter occurs while reduced sonic velocity decreases it. The higher vibration modes become excited as the fluid sonic velocity is continually lowered. The stability of the system is significantly affected since instability occurs in the higher modes before it takes place in the lower ones. Any return-to-stability associated with an increase in flow velocity can be eliminated by inclusion of a finite sonic velocity in the analysis of cantilevered, fluid-conveying beams.

Euler's method of equilibrium is applied to the partial differential equation pair described above in the simply supported case. The resultant stability problem also is amenable to solution using Muller's method. Results indicate that the critical flow velocity at which the tube buckles increases when the aspect ratio is raised if the flow is subsonic. When the flow is supersonic an increase in aspect ratio decreases the critical velocity. Decreased sonic velocity always reduces the critical velocity in the simply supported case.

TABLE OF CONTENTS

CHAPTER PAGE

CHAPTER PAGE

LIST OF TABLES

TABLE PAGE

TABLE PAGE

LIST OF FIGURES

FIGURE PAGE

FIGURE PAGE

FIGURE PAGE

LIST OF SYMBOLS

A	tube flow area $\pi d_i^2/4$ or alternate notational representation of γ_{1n}^*
dA	differential area element as indicated
A_s	annular cross-sectional area of tube $\pi(d_o^2 - d_i^2)/4$
A^*	tube aspect ratio r_i/L or $d_i/2L$
a_0, a_1, a_2	coefficients of second degree interpolating polynomial used in Muller's method
a_{2s}	coefficients in power series expansion of the quotient function of the first kind $\tilde{\mathcal{F}}_\nu(z)$
B	alternate notational representation of γ_{2n}^*
b_{2s}	coefficients in power series expansion of the compressibility factor f
C	alternate notational representation of γ_{3n}^*
C_1, C_2	integration constants
$C_{p'}$	integration constant
C_s^*	dimensionless internal strain rate damping coefficient of tube
C_v^*	dimensionless external viscous damping coefficient in medium surrounding tube
c	speed of sound of fluid
c_s	internal strain rate damping coefficient of tube
c_v	external viscous damping coefficient in medium surrounding tube

c^*	dimensionless sonic velocity of fluid
D	alternate notational representation of γ_{4n}^*
$\frac{D}{Dt}$	substantial derivative operator $\frac{\partial}{\partial t} + \vec{\nabla} \bullet \vec{\nabla}$
d	diameter of middle surface of tube
d_i	inside tube diameter $2r_i$
d_o	outside tube diameter
E	tube modulus of elasticity
$E_n(x)$	nth spatial component in solution representation of y(x,t)
$E_n^*(\xi)$	nth dimensionless spatial component in solution representation of $\eta(\xi,\tau)$
$\tilde{E}$	complex form of tube elastic modulus $E(1 + i\mu)$
e_{xx}	infinitesimal strain in the x-direction due to a stress in the x-direction
$F(\omega_n^*)$	frequency equation representation
$F_D(x)$	distributed external viscous damping force acting on tube
$\tilde{\mathfrak{J}}_\nu(z)$	quotient function of the first kind of integer order ν
dF	differential flow-induced force along the tube wall acting in the radial direction
$\frac{dF}{dx}$	flow-induced force per unit of tube length acting on inside periphery of tube [= w(x,t)]
f	compressibility factor* defined in Eq. (4.49)
f(z)	complex function representation
f_I	transverse inertia force of tube per unit of length

f_n	cyclic frequency in the nth mode
f_{jn}	compressibility factor of the jth component in the nth degree of freedom
G	tube modulus of rigidity
$\tilde{G}$	complex form of tube modulus of rigidity $G(1 + i\nu)$
g(z)	single complex equation representation
$g_N(z)$	deflated function used by the Muller algorithm to compute the N + 1 root
$g_1(z)$	deflated function used by the Muller algorithm to compute the second root
I	moment of inertia of annular tube cross section $\pi(d_o^4 - d_i^4)/64$
Im	imaginary part of a complex quantity
i	iteration counter for Muller's method or $\sqrt{-1}$
$\hat{i}_r$	unit vector in the radial direction
$\hat{i}_x$	unit vector in the axial or longitudinal direction
$\hat{i}_\theta$	unit vector in the circumferential or angular direction
J_m	Bessel function of first kind of integer order m
j	root counter for deflated function in Muller algorithm
k	tube shear coefficient
L	tube length
M	internal bending moment (resisting)
M_D	internal bending or resisting moment due to strain rate damping

M^*	Mach number $\left[= \frac{U}{c} = \frac{U^*}{c^*}\right]$
M_c^*	critical Mach number corresponding to U_c^*
m	axial wavenumber
m_I	rotary inertia
m_s	mass per unit length of beam $\rho_s A_s$
n	mode index counter or circumferential wavenumber
P	dynamic fluid pressure
P_0	mean fluid pressure
P'	dynamic fluid pressure perturbation
p	alternate notational representation for α_{1n}^*
$p_2(z)$	second degree polynomial representation
q	alternate notational representation for α_{2n}^*
R(r)	radial portion of the separated potential function where $\Phi(x,r,\theta,t) = R(r)\, S(x,\theta,t)$
R^*	dimensionless rotary inertia number
Re	real part of a complex quantity
r	radial coordinate or alternate notational representation for α_{3n}^*
r_i	inside tube radius
$S(x,\theta,t)$	radial independent portion of the separated potential function where $\Phi(x,r,\theta,t) = R(r)\, S(x,\theta,t)$
S^*	dimensionless shear number
s	entropy per unit mass of fluid or alternate notational representation for α_{4n}^*

T	axial or longitudinal tube tension or thermodynamic temperature
t	time coordinate
U	average fluid velocity component parallel to the horizonal x-axis
U^*	dimensionless fluid velocity $LU\sqrt{\rho_0 A/EI}$
U_c^*	smallest of the set of dimensionless critical fluid velocities $\{U_{nc}^* \mid n = 1,2,..., \infty\}$
U_{nc}^*	dimensionless critical fluid velocity in the nth mode
u	internal energy per unit of mass
$u(x,y)$	real part of the complex function $f(z)$
V	internal shear force in tube (resisting)
V_r	radial fluid velocity component
V_x	horizontal fluid velocity component
V_θ	circumferential fluid velocity component
V_r'	radial fluid velocity perturbation
V_x'	horizontal fluid velocity perturbation
V_θ'	circumferential fluid velocity perturbation
$\vec{V}$	fluid velocity vector $V_r\hat{i}_r + V_\theta\hat{i}_\theta + V_x\hat{i}_x$
$v(x,y)$	imaginary part of the complex function $f(z)$
$W(x,\theta,t;r_i)$	interfacial deflection along fluid-solid boundary
W'	interfacial deflection perturbation
$w(x,t)$	transverse beam loading per unit of length
$w(x,y)$	complex function to be minimized in Ward's method

x	axial, longitudinal, or horizontal coordinate or real part of the complex variable z
$\hat{x}$	cross or vector product of two vectors
Y_m	Bessel function of second kind of integer order m
y	tube deflection, lateral coordinate, or imaginary part of the complex variable z
z	complex variable $x + iy$
z_i, z_{i-1}, z_{i-2}	root estimates used by Muller's method
$\bar{z}_j$	jth root used to form a deflated function

Greek Letters

α	rotation angle of beam element
α_{jn}	dimensional coefficients in solution representation for $E_n(x)$
α_{jn}^*	dimensionless coefficients in solution representation for $E_n^*(\xi)$
β	fluid mass parameter $\rho_0 A/(\rho_s A_s + \rho_0 A)$ or shear distortion angle $\alpha - \partial y/\partial x$
γ_{jn}	dimensional coefficients in solution representation for $E_n(x)$
γ_{jn}^*	dimensionless coefficients in solution representation for $E_n^*(\xi)$

Δ	Laplacian operator ($= \nabla^2 = \vec{\nabla} \cdot \vec{\nabla}$) in cylindrical coordinates $\left[= \frac{\partial^2}{\partial r^2} + \frac{1}{r} \cdot \frac{\partial}{\partial r} + \frac{1}{r^2} \cdot \frac{\partial^2}{\partial \theta^2} + \frac{\partial^2}{\partial x^2} \right]$
δ	dimensionless radial coordinate r/r_i
$\bar{\delta}$	transformed dimensionless radial coordinate
η	dimensionless tube deflection y/L
θ	angular coordinate
κ	parameter defined by Eq. (4.41)
κ_{jn}	the value of the parameter κ for the jth component in the nth degree of freedom
Λ	dimensionless radial function R/L
$\bar{\Lambda}$	transformed dimensionless radial function
μ	tube hysteretic damping coefficient in tension
ν	tube hysteretic damping coefficient in shear
$\bar{\nu}$	Poisson's ratio for the tube
ξ	dimensionless axial coordinate x/L
Π	product of terms
ρ	fluid density
ρ_0	mean fluid density
ρ_s	density of tube material
ρ'	fluid density perturbation
σ	tube mass parameter $\rho_s A_s/(\rho_s A_s + \rho_0 A)$ which is equal to $1 - \beta$
σ_D	internal tube stress due to strain rate damping

σ_{xx}	stress on a plane normal to the x-direction from a force parallel to the x-direction
τ	dimensionless time coordinate $t\sqrt{EI/(\rho_s A_s + \rho_0 A)}/L^2$
τ_w	fluid frictional shear stress along the inside tube wall
υ	fluid specific volume ($= 1/\rho$)
Φ	velocity potential function
ω	circular frequency of harmonic motion
ω_n	circular frequency for the nth mode
ω_s	circular frequency of radial standing waves
ω_c^*	dimensionless circular frequency corresponding to U_c^*
ω_n^*	dimensionless circular frequency $\omega_n L^2\sqrt{(\rho_s A_s + \rho_0 A)/EI}$ in the nth mode
ω_s^*	dimensionless circular standing wave frequency $\omega_s L^2\sqrt{(\rho_s A_s + \rho_0 A)/EI}$

Mathematical Symbols

$\bullet$	dot or scalar product of two vectors where applicable
$\vert\,\vert$	absolute value or modulus of a complex quantity
$\vec{\nabla}$	vector operator del in cylindrical coordinates defined as $\hat{i}_r \frac{\partial}{\partial r} + \hat{i}_\theta \frac{1}{r} \cdot \frac{\partial}{\partial \theta} + \hat{i}_x \frac{\partial}{\partial x}$
!	factorial operation as in $3! = 1 \cdot 2 \cdot 3 = 6$

Superscripts

*	dimensionless quantities
′	total differentiation with respect to the independent variable ξ or a perturbed quantity

1. INTRODUCTION

In the past decade the subject of flow-induced vibrations has grown into a vast area demanding knowledge for problem solution from such disciplines as fluid and solid mechanics, dynamics, vibrations, nonlinear mechanics, and stability theory [1]. The emergence of this field of study has been stimulated by the numerous problems and associated failures that can be attributed to the complicated dynamic interaction between a solid and a flowing fluid. In particular, the nuclear industry has been plagued with a variety of flow-induced vibration problems in such components as the steam generators [2,3], the reactor fuel subassemblies [4], and the primary-circuit heat exchangers [5,6]. Flow-induced vibrations have even caused failure of heat exchangers during service and, in some cases, shutdown of major power plants has taken place [7]; moreover, monitoring of such heat exchanger vibrations is being carried out [8].

The atmospheric winds have also caused numerous catastrophic failures either related to or definitely influenced by flow-induced vibratory effects. A pilot plant model of the Madaras Rotor Power Plant which was erected in Burlington, New Jersey, and which powered an electric generator through application of the Magnus effect [9], blew down in a high wind [10]. Likewise, the famous failure of the Tacoma Narrows bridge was apparently caused by a combination of vortex shedding over the roadway and the resultant formation of torsional oscillations between the two main support towers [11]. The Ferrybridge cooling towers also collapsed under moderate wind loading in 1965

[12]. The monetary value of structural failures caused by atmospheric wind interactions is staggering when it is realized that hurricane Camille, which swept through the Gulf coast of Louisiana and Mississippi in 1969, was responsible for a total of 1.5 billion dollars worth of damage [13]. It is no surprise that modern building design must now account for wind interaction so that structures are both safe and comfortable for human occupancy [14].

Other applications of flow-induced vibrations include the analysis of liquid propellant feedlines for launch vehicle rocket engines [15], pump discharge lines [16], hydraulic and swing check valves [17,18], tow cables for moving underwater vessels with surface ships [1, pp. 47–51], and offshore and submerged marine structures at sea [19,20]. Significant research is presently going on to determine the effects of two-phase flow-induced vibrations in piping systems and heat exchangers [21]. For instance, it seems feasible to augment heat transfer rates in condenser tubes by allowing them to vibrate [22].

A fluid flowing through a pipe or tube also can excite flow-induced vibratory motion. The pressures imposed by the flowing fluid on the inside tube wall deflect it. Waterhammer is the term associated with the deflections of the tube when they are excited by an accelerating fluid flow [23]. A steady fluid flow also causes the tube to deflect. If the velocity of the steady internal flow becomes great enough, the tube can either buckle or flail about depending on how it is supported [24]. These deflections are now commonly known as instabilities of fluid-conveying tubes. The most familiar form of waterhammer is the rumbling of household plumbing that can be heard on quiet mornings when a faucet is first turned on while the most common instability associated with steady flow in a tube is the flailing about of an unrestricted garden hose. This problem of the lateral vibration of tubes containing a flowing fluid is of considerable practical importance. The basic theory has been used or applied to such problems as above-ground oil pipelines [25], flexible cylindrical fuel elements immersed in nuclear reactor coolant channels [26], the development of Dracone flexible barges [27], the swimming of slender fish [28,29], the design of coolant loops in sodium-cooled fast breeder reactors [30], many marine engineering problems such as submerged pipelines and risers [31], and the generation of Korotkoff sounds [32] occurring in the human arterial system [33].

Theoretical investigation of the instabilities associated with fluid-conveying tubes usually has coupled Bernoulli-Euler beam theory with an incompressible flow model. This dissertation extends the applicable range of these previous studies by considering the problem of a horizontal, damped, Timoshenko beam conveying a compressible fluid. The tube is assumed to be either simply supported or cantilevered. The three damping mechanisms incorporated into the problem formulation include external viscous damping as well as both internal strain rate and hysteretic damping. The Timoshenko beam theory accounts for both rotary inertia and shear deformation. The compressible flow formulation allows for the specification of a finite sonic velocity.

2. LITERATURE REVIEW

The subject of flow-induced vibrations has grown vastly in the past thirty years. The review article by Wambsganss [4] and the report by Nelms and Segaser [5] have summarized those aspects of flow-induced vibrations which apply to the nuclear industry as a whole and to heat exchangers, respectively. Recent review articles include the works of Shin and Wambsganss [2] and Chen [34,35]. The monograph by Blevins [1] treats most of the subjects in these articles just cited in considerably more detail. Four important conferences [36–39] have taken place which deal specifically with fluid-structure interaction phenomena for which published proceedings are available. Finally, an annotated bibliography [40] exists which summarizes many significant contributions on this subject prior to 1974.

Bernoulli-Euler beam theory coupled with a simple slug or plug type internal flow model has been used extensively to study the dynamics of fluid-conveying pipes [41–46]. These early investigations concentrated on the derivation of the correct governing partial differential equation and the prediction of a critical flow velocity which induced buckling or divergence instability* when exceeded. Analysis of this beam having internal fluid flow was complicated by the appearance of a Coriolis acceleration term consisting

*Buckling and divergence instability both refer to the failure of a structure to attain an equilibrium position under the action of static forces and moments. The term buckling arises in the study of elastic structures [47] while divergence instability refers to the study of lifting surfaces at critical air speeds in the field of aeroelasticity [48]. In either case, the elasticity of the structure or lifting surface as well as the flow-induced forces are essential to the instability while inertial forces are not involved.

of a mixed partial derivative in the temporal and spatial coordinates. The analysis performed by Niordson [43,44] was quite significant since the problem of a compressible inviscid fluid-conveying pipe was formulated using the theory of thin shells combined with a potential flow formulation. Results indicated that only when the wavelength of the transverse tube motion was small in comparison to the tube diameter did the effects of fluid compressibility become pertinent to the problem solution.

Considerable research was later performed which centered on understanding the existence of a critical flow velocity and the resultant instability [24, 49–59]. Study of a chain of articulated pipes [49] through which there passed simple slug flow indicated that the fluid forces were conservative when both ends of the articulated chain were simply supported while these forces were nonconservative when one of the ends was free or cantilevered. Two different forms of instability recognized in this discrete model of the continuous fluid-tube system were simple buckling or divergence similar to the failure of structures under static loading and self-excited oscillations or flutter. It was later demonstrated that continuous fluid-tube systems which were nonconservative could be destabilized by small velocity-dependent forces [50]. Continuous cantilevered fluid-tube systems were found to lose stability by torsional divergence or buckling (failure to obtain an equilibrium position under the action of static torsional loads) and by either torsional or transverse flutter (failure to obtain oscillations of limited finite amplitudes under the action of torsional or transverse loads); transverse divergence or buckling was not predicted in these nonconservative situations

[51–54, 58]. In the cantilevered case buckling could be totally eliminated if gravitational forces acted on the fluid-tube system in a particular manner [57]. Likewise, stability could be enhanced by the addition of suitably sized lumped masses positioned at select locations along the span of the fluid-conveying tube [58].

These discrepancies in stability behavior predicted for both the discrete and continuous cantilevered fluid-conveying pipes were traced to the higher response modes of the articulated chain of pipes which did not resemble at all the corresponding response modes of the continuous system regardless of the number of degrees of freedom used in the articulated model [56]. The disagreement became increasingly exaggerated as the flow velocity was increased. This perhaps helped to explain the extreme difficulty encountered by Naguleswaran and Williams [55] when using approximate one and two term Galerkin, Rayleigh-Ritz, and Fourier series to predict buckling frequencies for continuous fluid-tube systems at high flow velocities. This stability problem has recently become even more complicated since at yet higher flow velocities, above the classical critical velocity, pipes with both ends supported are subject to flutter [24] while short cantilevered pipes analyzed using Timoshenko theory lose stability by buckling or divergence [59].

Mathematical techniques employed to solve the eigenvalue problem (associated with the mathematical description of the fluid-conveying tube) that is complicated by the mixed derivative term include operational techniques that make use of the linear operator and the adjoint operator intrinsic to the governing equation of motion [60], Dunkerley's method [61], Galerkin's method [62], integral equation formulations [63], and the application of a simple transformation which reduces the determinant of the fourth-order equation system to a third-order one [15]. The most adaptable technique seems to be the Fourier transform method utilized by Satter and Yaghoubi [64]. Their analysis which was performed in the frequency domain successfully accommodated the Coriolis term and enabled them to obtain solutions for both free and forced vibrations in the simply supported case.

The transverse beam-type motions* that have been discussed thus far assume that the deflected cylinder cross section remains essentially circular. These motions are associated with the first circumferential wavenumber ($n=1$) when the cylinder is considered to be a simple beam. When flutter occurs the

---

*The definition of beam-type motions or vibrations depends predominately upon the $md/2L$ ratio where $d/2$ is the radius of the middle surface of the cylinder, L is the cylinder length, m is the axial wavenumber, and the cylinder is considered to be a hollow cylindrical thin shell [65, pp. 98–99]. For small $md/2L$ ratios with the circumferential wavenumber n equal to zero, the first mode ($m=1$) is torsional, the second mode ($m=2$) is axial or longitudinal, and the third mode ($m=3$) is a breathing mode involving essentially radial displacements; likewise, for large $md/2L$ ratios with n equal to zero, the first mode becomes the breathing mode, the second the torsional mode, and the third the axial or longitudinal mode. For $n \geqslant 1$ the first mode ($m=1$) is a flexural mode while the second mode ($m=2$) is an axial or longitudinal mode; moreover, the third mode ($m=3$) is a breathing mode (involving radial and tangential displacements) for small values of $md/2L$ while it is a shear mode (involving tangential and axial or longitudinal displacements) when $md/2L$ is large. Hence, beam-type flexural or bending vibrations are associated with the first axial wavenumber ($m=1$) for $n \geqslant 1$. The deflected circumferential shapes are actually oval for $m=1$ and $n \geqslant 1$ and only possess circular deflected shapes in "pure" breathing vibration modes. However, these oval shapes become essentially circular in the limit as the hollow cylinder wall thickness to length ratio becomes small (fundamental assumption of thin shell theory).

resultant self-limiting oscillatory motions are associated with the higher circumferential modes (n>1) of a circular cylindrical shell [66]. Paidoussis [67] has combined the thin shell equations for a circular cylinder with a potential flow analysis for the internal fluid motion. His analysis demonstrated that a tube supported at both ends that has no transverse loading does not exhibit the flutter phenomenon while flutter is the only form of instability displayed by a cantilevered tube. Weaver and Unny [68] performed a similar analysis using the Flügge shell equations given by Kempner [69] in which the vibratory mode shapes and critical flow velocity were predicted as a function of the internal fluid velocity as well as tube thickness and length. Recent results quoted by Weaver and Unny [70] have shown that the simpler beam theory approach agrees quite well with the results of thin shell theory when a long thin tube is being considered. The advantage of using beam theory is obvious since it does not require a complete spatial description of the static and dynamic fluid pressure along the fluid-shell interface.

Other investigations related to this study include the nonlinear theory for a fluid-conveying tube developed by Mote et al. [71,72] which showed that longitudinal tension variation during oscillation became increasingly important as the internal fluid velocity was increased and that, accordingly, the range of applicability of a linear analysis was significantly reduced. Chen [73] has studied a simply supported tube conveying a pulsating flow in which parametric resonance similar to a column subjected to periodic axial loads was found to occur. Clinch [74] and Lakis and Paidoussis [75] have investigated a fluid-conveying tube by treating the turbulent pressure field as a random process. Satter and Ahmadi [76] have solved for the expectation of the mean-squared amplitude of response of a hollow fluid-conveying Bernoulli-Euler beam subjected to different types of nonstationary random excitations. Finally, Widnall and Dowell [77] have treated the problem of supersonic flow through a finite length duct of constant circular cross section using a Fourier decomposition in the circumferential variable.

The related problem of a straight fluid-conveying cylinder subjected to an external axial flow parallel to the internal flow direction has been treated by Cesari and Curioni [30] and Hannoyer and Paidoussis [78]. The analysis by Hannoyer and Paidoussis has recently been extended to the case of slender tapered beams having both internal and external axial flows acting on them [79].

The only investigations that have considered the flow through the tube to be compressible are the ones performed by Niordson [43,44] and Anliker and Raman [33]. Mathematical descriptions of the eigenvalue problem associated with the stability of a Bernoulli-Euler beam conveying a compressible fluid were obtained in both of these studies. No general schemes were offered for solving this eigenvalue problem and no calculations were published which considered specific physical situations in which the flow through the tube was compressible. The related problem of a Timoshenko beam conveying a compressible fluid has received no attention in the open literature.

3. PROBLEM FORMULATION

3.1 Introduction

In this chapter the fundamental equations which describe the motion of a horizontal, damped, fluid-conveying Timoshenko beam are developed from the basic notions of continuum mechanics. External viscous damping as well as internal strain rate and hysteretic damping are included in the beam equation derivation. The dynamic pressure at the tube wall is determined using the compressible form of Euler's equations for inviscid fluid flow. Simply supported and cantilevered tubes are considered in the analysis. The emphasis in this study is on quantifying the stability of steady-state harmonic vibratory motion. The analysis of fluid motion presented here was first carried out by Niordson [43,44] in the context of vibrations of a cylindrical tube containing a compressible flowing fluid. The analysis of a fluid-conveying Timoshenko beam with an incompressible fluid was later performed by Paidoussis and Laithier [59]. They considered a vertical beam which unduly complicated the mathematics associated with the internal forces and moments in the beam itself. This study extends the analysis to the damped Timoshenko beam containing a compressible flowing fluid. The beam is assumed to be horizontal so that the operator associated with the resultant equation of motion of the Timoshenko beam will contain constant coefficients and therefore, somewhat simplify the mathematics embodied in its solution. Motivation for portions of this study came from the analysis by Benjamin [80] in which the stability of fluid-solid systems was shown to be greatly influenced by damping mechanisms.

3.2 Bernoulli-Euler Beam Theory

An analysis of Bernoulli-Euler beam theory can be found in many textbooks [81,82]. This theory is based upon the fundamental assumption that plane sections remain plane. This simply means that any plane cross section normal to the longitudinal axis through the beam remains plane in the deformed configuration. With this assumption it can be shown that the element e_{xx} of Cauchy's infinitesimal strain tensor (whose geometric interpretation represents the extension or change of length per unit of length) is distributed as a linear function of the lateral coordinate y. Additionally, the internal bending stress σ_{xx} is distributed as a linear function of y if a Hookean elastic solid is being considered.

Consider the Bernoulli-Euler beam shown in Figure 3.1. The beam is acted upon by a transverse loading per unit of length w(x,t) and a tensile force T(x) in the longitudinal direction. It is assumed that the direction of the tensile force does not change when the beam is deflected; therefore, transverse equilibrium is not affected by this tensile force. The forces and moments acting on a differential element of the beam in Figure 3.1 are shown in Figure 3.2. The internal forces and moments within the beam are denoted by V and M, respectively. The quantity $f_I \cdot dx$ is the distributed transverse inertia force. Its sense is determined by applying D'Alembert's principle which simply states that a mass develops an inertia force proportional to its acceleration acting in a direction which opposes the motion. In accordance with Newton's second law

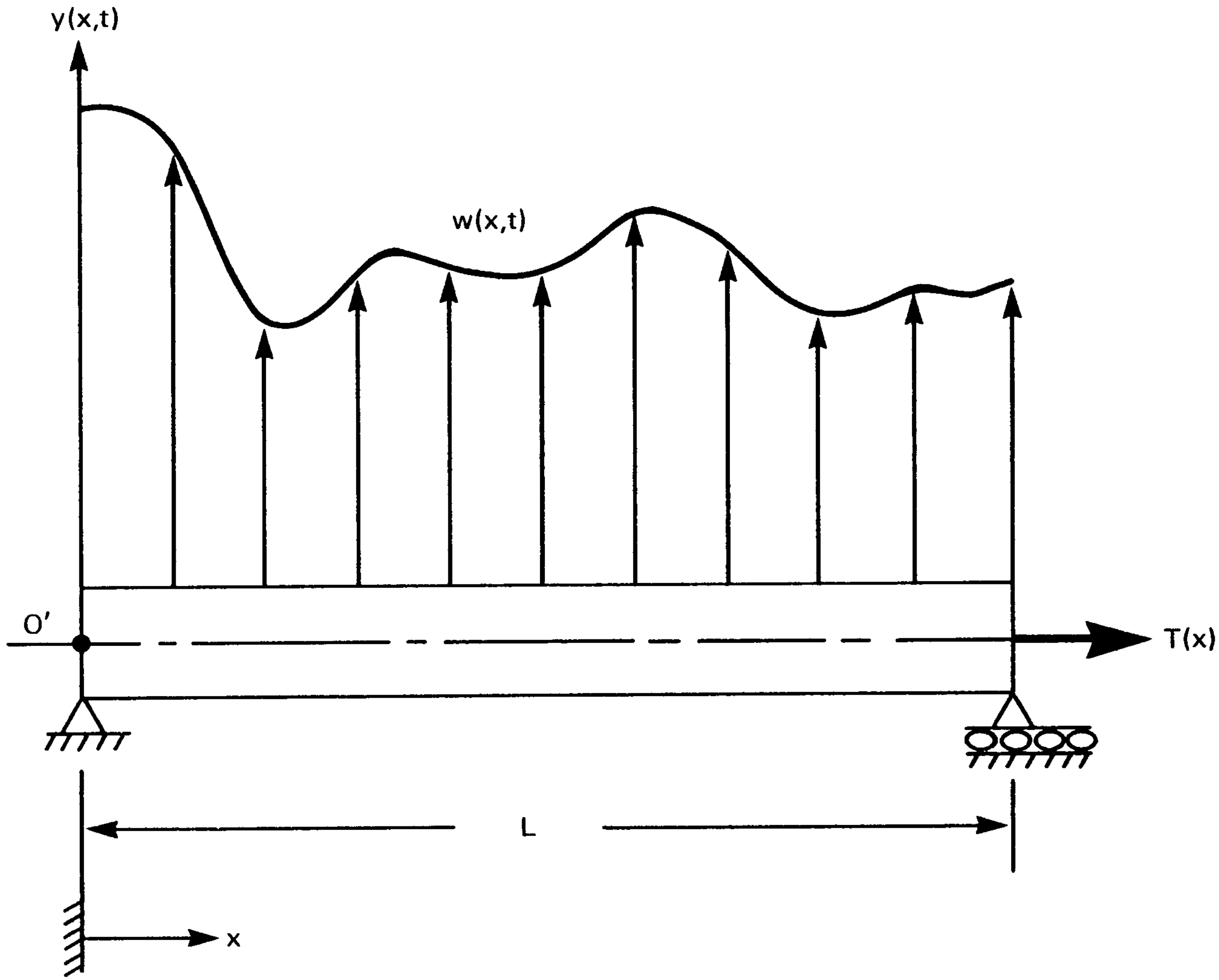

Figure 3.1. Bernoulli-Euler Beam Subjected to Transverse and Tensile Loadings.

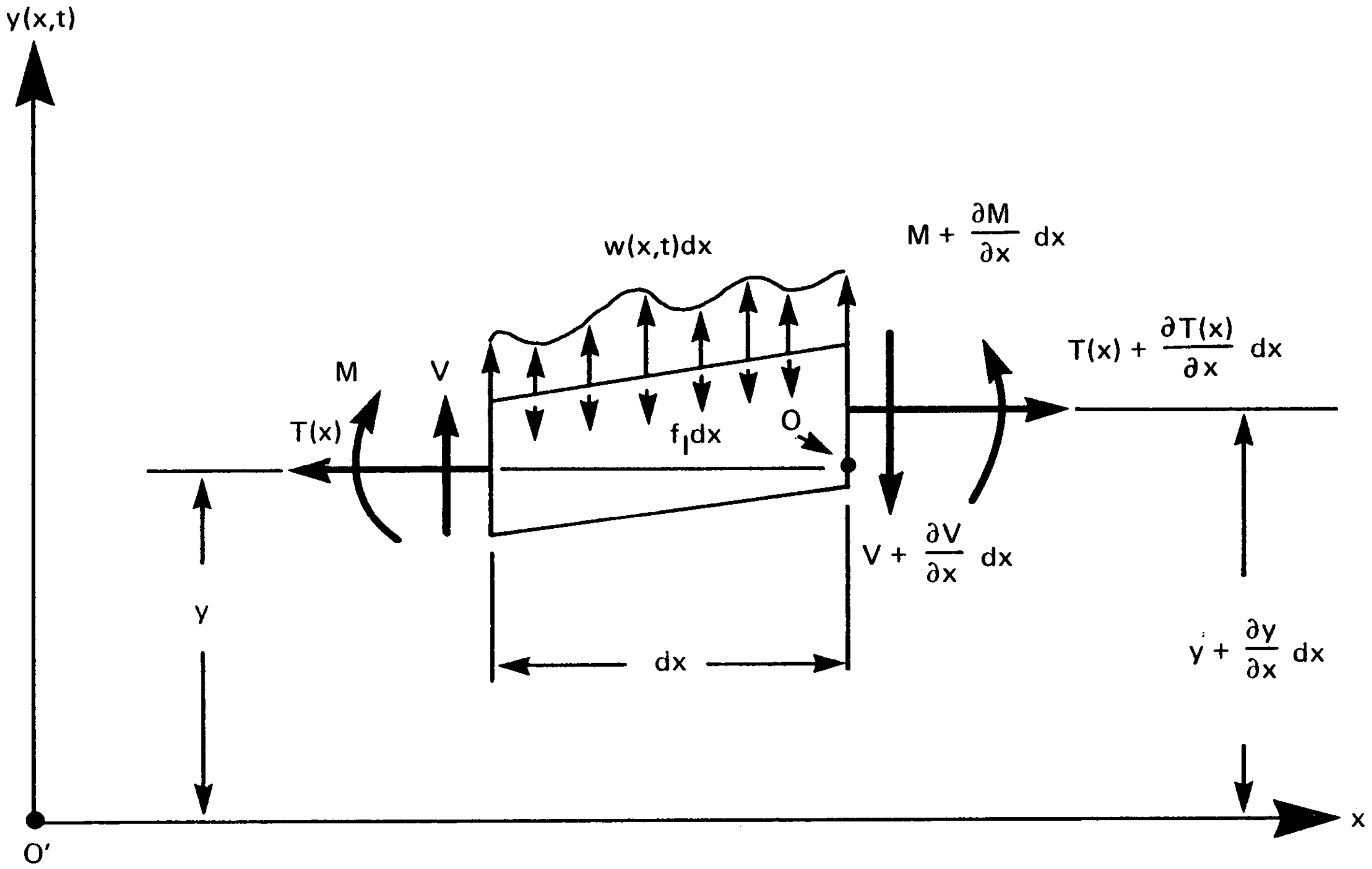

Figure 3.2. Forces and Moments Acting on a Differential Element of a Bernoulli-Euler Beam with Tension.

this transverse inertia force is simply the product of the mass and acceleration. It is representable as

$$f_I \bullet dx = \rho_s A_s \frac{\partial^2 y}{\partial t^2} \bullet dx \tag{3.1}$$

where ρ_s is the density of the material comprising the beam and A_s is its cross-sectional area. The quantity m_s which is defined to be the product $\rho_s A_s$ is the mass per unit length of beam.

The following three equations for equilibrium of the beam element in Figure 3.2 can be written by summing the forces in the transverse and longitudinal directions, taking the sum of the moments about point O, and taking the limit as dx→0:

$$\frac{\partial V}{\partial x} = w - \rho_s A_s \frac{\partial^2 y}{\partial t^2} \tag{3.2}$$

$$\frac{\partial T}{\partial x} = 0 \tag{3.3}$$

$$V = \frac{\partial M}{\partial x} - T\frac{\partial y}{\partial x} \tag{3.4}$$

It is concluded from Eq. (3.3) that the tension T does not vary along the length of the beam. The internal shear V can be eliminated by differentiating Eq. (3.4) with respect to x and then substituting this derivative into Eq. (3.2). The result is

$$\frac{\partial^2 M}{\partial x^2} - T\frac{\partial^2 y}{\partial x^2} + \rho_s A_s \frac{\partial^2 y}{\partial t^2} = w \tag{3.5}$$

For small deflections of beams the internal resisting moment M can be related to the deflection y through the moment-curvature formula [82]. It is expressable as

$$M = EI\frac{\partial^2 y}{\partial x^2} \tag{3.6}$$

where E is the modulus of elasticity and I is the moment of inertia with respect to the neutral axis which passes through the centroid of the beam cross section.

The Bernoulli-Euler beam equation with tension included may now be written as

$$EIy_{xxxx} - Ty_{xx} + \rho_s A_s y_{tt} = w \tag{3.7}$$

where the subscripts represent partial differentiation with respect to the independent variable x or t as indicated. For the tube under consideration the geometric parameters can be computed from $A_s = \pi(d_o^2 - d_i^2)/4$ and $I = \pi(d_o^4 - d_i^4)/64$ where d_i and d_o are the inner and outer tube diameters, respectively. It has been assumed that the tube properties ρ_s and E are constants in writing Eq. (3.7).

3.3 Damping Considerations

Three mechanisms which absorb energy from the beam can be incorporated into the analysis presented in the previous section without unduly complicating the resultant governing partial differential equation. These three mechanisms include an external viscous damping force, internal strain rate damping, and hysteretic damping. These forms of damping were selected as a matter of convenience because they can be represented by tractable mathematical forms. Many different formulations exist which can be employed to model internal or external damping of a structure [83,84].

Many physical situations concerning pipe flow occur in a fluid environment. In other words, the fluid-conveying tube is immersed in air, water, or some other fluid. In such situations the external damping is associated with the drag force on the outside of the vibrating tube. The mechanism producing this drag force is simply viscous shear. Each element of the tube experiences a drag force proportional to its velocity. The resistance to the transverse velocity is represented by the proportionality constant $c_v(x)$. Using the dashpot representation shown in Figure 3.3 as a basis the corresponding distributed damping force is

$$F_D(x) = c_v(x)\frac{\partial y(x,t)}{\partial t} \qquad (3.8)$$

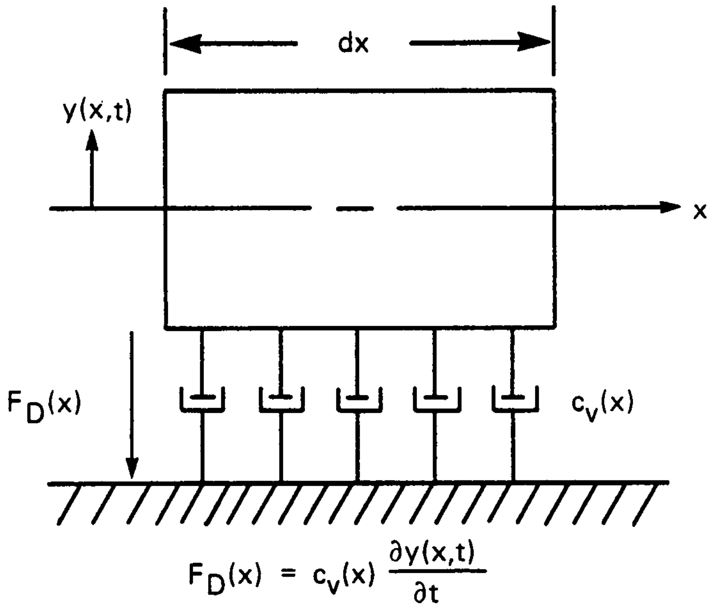

Figure 3.3. External Viscous Damping of a Beam Element.

This formulation is valid only if the external flow relative to the tube is laminar. More precisely, Eq. (3.8) implies that the external flow must be a creeping flow [85] for which the inertia forces can be neglected completely [86]. When the fluid-conveying tube itself becomes unstable this laminar flow requirement is violated since the tube oscillations grow into a limit cycle of large amplitude. This simple linear theory is not expected to predict the subsequent motion of a system which has already become unstable.

The situation for internal strain rate damping is illustrated in Figure 3.4. If the resistance to strain rate is represented by the simple constant $c_s(x)$, the resultant damping stress σ_D is then $c_s(x) \bullet \partial e_{xx}/\partial t$ where e_{xx} is the local

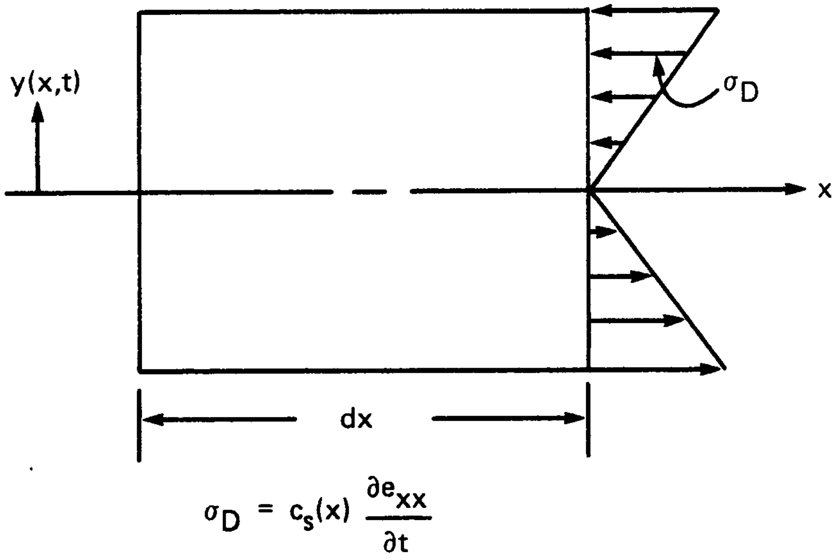

Figure 3.4. Internal Strain Rate Damping of a Beam Element.

normal strain. The resultant internal damping moment M_D attributable to strain rate damping can be evaluated from

$$M_D = \int_{A_s} \sigma_D y dA = c_s(x) \int_{A_s} \frac{\partial e_{xx}}{\partial t} \cdot y dA \tag{3.9}$$

where the integral is taken over the beam cross-sectional area A_s.

Utilizing Navier's hypothesis (which is a direct result deducible from Bernoulli's assumption that each plane cross section of the beam remains plane after bending) that the normal stresses σ_{xx} vary linearly over the beam cross-sectional area, it can be shown that the normal strain e_{xx} is given by

$$e_{xx} = y/r \tag{3.10}$$

where r is the radius of curvature which is assumed to be a function of the longitudinal coordinate x and time t in the deformed configuration. The expression for the internal strain rate damping moment then becomes

$$M_D = c_s(x)\frac{\partial}{\partial t}\left\{\frac{1}{r}\int_{A_s} y^2 dA\right\} = c_s(x)I(x)\frac{\partial}{\partial t}\left(\frac{1}{r}\right) \qquad (3.11)$$

where $\int_{A_s} y^2 dA$ is the moment of inertia I(x) of the beam cross-sectional area which is assumed to be time independent.

Assuming small deflections the curvature $1/r$ can be determined using the familiar curvature formula from the elementary calculus i.e., $1/r \approx \partial^2 y/\partial x^2$. Hence, the required expression for the internal strain rate damping moment becomes

$$M_D = c_s(x)I(x)\frac{\partial^3 y(x,t)}{\partial x^2 \partial t} \qquad (3.12)$$

Internal dissipation in the tube material also can be accommodated by using the complex representation of the elastic moduli were it is assumed that the material follows a hysteretic or structural damping model. This type of damping model is particularly useful for handling rubberlike materials [87]. The complex forms of the modulus of elasticity and modulus of rigidity may be written as

$$\tilde{E} = E(1 + i\mu) \tag{3.13}$$

$$\tilde{G} = G(1 + i\nu) \tag{3.14}$$

where μ and ν are small numbers. In the most general case μ and ν are frequency dependent. The hysteretic damping model can be inserted into the overall theoretical development by simply replacing E and G in the governing equations with $\tilde{E}$ and $\tilde{G}$.

Strictly speaking, this type of hysteretic damping model is valid only for simple harmonic motion. It then represents damping proportional to the displacement and in phase with the velocity [88]. This is not a severe restriction since the solutions to the equations of the type being studied in this investigation can be cast in the form of a complex Fourier series [64].

These three damping mechanisms can be added to the Bernoulli-Euler beam theory with axial tension included by performing an analysis similar to that appearing in the previous section. Figure 3.5 shows the forces and moments acting on a differential element of the damped beam. The resultant equation of motion is

$$\begin{aligned} c_s I y_{xxxxt} + E(1 + i\mu) I y_{xxxx} - T y_{xx} \\ + c_v y_t + \rho_s A_s y_{tt} = w \end{aligned} \tag{3.15}$$

where the beam properties and cross section again have been assumed to be constant with respect to the independent variables. The modulus of rigidity

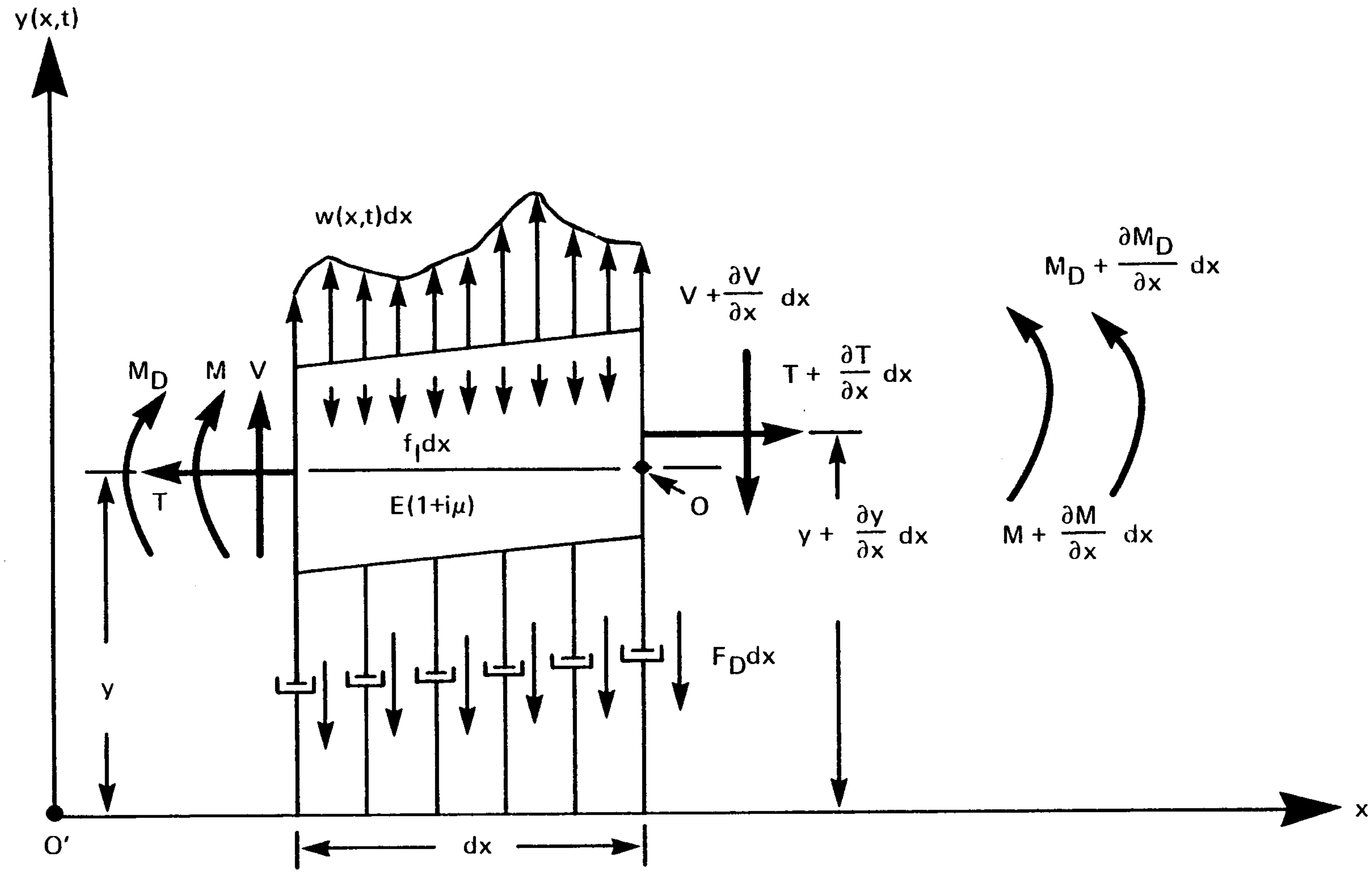

Figure 3.5. Forces and Moments Acting on a Differential Element of a Damped Bernoulli-Euler Beam with Tension.

does not appear in either Eq. (3.7) or Eq. (3.15) because Bernoulli-Euler beam theory neglects the effects of shear deformation.

If solutions to Eq. (3.15) are assumed that are proportional to $e^{i\omega t}$ where ω is the circular frequency of harmonic motion, it is clear that the complex parts of the first and second terms are identical when $\mu = c_s\omega/E$. Thus, strain rate damping is a special case of hysteretic damping in which the frequency dependence is linear. These two damping mechanisms are distinct since the beam properties in Eq. (3.15) are assumed to be time independent. This study deals exclusively with hysteretic damping ($c_s = c_v = 0$) in the calculations that are to be presented. This is simply a convenient choice since many computations exist in the literature which have considered each type of these three damping mechanisms [24]. The analysis and resultant computer program described in the remainder of this dissertation possess the capability to handle all three types of these damping mechanisms either separately or together. Interactions between the damping mechanisms are accounted for thus giving the overall theory great flexibility.

3.4 Timoshenko Beam Theory

The effects of shear deformation and rotary inertia on the dynamic response of the beam are accounted for in the Timoshenko beam theory [89,90]. These two effects can influence the motion of the beam appreciably when its aspect or depth-to-length ratio is large. High frequency vibratory response also can be affected by these two factors [91]. In Figure 3.6 are shown the components of beam deflection associated with shear distortion and

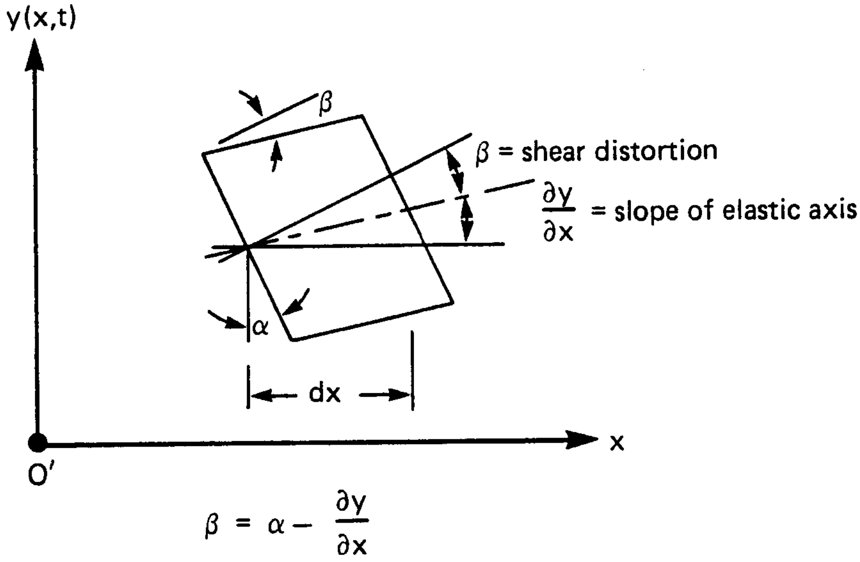

Figure 3.6. Effect of Shear Distortion on Beam Deflection.

rotary inertia. The presence of rotary inertia occurs because the beam cross sections rotate through some angle α from their original vertical positions. In the absence of shear the beam cross sections remain normal to the elastic axis and the rotation angle α would simply be equal to the slope of the elastic axis $\partial y/\partial x$. If shear distortion is considered and Bernoulli's hypothesis is again invoked, the shear distortion can be represented to a first approximation by the angle β shown in Figure 3.6. The slope of the elastic axis is actually reduced by this distortion angle β. The kinematic relationship between these angles can be expressed as

$$\beta(x,t) = \alpha(x,t) - \frac{\partial y(x,t)}{\partial x} \tag{3.16}$$

The analysis presented in the preceding section can now be extended to account for shear deformation and rotary inertia. No axial variation of material properties or of the beam cross-sectional area is accounted for in this development. Figure 3.7 shows the forces and moments acting on a differential element of this damped Timoshenko beam with tension. The transverse and longitudinal force balances can be written as follows:

$$V + w \bullet dx - f_I \bullet dx - F_D \bullet dx - \left[V + \frac{\partial V}{\partial x} \bullet dx \right] = 0 \tag{3.17}$$

$$T - \left[T + \frac{\partial T}{\partial x} \bullet dx \right] = 0 \tag{3.18}$$

The moment balance with rotary inertia included is

$$\begin{aligned} M + M_D + V \bullet dx + w \bullet dx \bullet \left[\frac{dx}{2} \right] - \left[M + \frac{\partial M}{\partial x} \bullet dx \right] \\ + \left[T + \frac{\partial T}{\partial x} \bullet dx \right] \left[\frac{\partial y}{\partial x} \right] \bullet dx - F_D \bullet dx \bullet \left[\frac{dx}{2} \right] \\ - \left[M_D + \frac{\partial M_D}{\partial x} \bullet dx \right] + m_I dx = 0 \end{aligned} \tag{3.19}$$

where m_I is the distributed rotational inertia. In writing these equilibrium equations the tensile force T on the tube is assumed to be independent of the deflection. Its direction and point of application do not change.

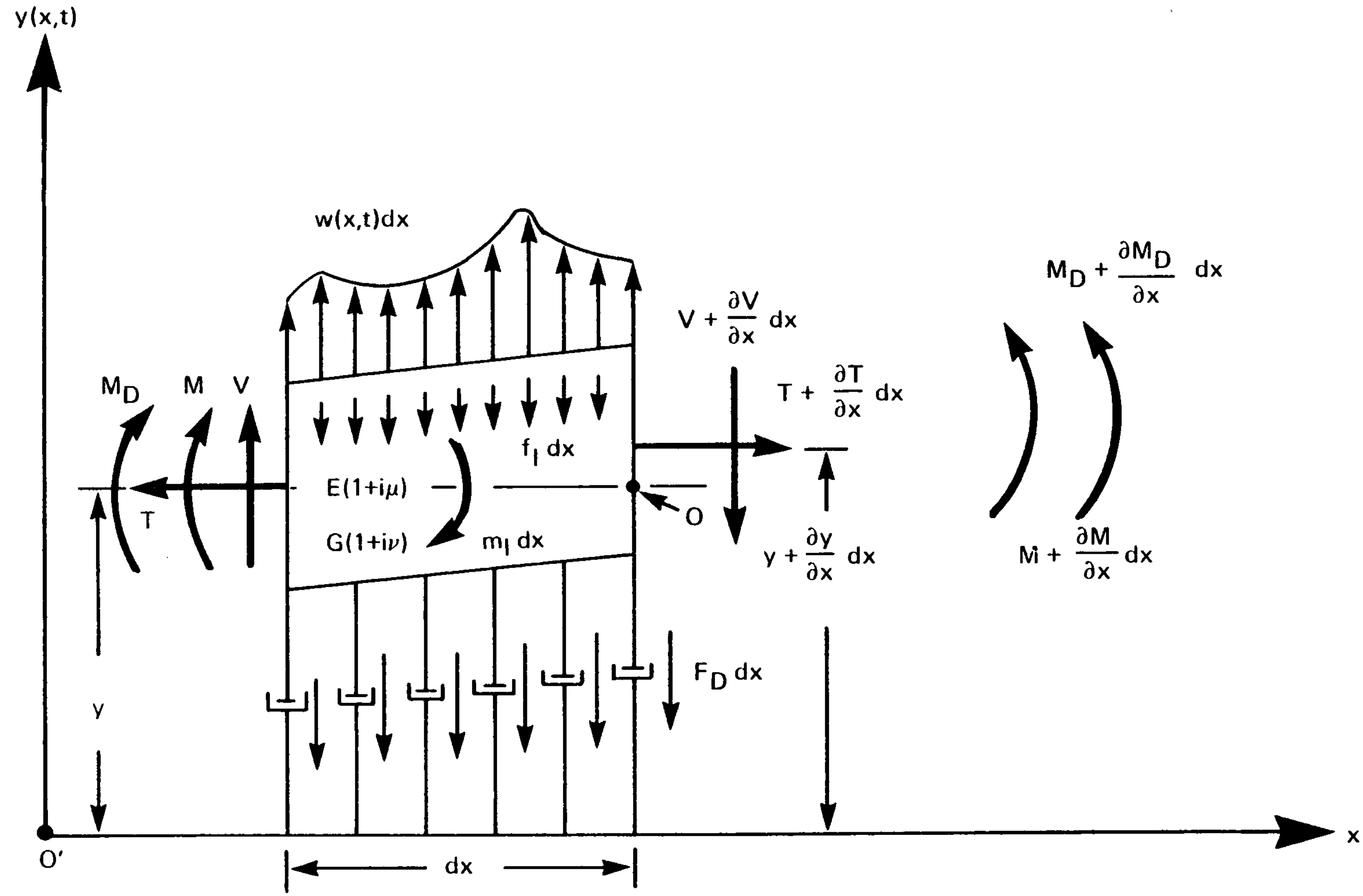

Figure 3.7. Forces and Moments Acting on a Differential Element of a Damped Timoshenko Beam with Tension.

The shear force acting on the beam cross section can be related to the distortion angle β by

$$V = kA_sG\beta \tag{3.20}$$

where the material is assumed to be isothermal, isotropic, elastic, and to obey Hooke's law.

The shear coefficient k for the annular cross section of a tube or pipe having inside diameter d_i and outside diameter d_o is given by

$$k = \frac{6(1 + \bar{\nu})\left[1 + \dfrac{d_i^2}{d_o^2}\right]^2}{(7 + 6\bar{\nu})\left[1 + \dfrac{d_i^2}{d_o^2}\right]^2 + (20 + 12\bar{\nu})\dfrac{d_i^2}{d_o^2}} \tag{3.21}$$

where $\bar{\nu}$ is Poisson's ratio [92]. The quantity kA_s represents the effective shear area of the beam cross section.

For modeling hysteretic damping, the shear modulus or modulus of rigidity G can be replaced with its complex representation $\tilde{G}$ as embodied in Eq. (3.14).

The rotary inertia is simply the product of the mass moment of inertia of the cross section and the angular acceleration

$$m_I = \rho_s I \frac{\partial^2 \alpha}{\partial t^2} = m_s \frac{I}{A_s} \bullet \frac{\partial^2 \alpha}{\partial t^2} \tag{3.22}$$

where the quotient I/A_s is the radius of gyration of the beam cross section.

The radius of curvature, internal resisting moment, and internal strain rate damping moment must be written in terms of the rotation angle α. Thus,

$$M = \frac{EI}{r} = EI\frac{\partial \alpha}{\partial x} \tag{3.23}$$

$$M_D = c_s I \frac{\partial^2 \alpha}{\partial x \partial t} \tag{3.24}$$

The transverse inertia force and the viscous damping force still depend explicitly on the beam deflection; hence, they retain their mathematical forms already presented in terms of y(x,t).

The transverse force balance Eq. (3.17) and the moment balance Eq. (3.19) may now be written as follows:

$$w - \rho_s A_s \frac{\partial^2 y}{\partial t^2} - kA_s G(1 + i\nu)\frac{\partial \beta}{\partial x} - c_v \frac{\partial y}{\partial t} = 0 \tag{3.25}$$

$$\begin{aligned} &kA_s G(1 + i\nu)\beta + T\frac{\partial y}{\partial x} + \rho_s I \frac{\partial^2 \alpha}{\partial t^2} \\ &- E(1 + i\mu) I \frac{\partial^2 \alpha}{\partial x^2} - c_s I \frac{\partial^3 \alpha}{\partial x^2 \partial t} = 0 \end{aligned} \tag{3.26}$$

The axial force balance Eq. (3.18) reduces to $\partial T/\partial x = 0$ implying that the tube tension is constant.

Equations (3.16), (3.25), and (3.26) constitute a system of three equations and three unknowns. The variable β can be eliminated from the other two equations by using Eq. (3.16). The resultant Eq. (3.25) can be differentiated to obtain derivatives of α as a function of y. These derivatives then may be substituted into Eq. (3.26) to obtain the desired equation for the deflection y. The result is

$$
\begin{aligned}
&\left\{c_s I y_{xxxxt} + E(1 + i\mu) I y_{xxxx} - T y_{xx} + c_v y_t + \rho_s A_s y_{tt}\right\} \\
&\quad - \frac{c_s \rho_s I(1 - i\nu)}{kG(1 + \nu^2)}\, y_{xxttt} \\
&- \left[\frac{c_v c_s I(1 - i\nu)}{kA_s G(1 + \nu^2)} + \frac{EI\rho_s(1 + i\mu)(1 - i\nu)}{kG(1 + \nu^2)} + \rho_s I\right] y_{xxtt} \\
&- \frac{EIc_v(1 + i\mu)(1 - i\nu)}{kA_s G(1 + \nu^2)}\, y_{xxt} + \frac{\rho_s I c_v(1 - i\nu)}{kA_s G(1 + \nu^2)}\, y_{ttt} \\
&\quad + \frac{\rho_s^2 I(1 - i\nu)}{kG(1 + \nu^2)}\, y_{tttt} = w \\
&- \frac{EI(1 + i\mu)(1 - i\nu)}{kA_s G(1 + \nu^2)}\, w_{xx} + \frac{\rho_s I(1 - i\nu)}{kA_s G(1 + \nu^2)}\, w_{tt} \\
&\quad - \frac{c_s I(1 - i\nu)}{kA_s G(1 + \nu^2)}\, w_{xxt}
\end{aligned}
\tag{3.27}
$$

The first set of terms in curly brackets { } is the Bernoulli-Euler contribution to the theory. The Bernoulli-Euler equation is obviously a special case of the more general beam equation including shear distortion and rotary inertia. It is emphasized that ν appearing in Eq. (3.27) is a hysteretic dissipation coefficient. The notation $\bar{\nu}$ is reserved to indicate Poisson's ratio.

3.5 Extension to a Fluid-Conveying Beam

In order to extend the analysis of the previous section to the case of a fluid-conveying Timoshenko beam the forces exerted by the flowing fluid on the tube itself must be accounted for in the overall force balance. As the fluid flows through the vibrating tube it is accelerated due to the changing curvature of the tube. This fluid flow generates a centrifugal force which is analogous to a compressive end load whose net effect is to reduce the natural frequencies of the tube. A Coriolis force also causes an asymmetrical distortion of the classical mode shapes of a Bernoulli-Euler beam because a mixed derivative term appears in the equation of motion [1, p. 292].

In Figure 3.8 are shown the flow-induced forces exerted on an element of the tube by the flowing fluid. The quantity $\pi d_i \tau_w dx$ is the fluid frictional force while $w(x,t)dx$ is the dynamic fluid pressure at the inside tube wall integrated over this inside surface. The distributed force $w(x,t)$ must be determined from an analysis of the equations of fluid motion. The frictional force $\pi d_i \tau_w dx$ can be neglected as long as only lateral vibrations are being considered. This implies that the equations of motion for an inviscid fluid can be utilized in this problem. The fluid is assumed to discharge into the atmosphere at the downstream end of the tube. The pressure at $x=L$ is then zero relative to atmospheric pressure.

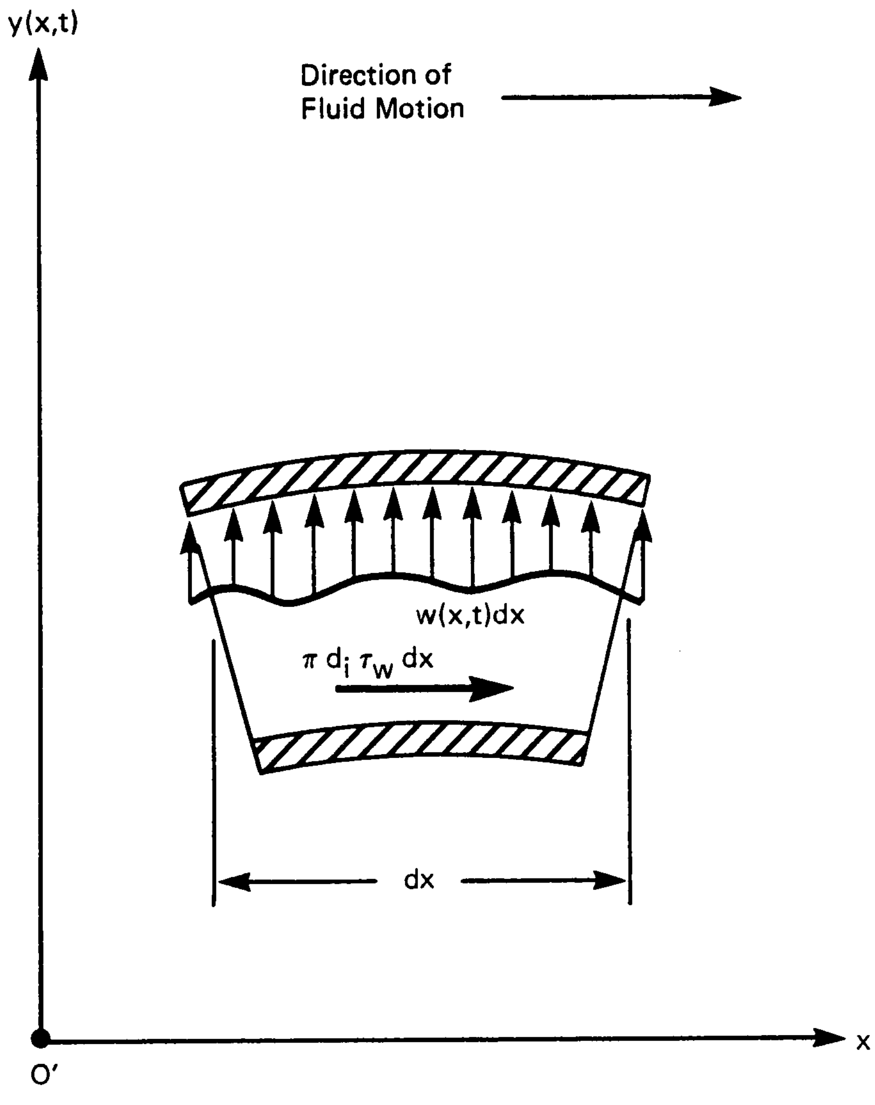

Figure 3.8. Fluid Forces Acting on Tube Element.

The tube is assumed to be either simply supported or cantilevered. In either of these cases the downstream end of the tube is free to slide axially. The tube tension T at x=L is then zero. This implies that T is zero in Eq. (3.27) since it can at most be a constant in this analysis. If fluid friction were being included this would not be the case; moreover, an axial equation of motion for a vibrating tube would then have to be added to the analysis.

The equation of motion for the damped, fluid-conveying Timoshenko beam is then Eq. (3.27) with the tube tension term $T \bullet \partial^2 y(x,t)/\partial x^2$ set equal to zero. The quantity w(x,t) can be determined using the equations of motion for an inviscid fluid.

3.6 Equations of Fluid Motion

The flow of a compressible fluid through a constant area circular duct or tube is now considered as shown in Figure 3.9. The tube itself is assumed to be horizontal to the surface of the earth. The radial coordinate r is assumed to be parallel to the earth's gravitational equipotentials. Its sense is opposite to the direction of the gravitational force. The fluid itself is assumed to be inviscid. The equations which govern the motion of the fluid are the Euler equations for mass and momentum transport [93]. In the absence of body forces they are

$$\frac{\partial \rho}{\partial t} + \vec{\nabla} \bullet (\rho \vec{V}) = 0 \tag{3.28}$$

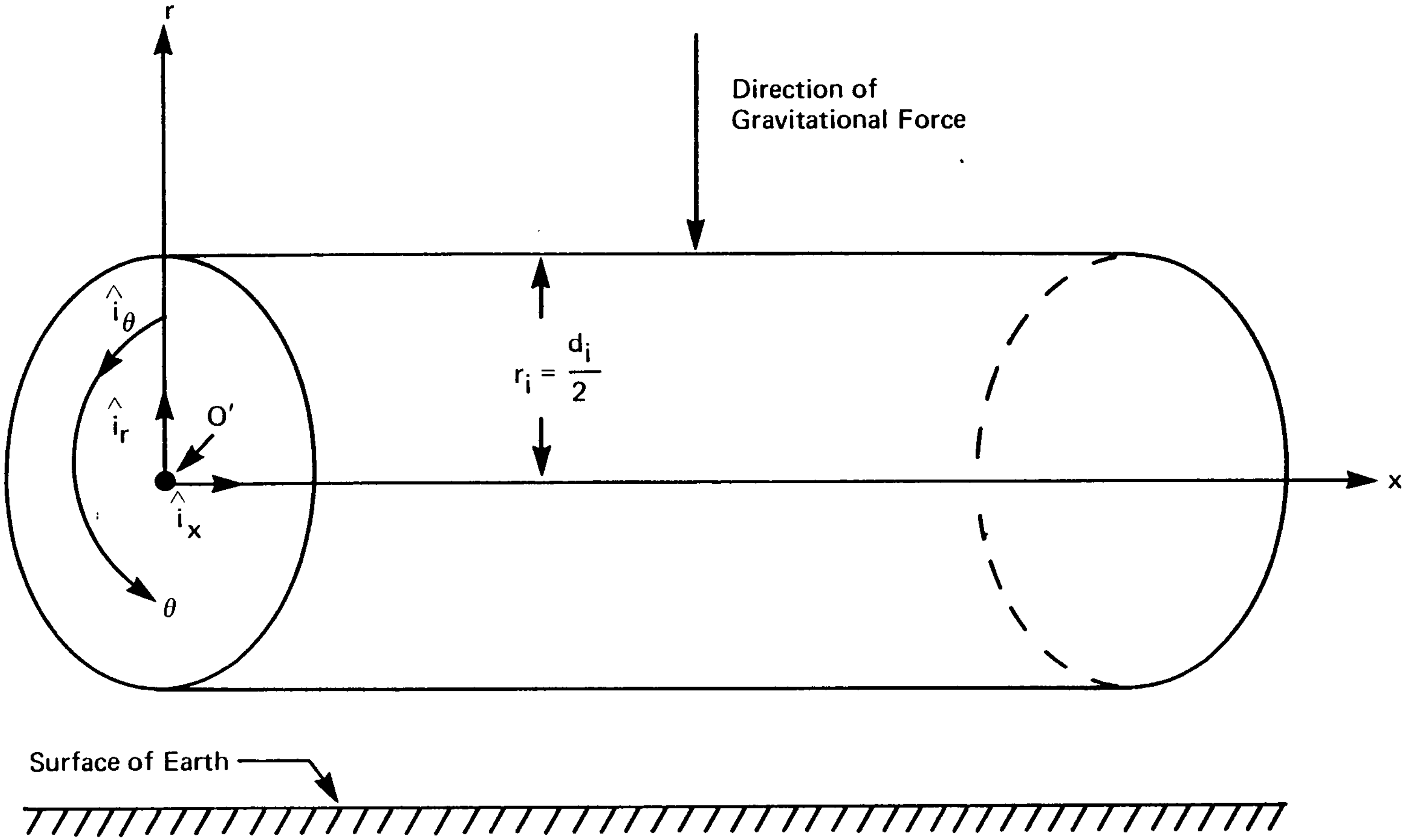

Figure 3.9. Coordinate System for Duct Flow.

$$\rho\frac{\partial\vec{V}}{\partial t} + \rho\vec{\nabla}\left(\frac{\vec{V}\bullet\vec{V}}{2}\right) - \rho\vec{V}\hat{x}(\vec{\nabla}\hat{x}\vec{V}) + \vec{\nabla}P = 0 \tag{3.29}$$

The momentum Eq. (3.29) is written in the form shown since it is invariant (in a tensorial sense) under coordinate change [94, p. 13].

A suitable energy transport equation can be developed if a condition of local thermodynamic equilibrium is assumed. This implies that thermodynamic functions of state exist for each fluid element whose functional values are determined by local state variables in accordance with equilibrium relations. The fluid media is assumed to be a perfect insulator whose thermal conductivity is zero; additionally, the fluid is assumed to be either transparent or opaque to radiative heat transfer. No internal sources or sinks of heat generation are present. The only work done is that due to compression or expansion of the fluid. This mode of energy interchange is reversible. The appropriate equation for the internal energy per unit mass u is

$$\rho\frac{\partial u}{\partial t} + \rho(\vec{V}\bullet\vec{\nabla})u + P\vec{\nabla}\bullet\vec{V} = 0 \tag{3.30}$$

where it is noted that no viscous dissipation terms appear since the fluid is inviscid [95, pp. 188–190]. Equation (3.30) is a statement of conservation of thermal energy only.

By introducing the substantial derivative operator D/Dt defined as $\partial/\partial t + \vec{V}\bullet\vec{\nabla}$ and the specific volume υ which is simply the reciprocal of the density $1/\rho$, the following result can be obtained when Eq. (3.30) is combined with the continuity Eq. (3.28):

$$\frac{Du}{Dt} + P\frac{D\upsilon}{Dt} = 0 \tag{3.31}$$

This equation is actually a defining relation fundamental to thermodynamics which combines the first and second laws of thermodynamics into a single equation, i.e.,

$$T\frac{Ds}{Dt} \equiv \frac{Du}{Dt} + P\frac{D\upsilon}{Dt} = 0 \tag{3.32}$$

where s is the entropy per unit mass. Since the temperature is nonzero it is concluded that Ds/Dt must be zero. This means that the changes of state of each fluid element are isentropic along a streamline.

The sonic velocity c may now be introduced without loss of generality since the flow is isentropic. The defining equation is

$$c^2 \equiv \left.\frac{\partial P}{\partial \rho}\right|_s = \frac{dP}{d\rho} \tag{3.33}$$

which is sometimes written functionally as $\rho = \rho(P)$. Equations (3.28), (3.29), and (3.33) govern the barotropic fluid motion in the tube shown in Figure 3.9.

Equation (3.33) implies that any acoustic wave propagating within the duct consists of weak rarefactions or expansions and compressions [96, p. 27]. The thermodynamic processes occurring across the wave are reversible, the wave itself is very thin, and property changes occur instantaneously. No heat transfer takes place between the fluid and its surroundings. The acoustic wave process is reversible as well as adiabatic; hence, it is isentropic.

The equations of fluid motion may now be written in cylindrical coordinates as follows:

Continuity:
$$\frac{\partial \rho}{\partial t} + \frac{\partial(\rho V_x)}{\partial x} + \frac{1}{r} \bullet \frac{\partial(\rho V_\theta)}{\partial \theta} + \frac{1}{r} \bullet \frac{\partial(r\rho V_r)}{\partial r} = 0 \tag{3.34}$$

Radial Momentum:
$$\frac{\partial(\rho V_r)}{\partial t} + \frac{\partial(\rho V_r V_x)}{\partial x} + \frac{1}{r} \bullet \frac{\partial(\rho V_r V_\theta)}{\partial \theta} + \frac{\partial(\rho V_r^2)}{\partial r} + \frac{\rho V_r^2}{r} - \frac{\rho V_\theta^2}{r} + \frac{\partial P}{\partial r} = 0 \tag{3.35}$$

Azimuthal Momentum:
$$\frac{\partial(\rho V_\theta)}{\partial t} + \frac{\partial(\rho V_\theta V_x)}{\partial x} + \frac{1}{r} \bullet \frac{\partial(\rho V_\theta^2)}{\partial \theta} + \frac{\partial(\rho V_\theta V_r)}{\partial r} + \frac{2\rho V_\theta V_r}{r} + \frac{1}{r} \bullet \frac{\partial P}{\partial \theta} = 0 \tag{3.36}$$

Axial Momentum:
$$\frac{\partial(\rho V_x)}{\partial t} + \frac{\partial(\rho V_x^2)}{\partial x} + \frac{1}{r} \bullet \frac{\partial(\rho V_x V_\theta)}{\partial \theta} + \frac{\partial(\rho V_x V_r)}{\partial r} + \frac{\rho V_x V_r}{r} + \frac{\partial P}{\partial x} = 0 \tag{3.37}$$

The sonic velocity Eq. (3.33) closes this system of equations. The momentum Eqs. (3.35), (3.36), and (3.37) have been written in conservative form [97].

3.7 Vibrations of the Fluid

As the fluid moves through the tube it remains attached to the inside tube wall; moreover, the boundary constraining the fluid motion also is moving. A compatibility condition must then exist which mathematically reflects this physical situation. As shown in Figure 3.10 the deflection surface r at the fluid-solid interface can be represented by the equation

$$r = r_i + W(r,x,\theta,t)\Big|_{r=r_i} = r_i + W(x,\theta,t;r_i) \qquad (3.38)$$

The quantity $W(x,\theta,t;r_i)$ is the interfacial deflection at the location of the inside tube radius r_i. The tube radius is constant in both the original and deflected configurations since beam vibrations are being considered. The tube cross section retains its annular shape. Hence, the tube radius r_i is really just a simple parameter. The semicolon notation emphasizes this functional independency.

The quantity $W(x,0,t;r_i)$ in Figure 3.10 is the actual displacement of the material line along the inside top ($r=r_i,\theta=0$) of the tube. In general, the quantity $W(x,\theta,t;r_i)$ does not represent material displacements but an interfacial deflection of a surface. The neutral axis on which the bending stress vanishes passes through the centroid of the cross section in the case of beam vibrations. For this annular tube this is simply the centerline. The quantity $y(x,t)$ is the deflection of this centroid. From the simple geometric construction

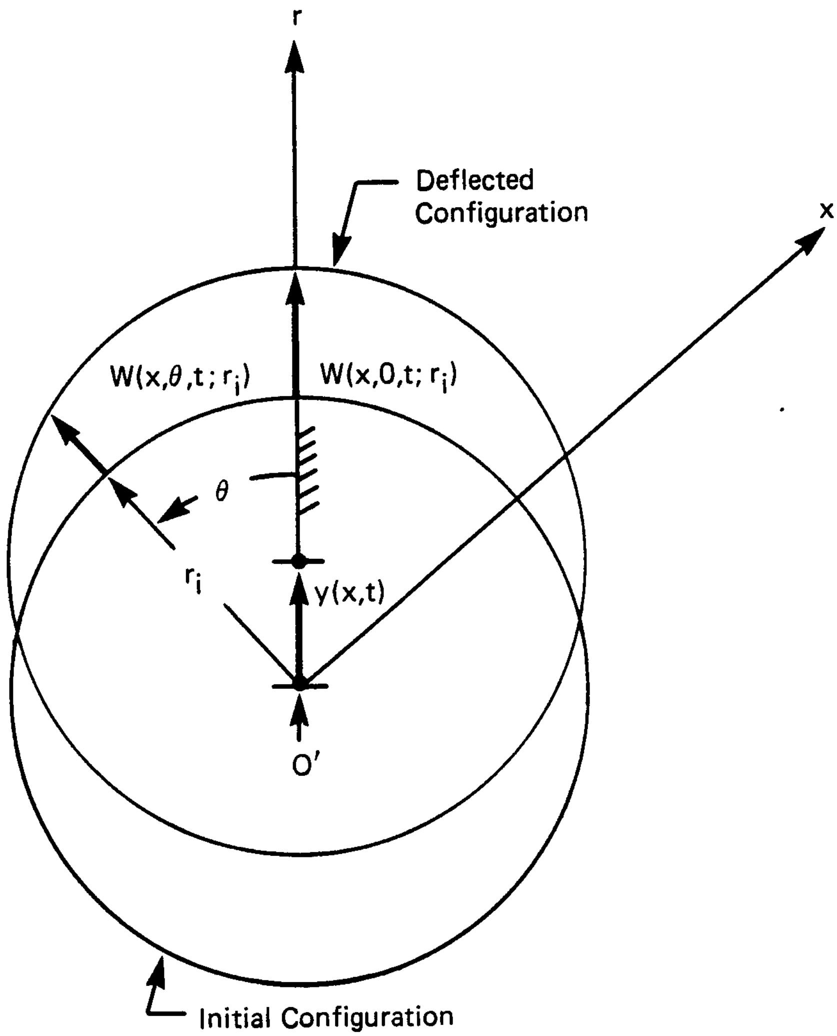

Figure 3.10. Radial Displacement of the Inside Tube Wall.

shown in Figure 3.10 the displacement $W(x,0,t;r_i)$ equals $y(x,t)$. In this problem torsion is not considered; thus, there is no azimuthal displacement component. The deflections resemble a simple rigid body translation.

The quantity $W(x,\theta,t;r_i)$ must be related to the centroidal motion $y(x,t)$. The appropriate geometric construction is shown in Figure 3.11. From the law of cosines side BC in triangle BCO′ is equal to $[(r_i + W)^2 + y^2 - 2(r_i + W)y\cos\theta]^{1/2}$. It is also equal to r_i. The quadratic formula can be used to relate W to y. The result is

$$W(x,\theta,t;r_i) = y\cos\theta - r_i + r_i\sqrt{1-(y/r_i)^2\sin^2\theta}$$

$$\approx y\cos\theta \quad \text{if} \quad y/r_i \ll 1 \tag{3.39}$$

The approximate form of Eq. (3.39) is used in this study.

The total derivative of Eq. (3.38) with respect to time is

$$\frac{dr}{dt} = \frac{\partial W}{\partial t} + \frac{\partial W}{\partial x} \bullet \frac{dx}{dt} + \frac{\partial W}{\partial \theta} \bullet \frac{d\theta}{dt} \quad \text{at } r=r_i \tag{3.40}$$

where dr/dt, dx/dt, and $rd\theta/dt$ are by definition the radial, axial, and azimuthal velocity components V_r, V_x, and V_θ, respectively. Equation (3.40) then can be rewritten as

$$V_r = \frac{\partial W}{\partial t} + V_x\frac{\partial W}{\partial x} + \frac{V_\theta}{r} \bullet \frac{\partial W}{\partial \theta} \quad \text{at } r=r_i \tag{3.41}$$

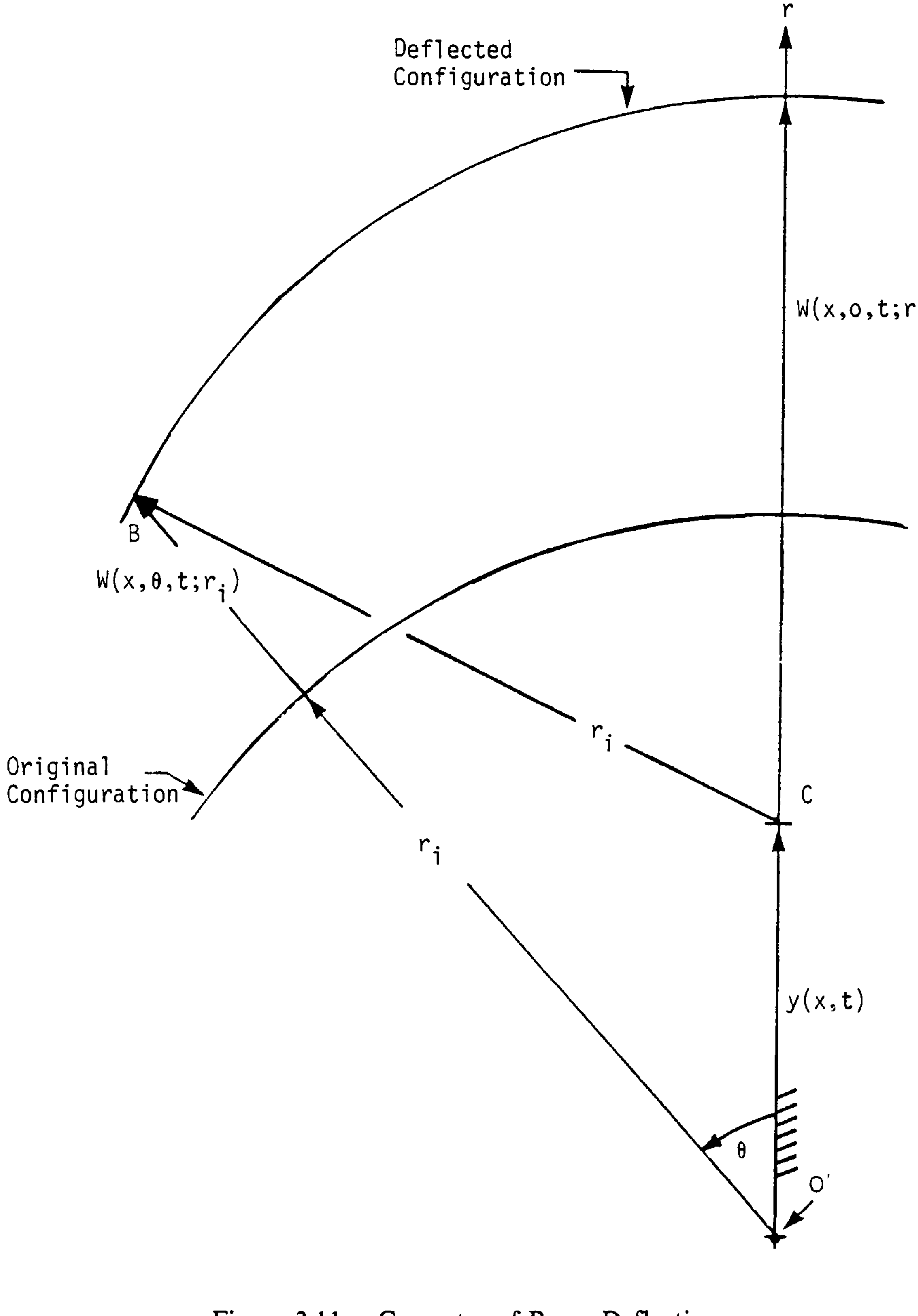

Figure 3.11. Geometry of Beam Deflections.

Equations (3.33) through (3.37) along with Eq. (3.41) can be linearized since small deflection theory has been used in the development of the beam Eq. (3.27) and because the flow through the duct is characterized by a nearly constant, though very large, axial velocity component. The appropriate perturbation variables are

$$\rho = \rho_0 + \rho' \tag{3.42a}$$

$$P = P_0 + P' \tag{3.42b}$$

$$V_x = U + V_x' \tag{3.42c}$$

$$V_r = 0 + V_r' \tag{3.42d}$$

$$V_\theta = 0 + V_\theta' \tag{3.42e}$$

$$W = 0 + W' \tag{3.42f}$$

where the primed quantities are small deviations from the assumed constant reference solution $(\rho_0, P_0, U, 0, 0, 0)$. It is noted that this reference solution satisfies Eqs. (3.34) through (3.37) as well as the compatibility Eq. (3.41).

When Eqs. (3.42) are substituted into Eqs. (3.33) through (3.37) as well as Eq. (3.41), the following set of linearized equations which describe the vibrations of the fluid can be derived:

$$\frac{\partial \rho'}{\partial t} + U\frac{\partial \rho'}{\partial x} + \frac{\partial(\rho_0 V_x')}{\partial x} + \frac{1}{r} \bullet \frac{\partial(\rho_0 V_\theta')}{\partial \theta} + \frac{\partial(\rho_0 V_r')}{\partial r} + \frac{\rho_0 V_r'}{r} = 0 \tag{3.43}$$

$$\frac{\partial(\rho_0 V_r')}{\partial t} + U\frac{\partial(\rho_0 V_r')}{\partial x} + \frac{\partial P'}{\partial r} = 0 \tag{3.44}$$

$$\frac{\partial(\rho_0 V_\theta')}{\partial t} + U\frac{\partial(\rho_0 V_\theta')}{\partial x} + \frac{1}{r} \bullet \frac{\partial P'}{\partial \theta} = 0 \tag{3.45}$$

$$\begin{aligned} U\frac{\partial \rho'}{\partial t} &+ \frac{\partial(\rho_0 V_x')}{\partial t} + U^2\frac{\partial \rho'}{\partial x} + 2U\frac{\partial(\rho_0 V_x')}{\partial x} \\ &+ \frac{U}{r} \bullet \frac{\partial(\rho_0 V_\theta')}{\partial \theta} + U\frac{\partial(\rho_0 V_r')}{\partial r} \\ &+ \frac{\rho_0 U V_r'}{r} + \frac{\partial P'}{\partial x} = 0 \end{aligned} \tag{3.46}$$

$$c^2 = \frac{dP'}{d\rho'} \text{ or } \rho' = \rho'(P') \tag{3.47}$$

$$V_r' = \frac{\partial W'}{\partial t} + U\frac{\partial W'}{\partial x} \text{ at } r = r_i \tag{3.48}$$

These first order perturbation equations were obtained by neglecting terms containing powers and products of ρ', P', V_r', V_θ', V_x', and W'.

The linearized continuity Eq. (3.43) allows the linearized axial momentum Eq. (3.46) to be reduced to

$$\frac{\partial(\rho_0 V_x')}{\partial t} + U\frac{\partial(\rho_0 V_x')}{\partial x} + \frac{\partial P'}{\partial x} = 0 \tag{3.49}$$

A velocity potential $\Phi(x,r,\theta,t)$ can be introduced as follows:

$$\frac{\partial \Phi}{\partial x} = \rho_0 V_x' \tag{3.50a}$$

$$\frac{1}{r} \bullet \frac{\partial \Phi}{\partial \theta} = \rho_0 V_\theta' \tag{3.50b}$$

$$\frac{\partial \Phi}{\partial r} = \rho_0 V_r' \tag{3.50c}$$

The linearized momentum equations become

$$\frac{\partial}{\partial x}\left[\frac{\partial \Phi}{\partial t} + U\frac{\partial \Phi}{\partial x} + P'\right] = 0 \tag{3.51a}$$

$$\frac{1}{r} \bullet \frac{\partial}{\partial \theta}\left[\frac{\partial \Phi}{\partial t} + U\frac{\partial \Phi}{\partial x} + P'\right] = 0 \tag{3.51b}$$

$$\frac{\partial}{\partial r}\left[\frac{\partial \Phi}{\partial t} + U\frac{\partial \Phi}{\partial x} + P'\right] = 0 \tag{3.51c}$$

or

$$\vec{\nabla}\left[\frac{\partial \Phi}{\partial t} + U\frac{\partial \Phi}{\partial x} + P'\right] = 0 \tag{3.52}$$

where $\vec{\nabla}$ is the operator defined by

$$\vec{\nabla} \equiv \hat{i}_r\frac{\partial}{\partial r} + \hat{i}_\theta\frac{1}{r} \bullet \frac{\partial}{\partial \theta} + \hat{i}_x\frac{\partial}{\partial x} \tag{3.53}$$

Equation (3.52) can be integrated such that

$$\frac{\partial \Phi}{\partial t} + U\frac{\partial \Phi}{\partial x} + P' = C_{P'} \tag{3.54}$$

By definition, the dynamic pressure perturbation P' is zero when the fluid is motionless (U=0); likewise, the velocity potential Φ can at most be a nonzero constant in this situation. Hence, the only logical choice for the integration constant $C_{P'}$ -- which in essence can be thought of as a datum -- is zero. Equation (3.54) then becomes

$$\frac{\partial \Phi}{\partial t} + U\frac{\partial \Phi}{\partial x} + P' = 0 \tag{3.55}$$

When the velocity potential defining Eqs. (3.50) is introduced into the linearized continuity Eq. (3.43) along with the linearized sonic velocity Eq. (3.47) and Eq. (3.55) which relates the dynamic pressure perturbation to the velocity potential the following equation for Φ results:

$$\Delta\Phi = \frac{1}{c^2}\left\{\frac{\partial^2\Phi}{\partial t^2} + 2U\frac{\partial^2\Phi}{\partial x \partial t} + U^2\frac{\partial^2\Phi}{\partial x^2}\right\} \tag{3.56}$$

The operator Δ is defined by

$$\Delta = \nabla^2 = \vec{\nabla} \bullet \vec{\nabla} = \frac{\partial^2}{\partial r^2} + \frac{1}{r} \bullet \frac{\partial}{\partial r} + \frac{1}{r^2} \bullet \frac{\partial^2}{\partial \theta^2} + \frac{\partial}{\partial x^2} \tag{3.57}$$

If the fluid is incompressible the sonic velocity c is infinite and the right-hand side of Eq. (3.56) is zero.

The quantity that is required is the force per unit length of tube w(x,t) exerted by the flowing fluid on the tube wall. This quantity as well as its derivatives appear on the right-hand side of Eq. (3.27). The differential force dF in the r-direction acting on the differential area element dA of the tube shown in Figure 3.12 is $P'(x,\theta,t;r_i)r_i\cos\theta d\theta dx$. Realizing that dw is simply dF/dx this expression can be integrated around the circumference of the inside tube wall to obtain the desired expression for w(x,t). The result is

$$w(x,t) = r_i \int_0^{2\pi} P'(x,\theta,t;r_i)\cos\theta d\theta \tag{3.58}$$

It is emphasized that only the dynamic fluid pressure perturbation at the tube wall is required to close the problem formulation.

3.8 Initial and Boundary Conditions

This study considers both simply supported and cantilevered tube spans. Boundary conditions for these two cases are written as

Simply Supported:

$$y(x,t)\Big|_{x=0} = y(x,t)\Big|_{x=L} = 0 \tag{3.59a}$$

$$\left.\frac{\partial^2 y(x,t)}{\partial x^2}\right|_{x=0} = \left.\frac{\partial^2 y(x,t)}{\partial x^2}\right|_{x=L} = 0 \tag{3.59b}$$

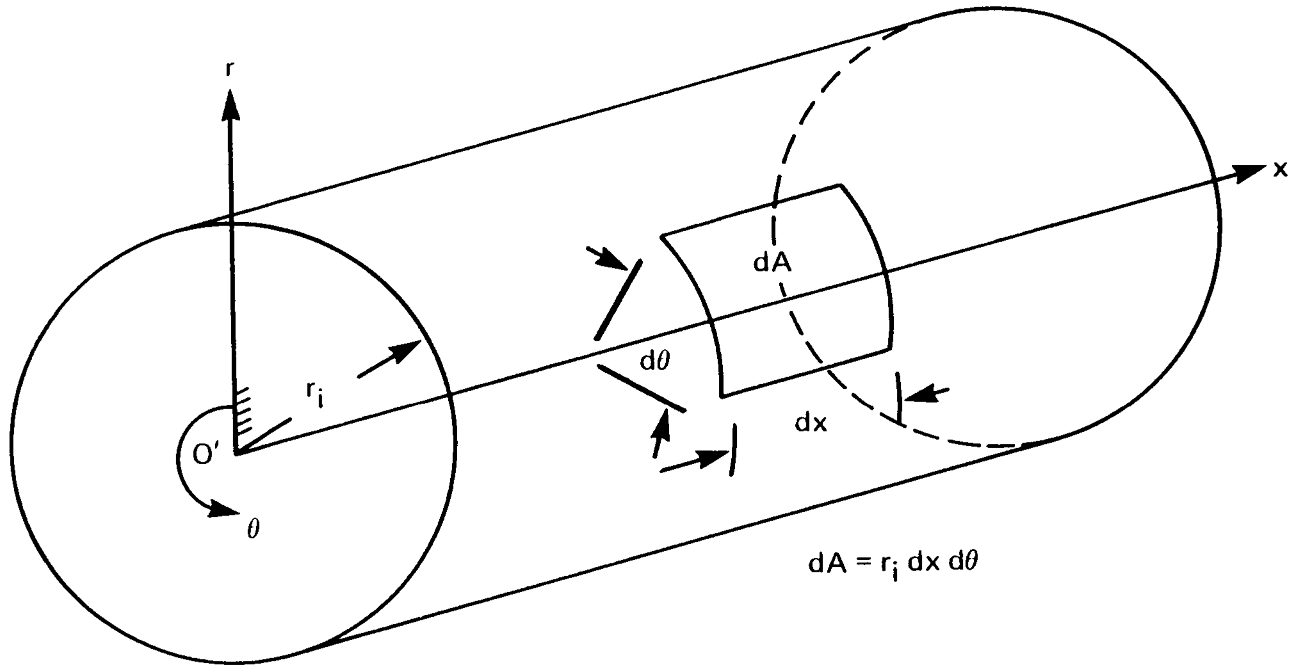

Figure 3.12. Differential Element Along Tube Wall.

Cantilevered:

$$y(x,t)\Big|_{x=0} = \frac{\partial y(x,t)}{\partial x}\Bigg|_{x=0} = 0 \tag{3.60a}$$

$$\frac{\partial^2 y(x,t)}{\partial x^2}\Bigg|_{x=L} = \frac{\partial^3 y(x,t)}{\partial x^3}\Bigg|_{x=L} = 0 \tag{3.60b}$$

The first derivative is the slope of the beam while the second and third derivatives are proportional to its moment and shear, respectively.

The primary emphasis in this investigation is determining when the steady-state harmonic vibratory motion of a damped Timoshenko beam conveying a compressible fluid is stable. Initial conditions are not required for determining whether the resultant lateral tube motion grows or decays in an exponential manner.

3.9 Problem Summary

A summary of the basic equations developed in this chapter is given in Table 3.1. These equations can be employed to investigate the stability of a horizontal, damped, fluid-conveying Timoshenko beam that is either cantilevered or simply supported. As originally shown by Niordson [43,44] sufficient information is available in the mathematical formulation of the fluid motion to allow resolution of the dynamic pressure perturbation along the fluid-solid interface. In the next chapter this stability problem is shown to be governed by a homogeneous partial differential equation pair. This work differs

Table 3.1. Basic Equation Summary.

$$\left\{c_s I y_{xxxxt} + E(1 + i\mu) I y_{xxxx} + c_v y_t + \rho_s A_s y_{tt}\right\}$$

$$- \frac{c_s \rho_s I(1 - i\nu)}{kG(1 + \nu^2)} y_{xxttt}$$

$$- \left[\frac{c_v c_s I(1 - i\nu)}{kA_s G(1 + \nu^2)} + \frac{EI\rho_s(1 + i\mu)(1 - i\nu)}{kG(1 + \nu^2)} + \rho_s I\right] y_{xxtt}$$

$$- \frac{EIc_v(1 + i\mu)(1 - i\nu)}{kA_s G(1 + \nu^2)} y_{xxt} + \frac{\rho_s I c_v(1 - i\nu)}{kA_s G(1 + \nu^2)} y_{ttt}$$

$$+ \frac{\rho_s^2 I(1 - i\nu)}{kG(1 + \nu^2)} y_{tttt} = w$$

$$- \frac{EI(1 + i\mu)(1 - i\nu)}{kA_s G(1 + \nu^2)} w_{xx} + \frac{\rho_s I(1 - i\nu)}{kA_s G(1 + \nu^2)} w_{tt}$$

$$- \frac{c_s I(1 - i\nu)}{kA_s G(1 + \nu^2)} w_{xxt} \qquad \text{(3.27) with } T = 0$$

$$\Phi_{rr} + \frac{1}{r}\Phi_r + \frac{1}{r^2}\Phi_{\theta\theta} + \Phi_{xx} =$$

$$\left[\Phi_{tt} + 2U\Phi_{xt} + U^2\Phi_{xx}\right]/c^2 \qquad (3.56)$$

$$P' = -\Phi_t - U\Phi_x \qquad (3.55)$$

$$V_r' = \frac{\partial W'}{\partial t} + U\frac{\partial W'}{\partial x} \text{ at } r = r_i = \frac{d_i}{2} \qquad (3.48)$$

$$W = W' = y\cos\theta \qquad (3.39)\ \&\ (3.42f)$$

$$w = r_i \int_0^{2\pi} P'\Big|_{r=r_i} \cos\theta d\theta \qquad (3.58)$$

Boundary Condition Eqs. (3.59) and (3.60) from that which already exists in the literature since it considers external viscous damping and internal strain rate and hysteretic damping in the formulation of the beam equation; likewise, a compressible fluid is assumed to be flowing through the tube. No calculations presently exist in the open literature which have accounted for the presence of a compressible fluid or all three of the above mentioned damping mechanisms in an analysis of a fluid-conveying Timoshenko beam.

4. MATHEMATICAL PROCEDURE

4.1 Introduction

The method of separation of variables [98, ch.8] is utilized in this chapter to obtain a pair of coupled partial differential equations which govern the stability of the damped, Timoshenko beam conveying a compressible fluid. Suitable dimensionless variables are selected and introduced into these equations to reduce them to a more suitable form. The partial differential equation set governing the motion of the fluid-tube system is shown to be homogeneous. Stability of the system is determined by the roots of a pair of simultaneous transcendental equations.

4.2 Separation of Variables

Let the velocity potential Φ be represented by the following functional form:

$$\Phi(x,r,\theta,t) = R(r)S(x,\theta,t) \tag{4.1}$$

The radial velocity perturbation V_r' at the tube wall can be determined from Eq. (3.50c). The result is

$$V_r'\Big|_{r=r_i} = \frac{S(x,\theta,t)}{\rho_0} \cdot \frac{dR(r)}{dr}\Big|_{r=r_i} \tag{4.2}$$

The linearized compatibility condition at the tube wall can be used to find S. From Eq. (3.48) obtain

$$S(x,\theta,t) = \rho_0 \left\{ \frac{\partial W'(x,\theta,t;r_i)}{\partial t} + U \frac{\partial W'(x,\theta,t;r_i)}{\partial x} \right\} \Big/ \left. \frac{dR(r)}{dr} \right|_{r=r_i} \tag{4.3}$$

Equations (3.39), (3.42f), and (4.3) may be substituted into the defining Eq. (4.1) to obtain an expression for Φ. It follows that

$$\Phi(x,r,\theta,t) = \rho_0 R(r) \left\{ y_t + U y_x \right\} \cos\theta \Big/ \left. \frac{dR(r)}{dr} \right|_{r=r_i} \tag{4.4}$$

In Eq. (4.4) the first appearance of R(r) means specifically this unknown function while its derivative in the denominator is evaluated at the tube wall.

From Eq. (3.55) the dynamic fluid pressure perturbation along the tube wall is given by

$$P'(x,\theta,t;r_i) = -\rho_0 R(r_i) \left\{ y_{tt} + 2U y_{xt} + U^2 y_{xx} \right\} \cos\theta \Big/ \left. \frac{dR(r)}{dr} \right|_{r=r_i} \tag{4.5}$$

The distributed lateral force along the tube wall now can be determined by performing the integration required in Eq. (3.58). The result is

$$w(x,t) = -\pi \rho_0 r_i R(r_i) \left\{ y_{tt} + 2U y_{xt} + U^2 y_{xx} \right\} \Big/ \Big[dR(r)/dr \Big]_{r=r_i} \tag{4.6}$$

Formal dependence on the angular coordinate θ has been removed by this integration process. The reference pressure P_0 has been set equal to zero for convenience; this is equivalent to assuming that P_0 is at or near atmospheric pressure (zero gauge pressure). No pressure excess exists at the discharge point $(x=L)$. This, of course, would not be true if the end of the tube were fitted with a convergent nozzle.

Equation (4.6) now must be substituted into Eq. (3.27) with the tension term set equal to zero. The following homogeneous partial differential equation results:

$$\Bigg\{ c_s I \left[1 - \frac{\rho_0 A f U^2 (1-i\upsilon)}{k A_s G (1+\upsilon^2)} \right] y_{xxxxt} + c_v y_t$$

$$+ E(1+i\mu) I \left[1 - \frac{\rho_0 A f U^2 (1-i\upsilon)}{k A_s G (1+\upsilon^2)} \right] y_{xxxx} + \left[\rho_s A_s + \rho_0 A f \right] y_{tt}$$

$$+ 2\rho_0 A f U y_{xt} + \rho_0 A f U^2 y_{xx} \Bigg\} - \frac{E I c_v (1+i\mu)(1-i\upsilon)}{k A_s G (1+\upsilon^2)} y_{xxt}$$

$$- \frac{c_s I (1-i\upsilon)}{k A_s G (1+\upsilon^2)} \left[\rho_s A_s + \rho_0 A f \right] y_{xxttt} + \frac{\rho_s I c_v (1-i\upsilon)}{k A_s G (1+\upsilon^2)} y_{ttt}$$

$$+ \frac{\rho_s I (1-i\upsilon)}{k A_s G (1+\upsilon^2)} \left[\rho_s A_s + \rho_0 A f \right] y_{tttt} - \frac{2\rho_0 A f U E I (1+i\mu)(1-i\upsilon)}{k A_s G (1+\upsilon^2)} y_{xxxt}$$

$$+\frac{2\rho_0 AfU\rho_s I(1-i\upsilon)}{kA_s G(1+\upsilon^2)}y_{xttt}-\frac{2\rho_0 AfUc_s I(1-i\upsilon)}{kA_s G(1+\upsilon^2)}y_{xxxtt}$$

$$-\left\{\frac{c_v c_s I(1-i\upsilon)}{kA_s G(1+\upsilon^2)}+\frac{EI(1+i\mu)(1-i\upsilon)}{kA_s G(1+\upsilon^2)}\left[\rho_s A_s+\rho_0 Af\right]\right.$$

$$\left.+\rho_s I\left[1-\frac{\rho_0 AfU^2(1-i\upsilon)}{kA_s G(1+\upsilon^2)}\right]\right\}y_{xxtt}=0 \qquad (4.7)$$

where A is simply the flow area πr_i^2 or $\pi d_i^2/4$ and f is a compressibility factor related to the sonic velocity c and tube geometry. This quantity f is defined as

$$f\equiv\left.\frac{R}{r\dfrac{dR}{dr}}\right|_{r=r_i} \qquad (4.8)$$

It is emphasized that this compressibility factor f has no direct relation to the coefficient of compressibility defined in elementary textbooks on fluid mechanics and thermodynamics. If the fluid is incompressible the sonic velocity is infinite and f is equal to one (this statement implies a tube of infinite length --see Section 5.2). If shear deformation is not considered whereby the terms in Eq. (4.7) which contain G are deleted, and all three damping coefficients are set equal to zero, the first term in curly brackets { } reduces to the classical Bernoulli-Euler, fluid-conveying beam equation when the fluid is incompressible.

A homogeneous partial differential equation for the function R(r) can be developed by substituting Eq. (4.4) into Eq. (3.56). The result is

$$\left[\frac{d^2R}{dr^2} + \frac{1}{r} \cdot \frac{dR}{dr} - \frac{R}{r^2}\right]\left[y_t + Uy_x\right]$$

$$+ R\left[y_{xxt} + Uy_{xxx}\right]$$

$$- \frac{R}{c^2}\left[y_{ttt} + 3Uy_{xtt} + 3U^2y_{xxt} + U^3y_{xxx}\right] = 0 \tag{4.9}$$

4.3 Dimensionless Equations

For convenience Eqs. (4.7) and (4.9) should be cast into a dimensionless form. To do this the following quantities are defined:

$$\eta = y/L \tag{4.10}$$

$$\xi = x/L \tag{4.11}$$

$$\tau = t\sqrt{EI/(\rho_s A_s + \rho_0 A)}/L^2 \tag{4.12}$$

This vibration problem has been shown to be a homogeneous one; hence, absolute deflections y (or η) cannot be determined. Only normalized deflections (i.e., mode shapes) can be computed. Otherwise, it probably would have been more logical to base the dimensionless deflection η on either the cylinder diameter or radius. Suffice it to say that using the length L as the fundamental factor for the normalized deflections permits easier comparison with existing work in the literature. It also simplifies the resultant equations somewhat by not having the aspect ratio r_i/L appearing in each term of Eqs. (4.7) and (4.9) after they have been cast in dimensionless form.

Equation (4.7) may be written in the following form with the use of Eqs. (4.10) through (4.12):

$$\Big\{C_s^*\Big[1 - fS^*U^{*2}(1 - i\upsilon)\Big]\eta_{\xi\xi\xi\xi\tau} + (1 + i\mu)\Big[1 - fS^*U^{*2}(1 - i\upsilon)\Big]\eta_{\xi\xi\xi\xi}$$

$$+ fU^{*2}\eta_{\xi\xi} + 2f\sqrt{\beta}U^*\eta_{\xi\tau} + C_v^*\eta_\tau + (\sigma + \beta f)\eta_{\tau\tau}\Big\}$$

$$- C_v^*S^*(1 + i\mu)(1 - i\upsilon)\eta_{\xi\xi\tau} - C_s^*S^*(\sigma + \beta f)(1 - i\upsilon)\eta_{\xi\xi\tau\tau\tau}$$

$$+ C_v^*R^*S^*(1 - i\upsilon)\eta_{\tau\tau\tau} + R^*S^*(\sigma + \beta f)(1 - i\upsilon)\eta_{\tau\tau\tau\tau}$$

$$- 2f\sqrt{\beta}S^*U^*(1 + i\mu)(1 - i\upsilon)\eta_{\xi\xi\xi\tau}$$

$$- \{C_s^*C_v^*S^*(1 - i\upsilon) + S^*(\sigma + \beta f)(1 + i\mu)(1 - i\upsilon) + R^*[1 - fS^*U^{*2}(1 - i\upsilon)]\}\eta_{\xi\xi\tau\tau}$$

$$+ 2f\sqrt{\beta}R^*S^*U^*(1 - i\upsilon)\eta_{\xi\tau\tau\tau} - 2f\sqrt{\beta}C_s^*S^*U^*(1 - i\upsilon)\eta_{\xi\xi\xi\tau\tau} = 0 \quad (4.13)$$

The dimensionless parameters in Eq. (4.13) which have obvious physical interpretations are given by

$$\beta = \rho_0 A/(\rho_s A_s + \rho_0 A) \tag{4.14}$$

$$\sigma = \rho_s A_s/(\rho_s A_s + \rho_0 A) \tag{4.15}$$

$$U^* = LU\sqrt{\rho_0 A/EI} \tag{4.16}$$

$$C_v^* = c_v L^2/\sqrt{EI(\rho_s A_s + \rho_0 A)} \tag{4.17}$$

$$C_s^* = c_s I/\left(L^2\sqrt{EI(\rho_s A_s + \rho_0 A)}\right) \tag{4.18}$$

$$R^* = \rho_s I/[L^2(\rho_s A_s + \rho_0 A)] \tag{4.19}$$

$$S^* = \frac{EI}{L^2 k A_s G(1 + \nu^2)} \tag{4.20}$$

As a general rule quantities which have an asterisk (*) for a superscript or that have been defined by Greek letters are dimensionless. The shear number S^* is the exact reciprocal of the one defined by Paidoussis and Laither [59] when ν is zero. Setting S^* equal to zero is equivalent to neglecting shear in the analysis, i.e., Bernoulli-Euler beam theory. The mass parameters σ and β are interdependent since their sum is equal to one. The quantity $\sigma + \beta f$ appearing in Eq. (4.13) can be rewritten as $1 + \beta(f\text{-}1)$ thus allowing the fluid-tube system mass to be determined by a single parameter. If the fluid is incompressible the sonic velocity is infinite and the compressibility factor f is unity; in this case the quantity $\sigma + \beta f$ is simply equal to one if the tube is infinitely long. If $C_v^* = C_s^* = R^* = S^* = 0$ and the fluid is incompressible, Eq. (4.13) reduces to the classical dimensionless Bernoulli-Euler fluid-conveying beam equation. The dimensionless parameters defined in Eqs. (4.14) through (4.20) conform with the convention established in previous investigations of this problem.

Now introduce the dimensionless quantities

$$\Lambda = R/L \tag{4.21}$$

$$\delta = r/r_i \tag{4.22}$$

into Eq. (4.9) and obtain

$$\begin{aligned}
&\left[\Lambda_{\delta\delta} + \frac{\Lambda_\delta}{\delta} - \frac{\Lambda}{\delta^2}\right]\left[\sqrt{\beta}\eta_\tau + U^*\eta_\xi\right] \\
&+ \Lambda A^{*2}\left[\sqrt{\beta}\eta_{\tau\xi\xi} + U^*\eta_{\xi\xi\xi}\right] \\
&- \Lambda A^{*2}\left\{\frac{M^{*2}\beta\sqrt{\beta}}{U^{*2}}\eta_{\tau\tau\tau} + 3\,\frac{M^{*2}\beta}{U^*}\eta_{\tau\tau\xi}\right. \\
&\left. + 3M^{*2}\sqrt{\beta}\eta_{\tau\xi\xi} + M^{*2}U^*\eta_{\xi\xi\xi}\right\} = 0
\end{aligned} \tag{4.23}$$

where the subscripts δ, ξ, and τ denote partial differentiation with respect to the independent variable as indicated. The parameter A^* is the aspect ratio

$$A^* = r_i/L = d_i/2L \tag{4.24}$$

while M^* is the Mach number.

$$M^* = \frac{U}{c} = \frac{U^*}{c^*} \tag{4.25}$$

The compressibility factor f becomes

$$f = \frac{1}{\delta} \cdot \left.\frac{\Lambda}{\Lambda_\delta}\right|_{\delta=1} \tag{4.26}$$

where the functional dependency $\Lambda = \Lambda(\delta)$ is noted.

The boundary condition Eqs. (3.59) and (3.60) may be written in dimensionless form as

Simply supported:

$$\eta(\xi,\tau)|_{\xi=0} = \eta(\xi,\tau)|_{\xi=1} = 0 \tag{4.27a}$$

$$\left.\frac{\partial^2\eta(\xi,\tau)}{\partial\xi^2}\right|_{\xi=0} = \left.\frac{\partial^2\eta(\xi,\tau)}{\partial\xi^2}\right|_{\xi=1} = 0 \tag{4.27b}$$

Cantilevered:

$$\eta(\xi,\tau)|_{\xi=0} = \left.\frac{\partial\eta(\xi,\tau)}{\partial\xi}\right|_{\xi=0} = 0 \qquad (4.28a)$$

$$\left.\frac{\partial^2\eta(\xi,\tau)}{\partial\xi^2}\right|_{\xi=1} = \left.\frac{\partial^3\eta(\xi,\tau)}{\partial\xi^3}\right|_{\xi=1} = 0 \qquad (4.28b)$$

The entire mathematical problem statement is represented in dimensionless form in Eqs. (4.10) through (4.28).

4.4 Solution Format

Simply stated, the purpose of this investigation is to determine when the amplitude of harmonic motion of a damped, Timoshenko beam conveying a compressible fluid increases without bound (in the context of linear partial differential equations with constant coefficients). The solution to Eq. (4.7) can be represented by

$$y(x,t) = \mathrm{Re}\left\{ \sum_{n=1}^{\infty} E_n(x)e^{i\omega_n t} \right\} \qquad (4.29)$$

where the circular frequency ω_n in rad/s is related to the cyclic frequency f_n in Hz by

$$\omega_n = 2\pi f_n \ , \ \ n = 1,2,\ldots,\infty \qquad (4.30)$$

In dimensionless form Eq. (4.29) becomes

$$7(\xi,\tau) = \mathrm{Re}\left[\sum_{n=1}^{\infty} E_n^*(\xi)\, e^{i\omega_n^*\tau} \right\} \tag{4.31}$$

where the relations between the dimensional and dimensionless quantities are given by

$$E_n^* = \frac{E_n}{L} \quad , \quad n=1,2,\ldots,\infty \tag{4.32}$$

$$\omega_n^* = \omega_n L^2 \sqrt{(\rho_s A_s + \rho_0 A)/EI} \quad , \quad n=1,2,\ldots,\infty \tag{4.33}$$

The system under consideration possesses an infinite number of degrees of freedom. The dimensionless circular frequency ω_n^* in the nth mode is in general a complex number. The system is defined to be stable or unstable depending on the imaginary component $\mathrm{Im}(\omega_n^*)$ of ω_n^*; the system is stable when $\mathrm{Im}(\omega_n^*)$ is positive and unstable when it is negative. A condition of neutral stability is said to have been reached when ω_n^* is real. As the flow velocity through the tube is increased the system can become unstable in one or more of its modes. Neutral stabiliy is achieved when $U^* = U_{nc}^*$ if $\mathrm{Im}(\omega_n^*) = 0$ for $U^* = U_{nc}^*$ and $\mathrm{Im}(\omega_n^*) > 0$ for $U_{nc}^* > U^* > 0$. The critical velocity U_c^* is defined as the smallest value of U_{nc}^* for any n; it represents physically the greatest flow velocity for which the system is stable in all of its modes. The critical dimensionless circular frequency ω_c^* is the frequency corresponding to U_c^*; it is a real quantity.

The equation system is fourth order in either the variable x or ξ. The solution in dimensional form can be further represented by

$$y(x,t) = \mathrm{Re}\left\{ \sum_{n=1}^{\infty} \sum_{j=1}^{4} \gamma_{jn}\, e^{\alpha_{jn}x} e^{i\omega_n t} \right\} \tag{4.34}$$

and in dimensionless form by

$$7(\xi,\tau) = \mathrm{Re}\left\{ \sum_{n=1}^{\infty} \sum_{j=1}^{4} \gamma_{jn}^* e^{\alpha_{jn}^*\xi} e^{i\omega_n^*\tau} \right\} \tag{4.35}$$

The coefficients are related through the expressions

$$\gamma_{jn}^* = \frac{\gamma_{jn}}{L} \tag{4.36}$$

$$\alpha_{jn}^* = \alpha_{jn} L \tag{4.37}$$

Equations (4.36) and (4.37) are valid for j=1,2,3,and 4 as well as n=1, 2, . . . , ∞. These coefficients are in general complex. Equations (4.34) and (4.35) must be altered with the usual modifications if two or more of the coefficients α_{jn} or α_{jn}^* coincide i.e., they are equal. It is noted that either Eq.

(4.34) or (4.35) can be written in the form of Fourier series. This is an expected result since the parent equation system contains mixed derivatives in the time and space variables.

4.5 Determination of the Compressibility Factor

Substitution of Eq. (4.35) into Eq. (4.23) results in

$$\left[\Lambda_{\delta\delta} + \frac{\Lambda_\delta}{\delta} - \frac{\Lambda}{\delta^2}\right]\left[\sqrt{\beta}\,(i\omega_n^*) + U^*\alpha_{jn}^*\right]$$

$$+ \Lambda A^{*2}\alpha_{jn}^{*2}\left[\sqrt{\beta}\,(i\omega_n^*) + U^*\alpha_{jn}^*\right]$$

$$-\Lambda\,\frac{A^{*2}M^{*2}}{U^{*2}}\left[\beta\sqrt{\beta}(i\omega_n^*)^3 + 3\beta U^*\,(i\omega_n^*)^2\,\alpha_{jn}^*\right.$$

$$\left. + 3U^{*2}\sqrt{\beta}(i\omega_n^*)\alpha_{jn}^{*2} + U^{*3}\alpha_{jn}^{*3}\right] = 0\ , \tag{4.38}$$

for n = 1, 2, . . . , ∞ and j = 1, 2, 3, or 4 only

Noting that the last quantity in brackets is equal to $[\sqrt{\beta}(i\omega_n^*) + U^*\alpha_{jn}^*]^3$ Eq. (4.38) may be written as follows when multiplied by δ^2 and divided by the quantity $[\sqrt{\beta}\,(i\omega_n^*) + U^*\,\alpha_{jn}^*]$:

$$\delta^2\Lambda_{\delta\delta} + \delta\Lambda_\delta - \Lambda + A^{*2}\alpha_{jn}^{*2}\delta^2\Lambda$$

$$- \delta^2\Lambda \frac{A^{*2}M^{*2}}{U^{*2}} \left[\sqrt{\beta}(i\omega_n^*) + U^*\alpha_{jn}^*\right]^2 = 0\,, \tag{4.39}$$

for n = 1, 2, . . . , ∞ and j = 1, 2, 3, 4 only

This equation can be written more compactly as

$$\delta^2\Lambda_{\delta\delta} + \delta\Lambda_\delta - (1)^2\Lambda + \kappa^2\delta^2\Lambda = 0 \tag{4.40}$$

where the parameter κ is given by

$$\kappa^2 = A^{*2}\left\{\alpha_{jn}^{*2} - \left(\frac{M^*}{U^*}\right)^2 \left[\sqrt{\beta}(i\omega_n^*) + U^*\alpha_{jn}^*\right]^2\right\}$$

$$= A^{*2}\left\{\alpha_{jn}^{*2} - \left[\frac{\sqrt{\beta}}{c^*}(i\omega_n^*) + \frac{U^*}{c^*}\alpha_{jn}^*\right]^2\right\}\,, \tag{4.41}$$

for n = 1, 2, . . . , ∞ and j = 1, 2, 3, 4 only

In writing Eq. (4.41) the dimensionless sonic velocity c* which is equal to cL $\sqrt{\rho_0 A/EI}$ has been introduced. The Mach number M^* obviously is given by the ratio U^*/c^*. It is better to define the fluid by specifying c^* rather than simply varying M^*. If the fluid is incompressible and stationary ($U^*=0$) then M^* will be indeterminate. In general, c^* must be greater than zero. A c^* of zero would imply a temperature of absolute zero which is not in the realm of the continuum description utilized throughout this development.

If Eq. (4.40) is transformed according to the two relations

$$\bar{\delta} = \kappa\delta \tag{4.42}$$

and

$$\bar{\Lambda}(\bar{\delta}) = \Lambda(\delta) \tag{4.43}$$

Eq. (4.41) can be written as

$$\bar{\delta}^2\bar{\Lambda}_{\bar{\delta}\bar{\delta}} + \bar{\delta}\bar{\Lambda}_{\bar{\delta}} + \left[\bar{\delta}^2 - (1)^2\right]\bar{\Lambda} = 0 \tag{4.44}$$

which can immediately be identified as Bessel's differential equation of integer order one [98, p. 384].

The general solution of Eq. (4.44) is

$$\bar{\Lambda}(\bar{\delta}) = C_1 J_1(\bar{\delta}) + C_2 Y_1(\bar{\delta}) \tag{4.45}$$

where J_1 and Y_1 are Bessel functions of the first and second kind, respectively, of integer order one. It is emphasized that $\bar{\delta}$ is in general a complex quantity. The parameters C_1 and C_2 are simple integration constants. Regularity of $\bar{\Lambda}\,(\bar{\delta})$ at $r = \delta = \bar{\delta} = 0$ requires that C_2 be set equal to zero.

The solution to Eq. (4.40) thus becomes

$$\Lambda(\delta) = C_1 J_1(\kappa\delta) \tag{4.46}$$

Equation (4.26) requires that Eq. (4.46) be differentiated with respect to δ. Bessel function recurrence relations [99] can be used to obtain the result for this derivative that

$$\frac{dJ_1(\kappa\delta)}{d(\kappa\delta)} = J_o(\kappa\delta) - \frac{J_1(\kappa\delta)}{\kappa\delta} = \frac{J_1(\kappa\delta)}{\kappa\delta} - J_2(\kappa\delta) \tag{4.47}$$

The required expression for the compressibility factor thus becomes

$$f = \left. \frac{C_1 J_1(\kappa\delta)}{\kappa\delta C_1 \left[J_o(\kappa\delta) - \dfrac{J_1(\kappa\delta)}{\kappa\delta} \right]} \right|_{\delta=1}$$

$$= \left. \frac{C_1 J_1(\kappa\delta)}{\kappa\delta C_1 \left[\dfrac{J_1(\kappa\delta)}{\kappa\delta} - J_2(\kappa\delta) \right]} \right|_{\delta=1} \tag{4.48}$$

or

$$f = \left[\kappa \frac{J_o(\kappa)}{J_1(\kappa)} - 1 \right]^{-1} = \left[1 - \kappa \frac{J_2(\kappa)}{J_1(\kappa)} \right]^{-1} \tag{4.49}$$

where κ is given by Eq. (4.41). Both of the parameters κ and f are in general complex quantities.

4.6 Characteristic Equation

When Eq. (4.35) is substituted into Eq. (4.13) the following characteristic or auxiliary equation associated with the parent partial differential equations can be obtained:

$$\Big\{ c_s^*\Big[1 - fS^*U^{*2}(1-i\nu)\Big] i\omega_n^*\alpha_{jn}^{*4} + (1+i\mu)\Big[1 - fS^*U^{*2}(1-i\nu)\Big] \alpha_{jn}^{*4}$$

$$+ 2if\sqrt{\beta}U^*\omega_n^*\alpha_{jn}^* + fU^{*2}\alpha_{jn}^{*2} + C_v^* i\omega_n^* - (\sigma+\beta f)\,\omega_n^{*2}\Big\}$$

$$-iC_v^*S^*(1+i\mu)(1-i\nu)\omega_n^*\alpha_{jn}^{*2} + iC_s^*S^*(\sigma+\beta f)(1-i\nu)\omega_n^{*3}\alpha_{jn}^{*2}$$

$$-iC_v^*R^*S^*(1-i\nu)\omega_n^{*3} + R^*S^*(\sigma+\beta f)(1-i\nu)\omega_n^{*4}$$

$$- 2if\sqrt{\beta}S^*U^*(1+i\mu)(1-i\nu)\omega_n^*\alpha_{jn}^{*3}$$

$$+\left\{C_s^*C_v^*S^*(1-i\nu)+S^*(\sigma+\beta f)(1+i\mu)(1-i\nu)+R^*\left[1-fS^*U^{*2}(1-i\nu)\right]\right\}\omega_n^{*2}\alpha_{jn}^{*2}$$

$$-2if\sqrt{\beta}R^*S^*U^*(1-i\nu)\,\omega_n^{*3}\alpha_{jn}^*$$

$$+2f\sqrt{\beta}C_s^*S^*U^*(1-i\nu)\,\omega_n^{*2}\alpha_{jn}^{*3}=0\,, \tag{4.50}$$

for $n = 1, 2, \ldots, \infty$ and $j = 1, 2, 3, 4$ only

The compressibility factor is given by Eq. (4.49) and its argument κ is determined using Eq. (4.41). Equation (4.50) is a transcendental equation; moreover, there are four values of the unknown α_{jn}^* corresponding to each of the dimensionless circular frequencies ω_n^*.

4.7 Frequency Equation

The frequency equation is developed by using the boundary conditions given by either Eqs. (4.27) or (4.28) in conjunction with the solution form given by Eq. (4.35). The exact equational statement is obtained by setting the determinant of the γ_{jn}^* coefficient matrix equal to zero. This is simply the mathematical condition required for the existence of nontrivial solutions [98, p. 159]. The frequency equation is developed here for the simply supported case with four distinct or unequal roots α_{jn}^*. The other required cases are summarized in Appendix A.

From a comparison of Eqs. (4.31) and (4.35) it is evident that

$$E_n^*(\xi) = \sum_{j=1}^{4} \gamma_{jn}^* e^{\alpha_{jn}^* \xi}, \text{ for } n=1,2,\ldots,\infty \tag{4.51}$$

The boundary conditions associated with this $E_n^*(\xi)$ then become

Simply Supported:

$$E_n^*(0) = E_n^*(1) = E_n^{*''}(0) = E_n^{*''}(1) = 0, \tag{4.52}$$

$$\text{for } n = 1, 2, \ldots, \infty$$

Cantilevered:

$$E_n^*(0) = E_n^{*'}(o) = E_n^{*''}(1) = E_n^{*'''}(1) = 0, \tag{4.53}$$

$$\text{for } n = 1, 2, \ldots, \infty$$

where the simple primes (′) denote total differentiation with respect to the independent variable ξ.

For notational simplification the following definitions are used:

$$\alpha_{1n}^* \equiv p \tag{4.54a}$$

$$\alpha^*_{2n} \equiv q \tag{4.54b}$$

$$\alpha^*_{3n} \equiv r \tag{4.54c}$$

$$\alpha^*_{4n} \equiv s \tag{4.54d}$$

$$\gamma^*_{1n} \equiv A \tag{4.55a}$$

$$\gamma^*_{2n} \equiv B \tag{4.55b}$$

$$\gamma^*_{3n} \equiv C \tag{4.55c}$$

$$\gamma^*_{4n} \equiv D \tag{4.55d}$$

$$\text{for } n = 1, 2, \ldots, \infty$$

Using this notation Eq. (4.51) may be written as

$$E^*_n(\xi) = Ae^{p\xi} + Be^{q\xi} + Ce^{r\xi} + De^{s\xi} \tag{4.56}$$

while the second derivative of this equation is

$$E^{*\prime\prime}_n(\xi) = Ap^2e^{p\xi} + Bq^2e^{q\xi} + Cr^2e^{r\xi} + Ds^2e^{s\xi} \tag{4.57}$$

Equations (4.52), (4.56), and (4.57) can be used to obtain the following set of equations:

$$E_n^*(0) = A + B + C + D = 0 \tag{4.58a}$$

$$E_n^*(1) = Ae^p + Be^q + Ce^r + De^s = 0 \tag{4.58b}$$

$$E_n^{*\prime\prime}(0) = Ap^2 + Bq^2 + Cr^2 + Ds^2 = 0 \tag{4.58c}$$

$$E_n^{*\prime\prime}(1) = Ap^2e^p + Bq^2e^q + Cr^2e^r + Ds^2e^s = 0 \tag{4.58d}$$

Existence of a nontrivial solution requires that the determinant of the coefficient matrix of the column vector $\{A, B, C, D\}^T$ be zero. Hence, the frequency equation for this simply supported case with four unequal roots is given by

$$F(\omega_n^*) = \det \begin{bmatrix} 1 & 1 & 1 & 1 \\ e^p & e^q & e^r & e^s \\ p^2 & q^2 & r^2 & s^2 \\ p^2e^p & q^2e^q & r^2e^r & s^2e^s \end{bmatrix} = 0 \tag{4.59}$$

where the functional dependency on ω_n^* is emphasized by the $F(\omega_n^*)$ notation. Five cases in all must be considered for the two support schemes. All ten of the frequency equation forms are summarized in Appendix A.

4.8 Summary

In this chapter it has been shown that the problem of determining the onset of unstable motion of a specified (the values of β or σ, U^*, C_v^* C_s^*, R^*, S^*, A^*, M^* or c^*, μ, and ν being given) fluid-conveying Timoshenko beam that is either simply supported or cantilevered reduces to the problem of finding the roots (α_{jn}^* and ω_n^*) of two simultaneous transcendental algebraic equations. The equation system just derived has been set up with the notion that it would be implemented on a digital computer. In the case of a compressible fluid the resulting equation system is too complicated to warrant attempting closed-form solutions.

5. NUMERICAL PROCEDURE

5.1 Introduction

In order to investigate the effects of compressibility on the stability of fluid-conveying beams the system of equations developed in the preceding chapter must be solved. Closed form solutions to such complex systems of nonlinear transcendental equations do not appear possible; therefore, numerical techniques must be employed. By selecting a suitable numerical scheme, this system of equations can be solved numerically to approximate the critical velocities and frequencies of the fluid-conveying tube.

This chapter is intended to outline the significant steps in the numerical solution technique. The actual computer program is quite lengthy and inclusion of a listing is not considered practical. Flow charts are utilized to illustrate the details of the numerical procedure.

5.2. Problem Classification

Equation (4.50) can be written as a quartic polynomial equation in terms of α_{jn}^* as

$$\left\{[1 + i(\mu + C_s^*\omega_n^*)][1 - f_{jn}S^*U^{*2}(1 - i\nu)]\right\}\alpha_{jn}^{*4}$$

$$-\left\{[1 + i(\mu + C_s^*\omega_n^*)][2if_{jn}\sqrt{\beta}S^*U^*(1 - i\nu)]\omega_n^*\right\}\alpha_{jn}^{*3}$$

$$+\left\{\left[[1+i(\mu+C_s^*\omega_n^*)][S^*(1-(1-f_{jn})\beta)(1-i\nu)]\right.\right.$$

$$\left.+R^*[1-f_{jn}S^*U^{*2}(1-i\nu)]\right]\omega_n^{*2}$$

$$\left.-[1+i(\mu+C_s^*\omega_n^*)][iC_v^*S^*(1-i\nu)]\omega_n^*+f_{jn}U^{*2}\right\}\alpha_{jn}^{*2}$$

$$+\left\{[1-R^*S^*(1-i\nu)][2if_{jn}\sqrt{\beta}U^*]\omega_n^{*3}\right\}\alpha_{jn}^*$$

$$+\left\{[iC_v^*-(1-(1-f_{jn})\beta)\omega_n^*][1-R^*S^*(1-i\nu)\omega_n^{*2}]\omega_n^*\right\}$$

$$=0 \tag{5.1}$$

where n = 1,2, ..., ∞ and j = 1,2,3, or 4 only. The subscripts j and n must be added to the compressibility factor since it is directly dependent on both α_{jn}^* and ω_n^*. The appropriate expression for the compressibility factor is then

$$f_{jn}=\left[1-\kappa_{jn}\frac{J_2(\kappa_{jn})}{J_1(\kappa_{jn})}\right]^{-1} \tag{5.2}$$

where

$$\kappa_{jn}^2=A^{*2}\left\{\alpha_{jn}^{*2}-\left[\frac{\sqrt{\beta}}{c^*}(i\omega_n^*)+\frac{U^*}{c^*}\alpha_{jn}^*\right]^2\right\} \tag{5.3}$$

The same numbering scheme on j and n is understood in these two equations.

Equation (5.2) can be expanded in a power series near the origin. The details of this expansion are summarized in Appendix B. The resultant series is given by

$$f_{jn} = 1 + \frac{2}{2!1!}\left(\frac{\kappa_{jn}}{2}\right)^2 + \frac{14}{3!2!}\left(\frac{\kappa_{jn}}{2}\right)^4$$

$$+ \frac{198}{4!3!}\left(\frac{\kappa_{jn}}{2}\right)^6 + \frac{4672}{5!4!}\left(\frac{\kappa_{jn}}{2}\right)^8$$

$$+ \frac{165380}{6!5!}\left(\frac{\kappa_{jn}}{2}\right)^{10} + \frac{8195910}{7!6!}\left(\frac{\kappa_{jn}}{2}\right)^{12}$$

$$+ \frac{541565290}{8!7!}\left(\frac{\kappa_{jn}}{2}\right)^{14} + \cdots \tag{5.4}$$

where κ_{jn} is defined in Eq. (5.3). It is now obvious that the $\lim_{\kappa_{jn}\to 0} f_{jn} = 1$. This occurs when $A^* \to 0$ (beam of infinite length). Specification of an incompressible fluid ($c^* \to \infty$) alone does not imply that $f_{jn} = 1$. Equation (5.4) is valid for small κ_{jn} only.

The frequency equation can best be represented by

$$F(\omega_n^*) = 0 \ , \ \text{for } n = 1,2,\ldots,\infty \tag{5.5}$$

It can be evaluated as a determinant after α_{1n}^*, α_{2n}^*, α_{3n}^*, and α_{4n}^*, for $n = 1,2,\ldots,\infty$, have been made available.

In viewing this equation system it is apparent that it is transcendental and nonlinear. For each dimensionless circular frequency ω_n^* there are four distinct values of the unknown α_{jn}^*. This is a system of two simultaneous transcendental equations for the general case of a compressible fluid. If the fluid is incompressible the compressibility factor is unity and Eq. (5.1) reduces to a complex quartic polynomial equation with complex coefficients. By considering the incompressible case the logical way to set up this equation system can be discerned. If an initial guess for ω_n^* is assumed then, Eq. (5.1) can be solved for the four α_{jn}^* which correspond to ω_n^*. Equation (5.5) then can be evaluated (since the α_{jn}^* are now available) to check how good the initial guess for ω_n^* really is. A suitable correction then can be made and the process repeated until some suitable prescribed accuracy level has been achieved.

5.3 Selection of a Numerical Method

Many methods have been developed for the solution of nonlinear equations and sets of nonlinear equations. The classic work on the subject is the book by Traub [103]. A more recent reference has been compiled by Rabinowitz [104]. Ortega and Rheinboldt [105] explore the fundamental mathematical aspects of this subject in detail in their treatise. Moré and Cosnard [106] have compared the various algorithms that are available for computing the numerical solution of sets of simultaneous nonlinear equations. When selecting an algorithm consideration must be given to the class of problems to which the method can be applied, the number of function evaluations which must be carried out, whether or not the derivative or

Jacobian (in the case of equation systems) must be computed, the convergence rate of the method, the availability of software, and of course, the actual core and central processing unit (CPU) time required by the computer. Attention also must be given to the accuracy requirements of initial estimates to the problem solution that must be supplied by the user to start the numerical procedures (or algorithms).

Numerical methods for solving nonlinear equations can be divided into two broad categories depending on whether the equation being solved is algebraic (expressible by equating polynomials to zero and having finitely many zeros) or transcendental (not representable by polynomials and having an infinite number of zeros). Methods based on iterated synthetic division in which either linear [107, p. 198] or quadratic [108] factors are removed in a consecutive manner from the original polynomial equation as well as methods utilizing both fixed-point and multipoint iteration [109] have been applied successfully to the solution of algebraic equations. These methods probably could be expected to generate valid results for the numerical solution of the incompressible form of Eq. (5.1). However, in the more general compressible case synthetic division cannot be applied to this equation because it is transcendental. In this context iteration methodology does not offer any more of a promising alternative because the selection of suitable iteration functions for such complicated problems does not appear possible.

Numerical methods applicable to the larger class of problems of transcendental equations include the bisection, Newton-Raphson, and secant methods [110] as well as the down-hill or Ward's method [111]. Each of these methods offers certain advantages or disadvantages when applied to the problem being studied in this investigation. The bisection method or interval-halving technique almost always converges although it is the slowest of the methods listed. It works for any continuous function, requires only function evaluations, and is relatively insensitive to roundoff errors. The method requires accurate initialization and no simple extension can be made to handle sets of equations. The greatest drawback of the bisection method is its low convergence rate which can cause it to consume vast amounts of computer time; moreover, the method is not directly applicable to complex equations.

The Newton-Raphson method converges quadratically, requires evaluation of the derivative of the function, and can be extended to sets of equations [106, 112] as well as complex equations. This method is known to be quite sensitive to initial root estimates. Its biggest drawback is its need for analytical expressions for the derivative (or the determinant of the Jacobian matrix in the case of equation sets) although software does exist which employs finite-difference approximations to calculate the required derivatives [113].

Ward's method seeks to minimize the function $w(x,y) = |u(x,y)| + |v(x,y)|$ where $f(z) = u(x,y) + iv(x,y)$ and $z = x + iy$. It requires that the given equation be written in component form (i.e., u and v) and the use of an optimization routine. The first of these requirements is particularly unappealing for the problem under study. Ward's method is well suited for finding complex roots and does not require any derivative evaluations.

Secant methods utilize interpolating polynomials $p_n(z)$ which are passed through a required number of root estimates to establish an iterative process [the next root estimate is actually extrapolated from the preceding root estimates by application of $p_n(z)$]. The classical secant method (which can be derived from the Newton-Raphson scheme by simply backward differencing the derivative) is based on a first degree interpolating polynomial $p_1(z)$ while a variant known as Muller's method [114] can be developed using $p_2(z)$. Muller's method has been applied with remarkable success to the solution of a variety of eigenvalue problems [115] and polynomial equations of large degree [116]. This iterative method is extremely powerful in the sense that it determines complex roots (even if their multiplicity is greater than one) of arbitrary functions, exhibits nearly quadratic convergence in the vicinity of a root, and requires no derivative evaluations; moreover, Muller's method is probably the most insensitive of the methods that have been discussed to initial root estimates and software is readily available [110]. Muller's method was selected for approximating the solution to the transcendental equation pair developed in the preceding chapter.

5.4 Muller's Method

Muller's method seeks roots to the single complex equation $g(z) = 0$. If three initial estimates to the root are designated by z_i, z_{i-1}, and z_{i-2} then the corresponding functional values are $g(z_i)$, $g(z_{i-1})$, and $g(z_{i-2})$. A second degree interpolating polynomial can be passed through these three points such that

$$g(z) \approx p_2(z) = a_0 + a_1 z + a_2 z^2 \tag{5.6}$$

where the coefficients of the polynomial must be determined from the expression

$$\begin{Bmatrix} a_0 \\ a_1 \\ a_2 \end{Bmatrix} = \begin{bmatrix} 1 & z_i & z_i^2 \\ 1 & z_{i-1} & z_{i-1}^2 \\ 1 & z_{i-2} & z_{i-2}^2 \end{bmatrix}^{-1} \begin{Bmatrix} g(z_i) \\ g(z_{i-1}) \\ g(z_{i-2}) \end{Bmatrix} \tag{5.7}$$

Once the quantities a_0, a_1, and a_2 have been computed Eq. (5.6) can be set equal to zero and the quadratic formula utilized to calculate z_{i+1} which is the next approximation to the desired root. The relevant expression is,

$$z_{i+1} = \frac{2\,a_0}{-\,a_1 \pm \sqrt{a_1^2 - 4\,a_0 a_2}} \tag{5.8}$$

where the sign in front of the radical is selected to maximize the denominator. The process is then repeated using z_{i+1}, z_i, and z_{i-1} to compute z_{i+2}. In essence, this procedure [which represents a sequence of fitting successive second degree polynomials to the equation $g(z) = 0$] is repeated iteratively until convergence occurs.

Muller's method determines one root at a time to the given equation. For multiple roots, a procedure known as deflation is used to determine the next root. For example, if one root $\bar{z}_1$ has been found the appropriate deflated function for computing the second root is

$$g_1(z) = \frac{g(z)}{z - \bar{z}_1} \tag{5.9}$$

If N roots have been computed the deflated function is representable by

$$g_N(z) = \frac{g(z)}{\prod_{j=1}^{N} (z - \bar{z}_j)} \tag{5.10}$$

where $\bar{z}_j$ is the jth root and $g_N(z)$ is the function to deploy to find the N+1 root.

Figure 5.1 displays a flow chart of Muller's method which can be used to write a FORTRAN program for machine calculation [117]. Conte and deBoor [110] have already published this software. Their subroutine was used with minor modification to perform the calculations quoted in this dissertation.

5.5 Program Description

5.5.1 Overall Implementation

An overall program flow chart is shown in Figure 5.2. Two separate compilations of the Muller algorithm are required by this nested root solver because a subroutine cannot call itself. The first compilation is associated with the frequency equation [see Eqs. (4.59) and (5.5) or Appendix A] while the second one is used in conjunction with Eqs. (5.1) through (5.3). Once the program is initialized with the Bernoulli-Euler beam equation solution for the

Comments: A subroutine based on this flow chart will find the first n real roots of a function $f(x)$; ϵ = the error criterion; $h = x_i - x_{i-1}$; rt (k) = approximation to kth root; if rt (k) = 0 initially, take $x_1 = -1$, $x_2 = 1$, $x_3 = 0$ as the first three approximations; if rt (k) is supplied initially, take $x_1 = 0.9$ rt (k), $x_2 = 1.1$ rt (k), x_3 = rt (k) as first three approximations; RT is the latest approximation to the kth root. The elliptical box in (β) is an *assigned go to* statement. This flow chart is sufficiently detailed to allow a program to be written directly.

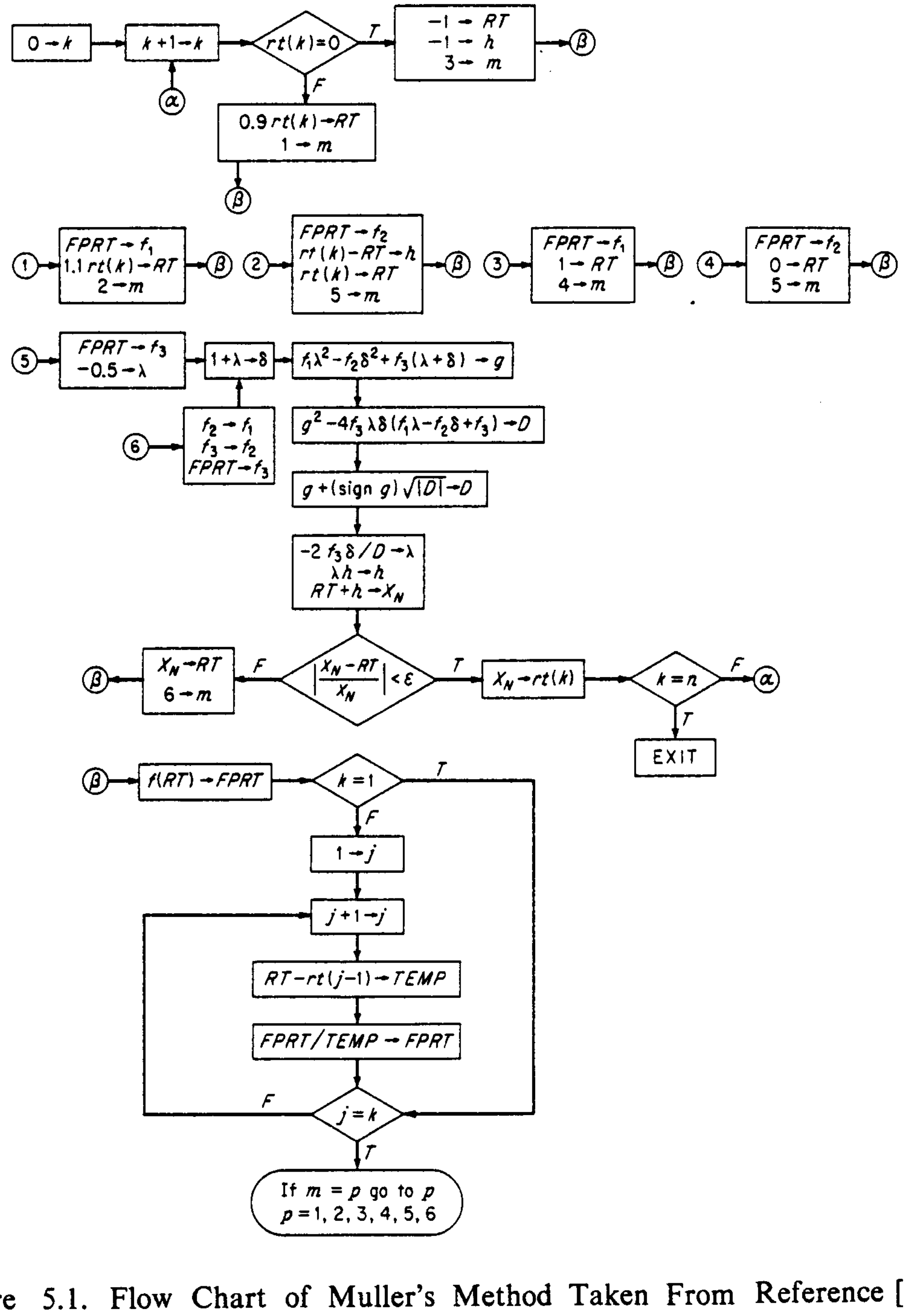

Figure 5.1. Flow Chart of Muller's Method Taken From Reference [117].

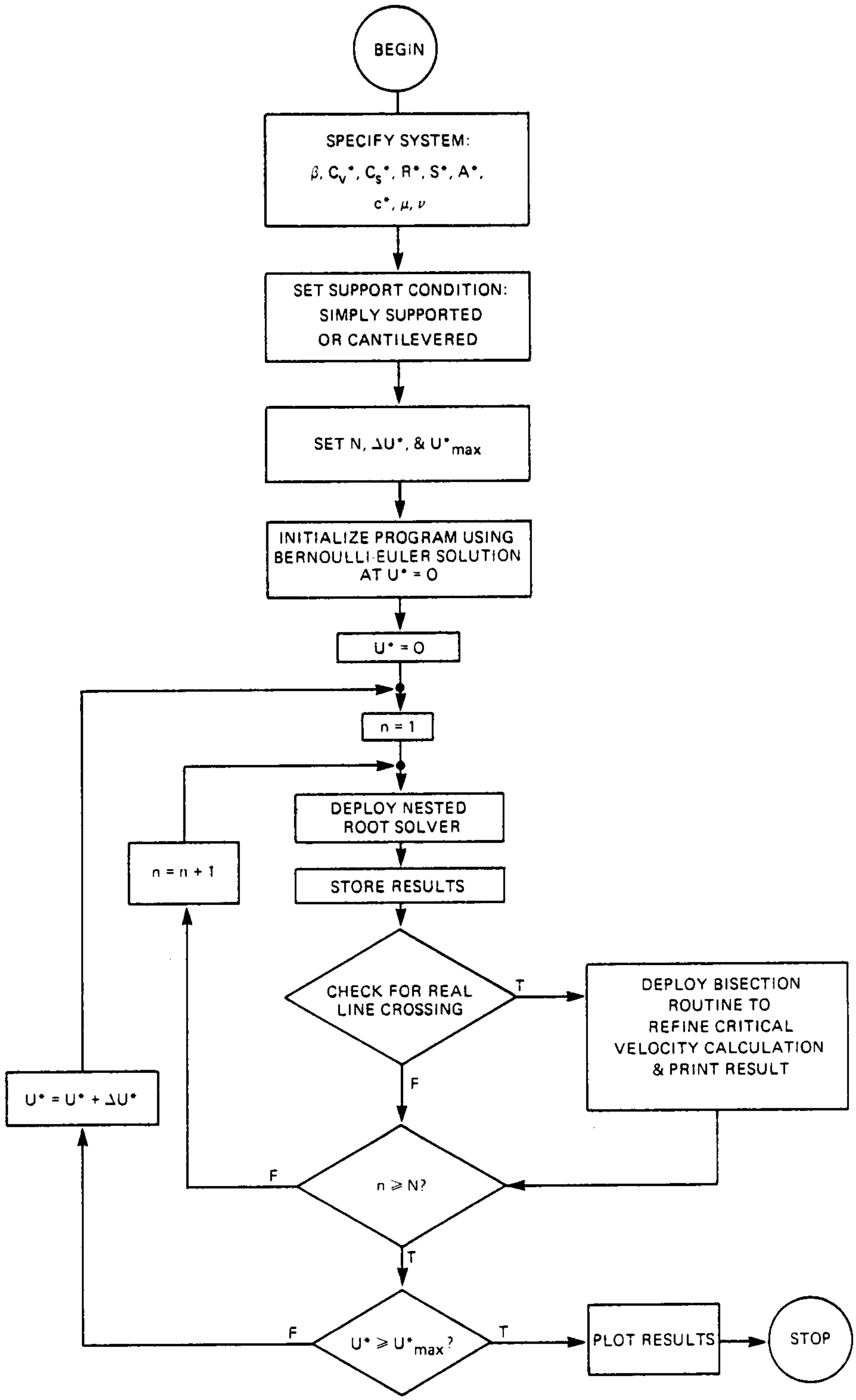

Figure 5.2. Overall Program Flow Chart.

stagnant flow condition ($U^* = 0$) the equation solver continuously calculates roots (ω_n^*) for incremental values in U^* of magnitude ΔU^* in up to nine modes. A more general procedure does not appear feasible because the map of ω_n^* is multi-valued; moreover, cusps and loops are usually exhibited. Frequency points along the real line which correspond to critical velocity points are further resolved using a bisection routine that iterates on U^* until the condition $\mathrm{Im}(\omega_n^*) = 0$ is satisfied. The program halts once some prescribed maximum value of U^* has been achieved. Calculated values of ω_n^* are then plotted in the complex plane as a function of U^*.

5.5.2 The Root Solver

Figure 5.3 is a flow chart of the nested root solver which employs two separate compilations of the Muller algorithm. The outer portion of the nest is concerned with the computation of ω_n^* while the inner nest determines p, q, r, and s (or α_{jn}^*) for each approximation to ω_n^* as dictated by the outer nest. Implicit in the inner nest is the calculation of κ_{jn} and f_{jn}. Deflation was found to work well for the determination of the four α_{jn}^* but not in the calculation of the ω_n^* whose defining equation $F(\omega_n^*) = 0$ was programmed as a complex matrix whose determinant was calculated using expansion by minors. A loop was placed around the entire computational procedure in terms of the mode number n so that deflation of the frequency equation would not be required as shown in Figure 5.2.

The Bessel functions of a complex argument were calculated using the routines developed by Sookne [118–121]. For values of κ_{jn} that were small in

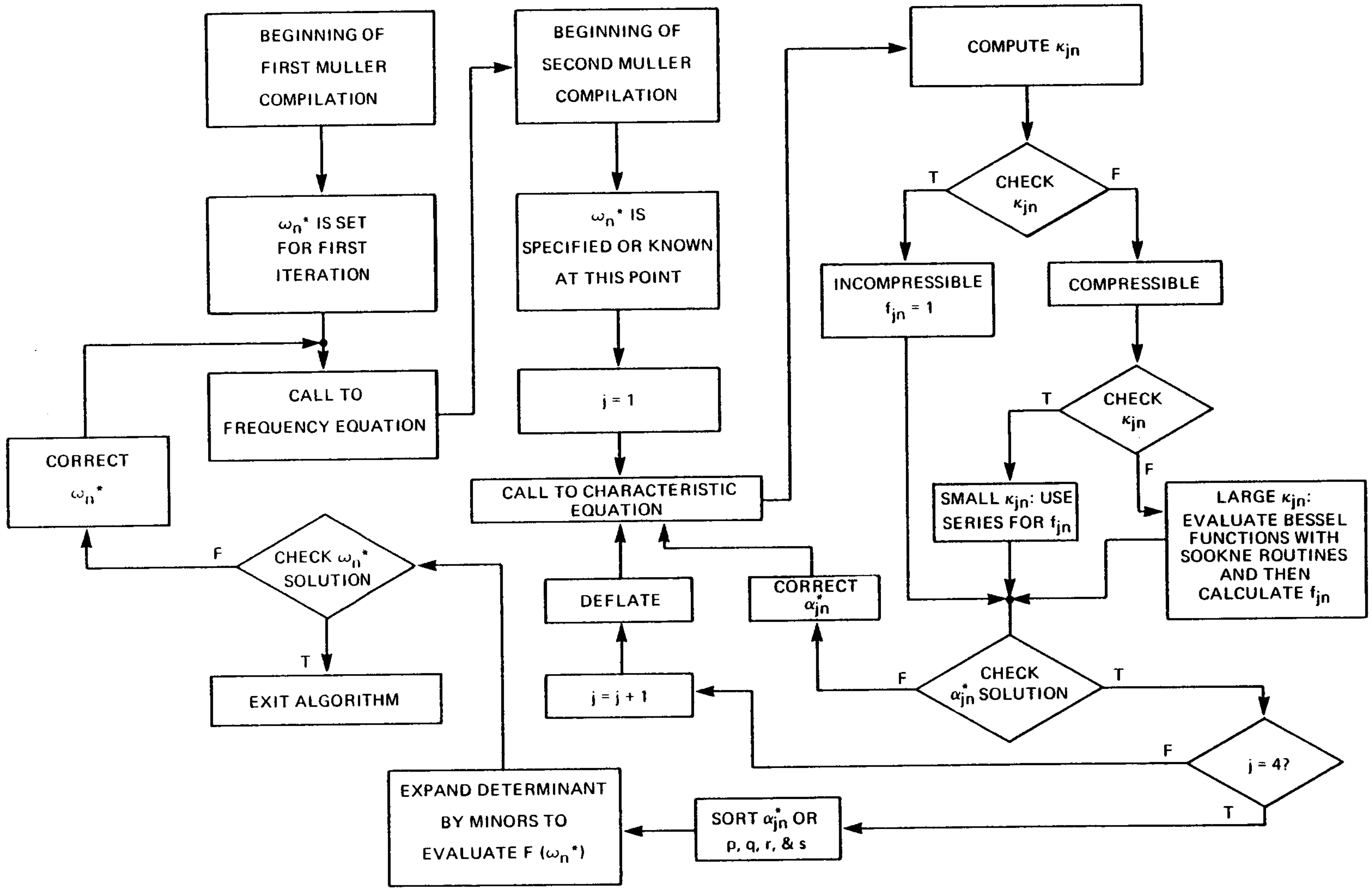

Figure 5.3. Flow Chart of Nested Root Solver.

magnitude Eq. (5.4) was employed to calculate f_{jn} directly rather than evaluating the Bessel functions. The logic associated with the different root cases embodied in Eq. (5.5) -- two equal roots, three equal roots, etc. -- was decreased by a factor of two by employing a bubble sort routine [122] which put the roots in ascending order according to their real part only. Frequency points along the real axis were further resolved with a bisection algorithm. It was a simple matter to check the sign of $\mathrm{Im}(\omega_n^*)$ to search for axis crossings. Iteration on U^* using bisection then achieved the actual neutral stability point.

5.5.3 Problem Initialization

The code is initialized using the solution to the Bernoulli-Euler beam equation assuming an incompressible, motionless fluid ($U^* = 0$, $c^* \rightarrow \infty$, and $f = 1$). No damping is considered. From Eq. (4.13) the defining equation for these initial root estimates is

$$\eta_{\xi\xi\xi\xi} + \eta_{\tau\tau} = 0 \tag{5.11}$$

In the simply supported case the real eigenvalues are given by

$$\omega_n^* = n^2\pi^2 \quad , \quad \text{for} \quad n = 1,2,\ldots,\infty \tag{5.12}$$

while in the cantilevered case the appropriate frequency equation is

$$\cos\sqrt{\omega_n^*}\cosh\sqrt{\omega_n^*} + 1 = 0 \quad , \quad \text{for } n = 1,2,\ldots,\infty \tag{5.13}$$

where the roots are given in Table 5.1 [123].

Table 5.1.
Initial Root Estimates
for the Cantilevered Beam [123].

$\sqrt{\omega_n^*}$	n
1.87510410	1
4.69409113	2
7.85475743	3
10.99554074	4
14.13716839	5
$(2n - 1)\,\pi/2$	6,7, ... , ∞

It is noted in Figure 5.2 that the solution at $U^* = 0$ is computed by the program so that corrections to the initial guesses can be made for various types of damping, shear, and rotary inertia.

5.5.4 General Comments

Results were not obtainable in the cantilevered case with the computer program described in this chapter for values of c^* less than one or values of A^* greater than 0.5. The curves of ω_n^* became closely spaced to each other in these situations. The numerical scheme could not resolve distinct values of ω_n^* for each of the prescribed number of modes n. The final computed solution consisted of n curves of ω_n^* which coalesced into a single one that was obviously incorrect. A related problem occurred near the origin when $|\omega_n^*| < 1$. Once a small value (although not zero) of ω_n^* was returned by the numerical scheme in a specified mode it would continue to return nearly this value as U^* was increased. Reduction of ΔU^* failed to alleviate either of these problems.

In the simply supported case the code could be used to predict the critical velocities associated with Euler's method of equilibrium. This, of course, amounts to Eq. (4.13) with the terms containing time derivatives eliminated. Results obtained with the code made possible considerable simplification of this problem. These findings are summarized in the next chapter. The code was unable to handle the coupled-mode flutter predicted by Paidoussis and Issid [24]. However, coupled-mode flutter may well require a shell analysis rather than a beam theory for its prediction since occurrence of this phenomenon is related to motion in the second circumferential shell mode [66].

In the case of cantilevered, incompressible fluid-conveying Timoshenko beams excellent agreement was obtained with the results quoted by Paidoussis and Laithier [59]. Their results included gravitational effects; however, the trends in the results were virtually identical.

The complete code package was implemented on an IBM 360/195 computer. Approximately twenty minutes of CPU time was required to run nine modes in the incompressible case with a maximum U^* of 20 and ΔU^* = 0.05. Compressible cases took roughly twice as much CPU time.

In Figure 5.3 the logic and coding associated with each of the root cases (two equal roots, three equal roots, etc.) was not really required in the cantilevered case. In theory all of these conditions should be in the code; in practice it turns out that the only case ever used by the code is four unequal roots.

Initial attempts to solve this problem were made using the Newton-Raphson method in a rested root solver scheme nearly identical to the one shown in Figure 5.3. The required analytic forms were derived directly from the matrices in Appendix A and by using implicit differentiation on Eq. (5.1). Little success was obtained with this method because the root solver always diverged. Initial root estimates that were compatible with the root solver could not be obtained. It was concluded that the Muller algorithm was superior to the Newton-Raphson method in nested root solver applications because the latter technique was too sensitive to initial root estimates.

In order to obtain smooth results from the code the inner nest had to have its error tolerances set at near machine accuracy (in double precision) regardless of those set on the outer nest. In the higher modes (when $|\omega_n^*|$ neared 1000) both nests had to have tolerances near machine accuracy if oscillations were to be avoided in the final plots.

6. RESULTS AND DISCUSSION

6.1 Introduction

This study is primarily concerned with determining the effects of compressibility on the stability of cantilevered and simply supported fluid-conveying tubes. The first section of this chapter defines a suitable parameter range over which fluid compressibility should influence the predicted results. The cantilevered tube is then studied by presenting complex frequency maps and the corresponding critical velocities for both Bernoulli-Euler and Timoshenko fluid-conveying beams. The effects of fluid compressibility on the Euler critical flow velocities for a simply supported tube are then evaluated. The results that are presented have been selected so that the capabilities of the computer code described in the preceding chapter are demonstrated.

6.2 Parameter Range of Interest

Tables 6.1 and 6.2 summarize the properties of solids and fluids, respectively, which are needed to define a fluid-tube system. The materials or substances were selected so that a continuous extended range of property data would occur. Table 6.3 lists values of the mass parameter β for the various system combinations which can be envisioned using the property data in Tables 6.1 and 6.2. The tube is assumed to have the dimensions [d_i = 0.02664 m (1.049 in) and d_o = 0.03340 m (1.315 in)] of a standard weight nominal 0.0254 m (1 in) diameter pipe [127]. It is apparent from Table 6.3 that values of β anywhere from nearly zero to almost one are achievable in practice.

Table 6.1.
Properties of Solids.

Material	$\rho_s(\mathrm{kg/m^3})$	$E\,(\mathrm{N/m^2})^*$	Reference
Platinum (pure)	21450	1.47×10^{11}	[124]
Steel (1040)	7850	2.07×10^{11}	[125]
Silicon Rubber (Silastic, type E)	1117	1.89×10^{6}	[59]
Balsa Wood	140	3.45×10^{9}	[126]

*Divide $\mathrm{N/m^2}$ by 6894.757 to obtain psi.

Table 6.2.
Properties of Fluids* [124].

Substance	$\rho_0(\mathrm{kg/m^3})$	$c(\mathrm{m/s})$
Mercury (298 K)	13633	1450
Water (298 K)	1000	1498
Air (100 K)	3.599	198
Air (300 K)	1.177	347
Air (2800 K)	0.125	983
Diatomic Hydrogen (298 K)	0.0823	1315

*All at atmospheric pressure.

Table 6.3.
Values of the Mass Parameter β for Various
Fluid-Tube Combinations*.

Fluid**	Tube: Platinum (pure)	Steel (1040)	Silicon Rubber (Silastic, type E)	Balsa Wood
Mercury (298 K)	0.526	0.752	0.955	0.994
Water (298 K)	0.0754	0.182	0.610	0.926
Air (100 K)	2.93×10^{-4}	8.01×10^{-4}	5.60×10^{-3}	4.30×10^{-2}
Air (300 K)	9.59×10^{-5}	2.62×10^{-4}	1.84×10^{-3}	1.45×10^{-2}
Air (2800 K)	1.02×10^{-5}	2.78×10^{-5}	1.96×10^{-4}	1.56×10^{-3}
Diatomic Hydrogen (298 K)	6.71×10^{-6}	1.83×10^{-5}	1.29×10^{-4}	1.03×10^{-3}

*Assumed nominal 0.0254 m (1 in) diameter standard weight pipe [127].

**All at atmospheric pressure.

Table 6.4 contains the corresponding values of the ratio c^*/L in m^{-1} for these fluid-tube systems. For a finite length tube (say 1 m) it can be stated arbitrarily that liquids correspond to c^* values of roughly 10 or 100 and above while gases dominate the region below this range. This statement is strongly dependent on the length of tube chosen as a representative value. Obviously, stronger tubes made from metals will see longer spans (say 1 to 10 m) in practice while more flexible ones made of elastomers may see runs of only a fraction of a meter in length.

It is instructive to compute the frequency of radial standing waves in the tube so that a stronger appreciation of when fluid compressibility affects the frequency of natural vibration can be gained. This condition is

$$\pi c = \omega_s d_i \tag{6.1}$$

The equivalent dimensionless expression is

$$\omega_s^* = \pi c^*/2A^*\sqrt{\beta} \tag{6.2}$$

where ω_s^* is the dimensionless circular frequency ($\equiv \omega_s L^2\sqrt{(\rho_s A_s + \rho_0 A)/EI}$) of the fundamental radial standing wave. The nodes and antinodes of such standing waves are spaced one-half of a wavelength apart [128]. This frequency is shown in Figure 6.1 over the parameter range of interest for a tube having a finite aspect ratio A^* of 0.1. Based on previous work [129] it is expected that the complex frequency ω_n^* will have a magnitude $|\omega_n^*|$ of

Table 6.4.
Values of the Ratio c^*/L in m^{-1} for Various
Fluid-Tube Combinations*.

	Tube			
Fluid**	Platinum (pure)	Steel (1040)	Silicon Rubber (Silastic, type E)	Balsa Wood
Mercury (298 K)	54.7	46.1	1.52×10^4	357
Water (298 K)	15.3	12.9	4.27×10^3	99.9
Air (100 K)	0.121	0.102	33.8	0.792
Air (300 K)	0.122	0.102	33.9	0.794
Air (2800 K)	0.112	0.0946	31.3	0.733
Diatomic Hydrogen (298 K)	0.122	0.103	34.0	0.795

*Assumed nominal 0.0254 m (1 in) diameter standard weight pipe [127].

**All at atmospheric pressure.

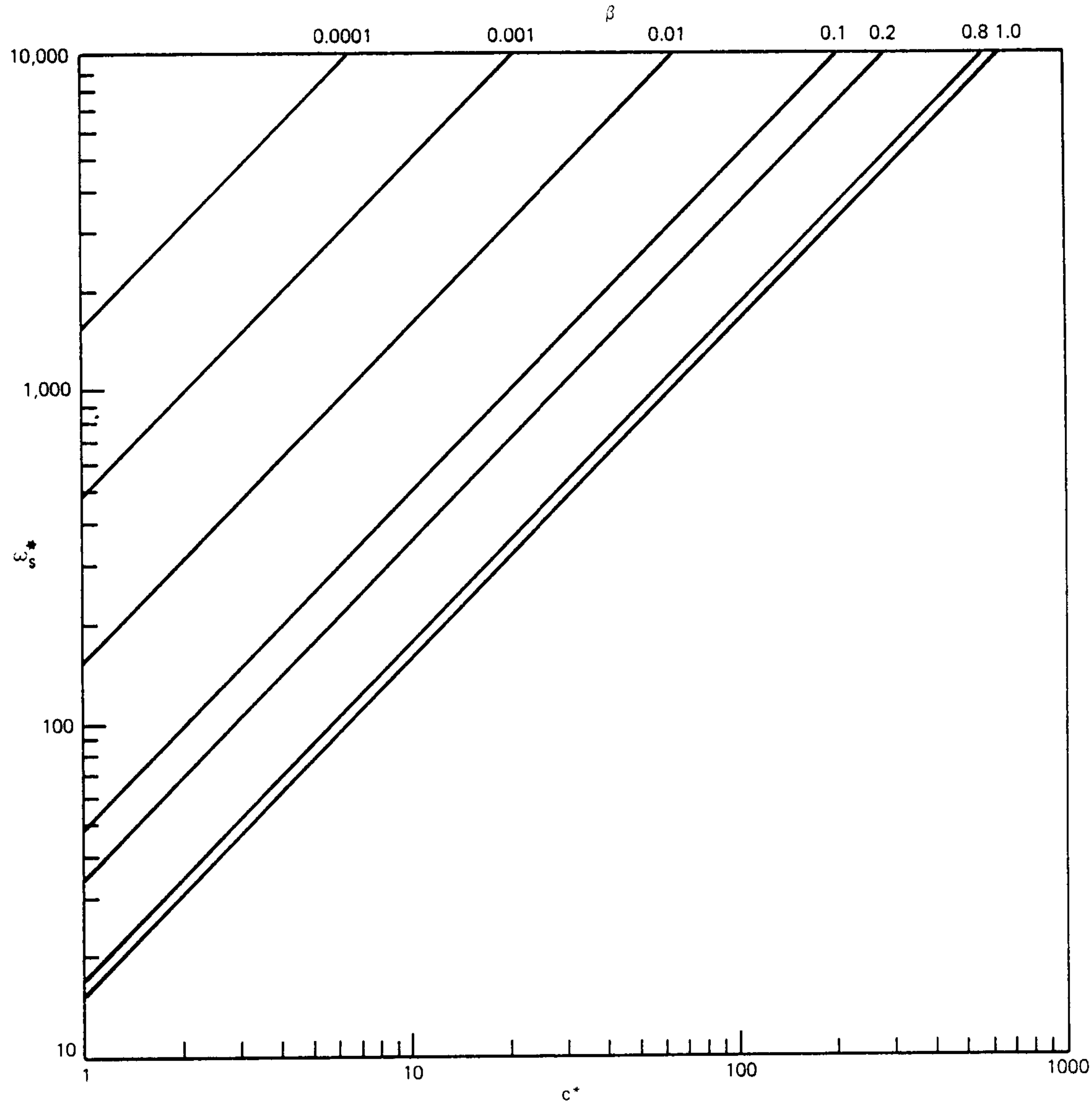

Figure 6.1. Dimensionless Radial Standing Wave Frequency as a Function of β and c^* for $A^* = 0.1$.

approximately 10 or 100. It is then apparent from Figure 6.1 that compressibility (as embodied in the relation between A^*, β, and c^*) only affects the results when c^* is low (say less than 100). Only then can resonance occur such that that the motion of both the fluid and the tube become coupled and dependent on the compressibility of the fluid.

Paidoussis and Laithier [59] have considered the influence of shear and rotary inertia in the case of incompressible, fluid-conveying Timoshenko beams. Typical values of S^* (which is the reciprocal of the Λ quoted by Paidoussis and Laither) range from 0.1 to 10^{-4} with 10^{-4} effectively being zero (the Timoshenko theory then yielding results nearly identical to Bernoulli-Euler beam theory since the shear deformation is minimal). In the range of S^* between 10^{-2} and 10^{-3} the second and third modes can switch with instability occurring in the third mode rather than in the second mode when gravitational body forces are included in the analysis. With S^* of 0.1 buckling rather than flutter occurred in the third mode when the tube was cantilevered (reported by Paidoussis and Laithier).

Practical values of R^* for real systems occur in the range from 10^{-3} to 10^{-4} [59]. The effect of R^* is small although it usually acts to destabilize the system by reducing the critical velocity. Its net effect is nonuniform and depends directly on all the other system parameters.

Typical values of the viscous damping coefficient C_v^* range from 0.23 to 1.42 [53]. This assumes the tube is surrounded by air and that the external flow relative to the tube is laminar. Representative values of the hysteretic damping coefficient μ have appeared in the range from 0.02 [59] to 0.1 [24].

This type of dissipative mechanism is representative of some metals and rubbers over practical frequency ranges; its use is restricted to harmonic or nearly harmonic motions [130]. It is assumed here that the hysteretic damping coefficient in shear ν possesses magnitudes equal to μ. A typical value for the strain rate damping coefficient C_s^* is 0.02 [24].

It is expected that inclusion of damping mechanisms (either internal, external, or hysteretic) will destabilize the system by lowering the predicted critical velocities. This will dramatically affect the shape of the loci of individual modes of ω_n^* in the complex plane. It is well known that dissipative forces destabilize nonconservative gyroscopic systems [50,57,131] and systems consisting of flexible surfaces coupled to inviscid flows [80].

6.3 Frequency Maps for a Cantilevered Bernoulli-Euler Tube

A series of calculations were performed for the case of an incompressible fluid which could be compared against results published by previous investigators. Figures 6.2 and 6.3 show the results for two of these calculations with $\beta = 0.2$ and 0.8. The dimensionless complex frequency is mapped as a function of the dimensionless flow velocity U^*. The markers along the curves signify consecutive increases in velocity of magnitude two; the end points along the real axis where each of the curves begin correspond to $U^* = 0$. The first nine modes have been plotted and are identifiable by counting these initial real axis end points beginning at the origin and preceding to the right. The first four modes for $\beta = 0.2$ are virtually identical with those published by Gregory and Paidoussis [53]. Tables 6.5 and 6.6 contain the

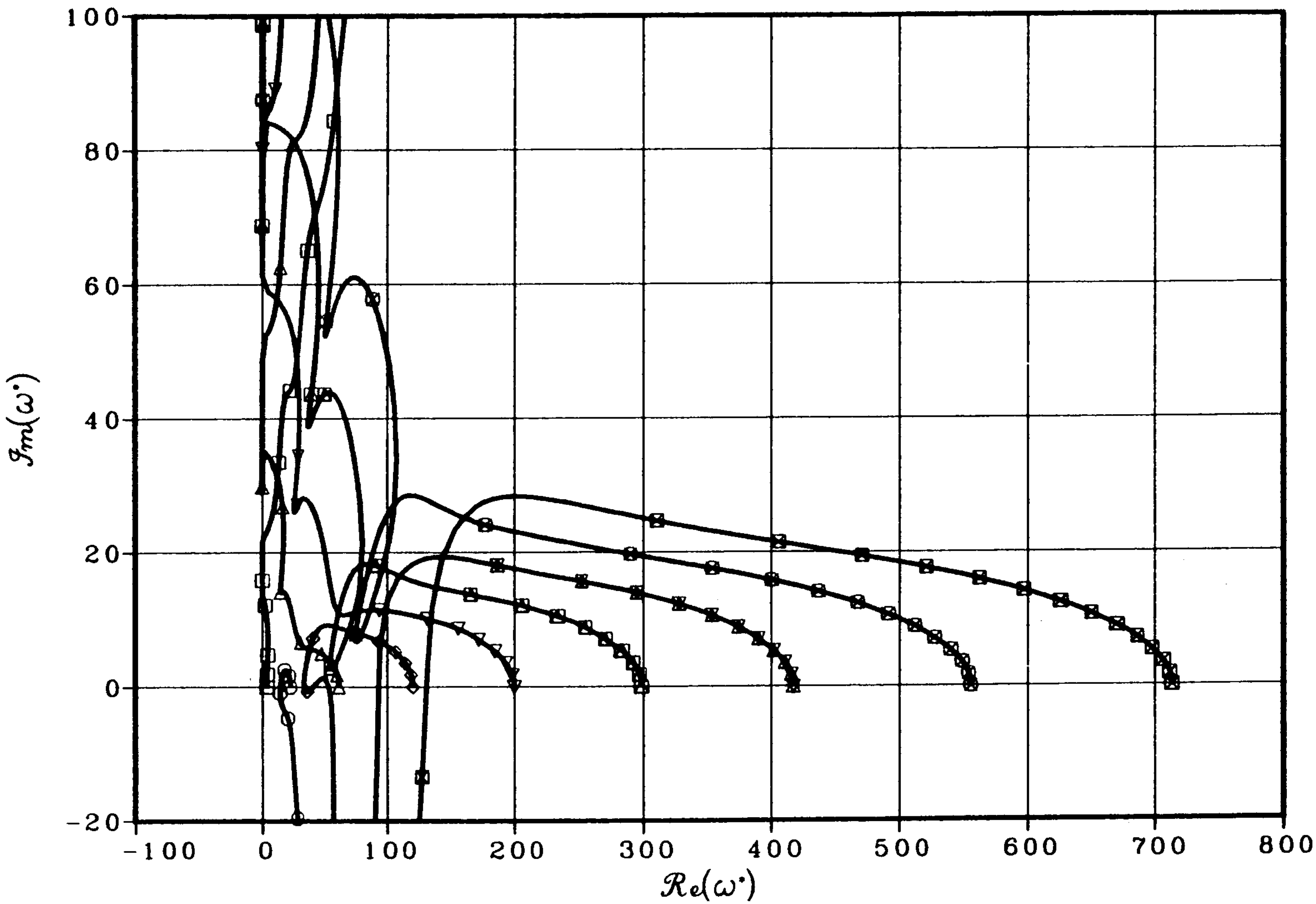

Figure 6.2. Complex Frequency Map for $A^* = 0$, $c^* \rightarrow \infty$, and $\beta = 0.2$.

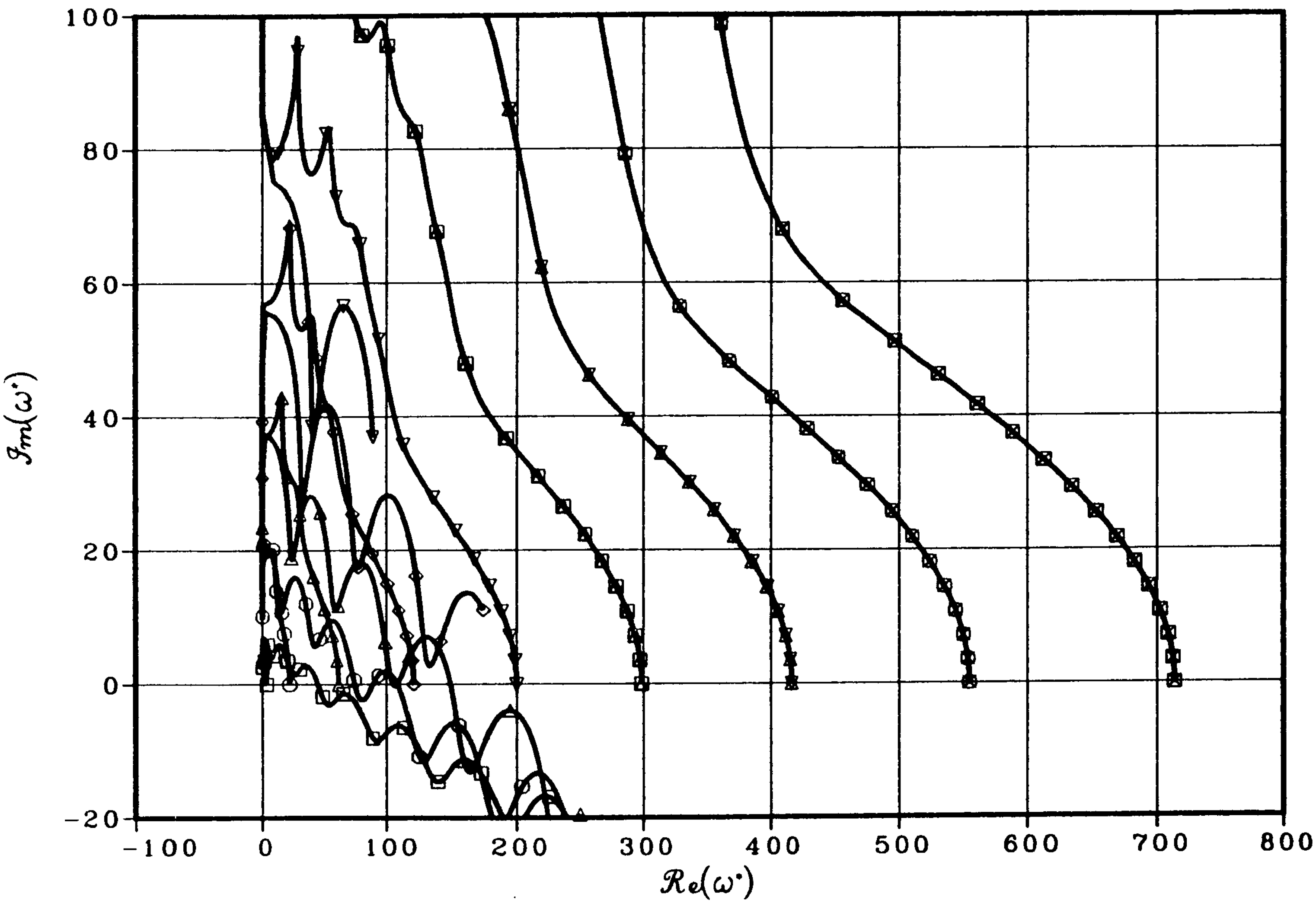

Figure 6.3. Complex Frequency Map for $A^* = 0$, $c^* \rightarrow \infty$, and $\beta = 0.8$.

Table 6.5.
Critical Velocity Summary
for $A^* = 0$, $c^* \rightarrow \infty$, and $\beta = 0.2$.

Mode Number	First Critical Velocity	Stability Reattained	Second Critical Velocity
2	5.59	--	--
4	13.32	14.42	.14.85
7	21.40	--	--
9	27.83	--	--

Table 6.6.
Critical Velocity Summary
for $A^* = 0$, $c^* \rightarrow \infty$, and $\beta = 0.8$.

Mode Number	First Critical Velocity	Stability Reattained	Second Critical Velocity
1	13.49	--	--
2	20.10	21.72	22.71
3	26.86	27.27	29.13

critical velocities where the curves in Figures 6.2 and 6.3 cross the positive real axis. It is evident that some of the modes exhibit a return to stability with an increase in flow velocity; a further increase in velocity then produces instability a second time. The dramatic effect of the mass parameter β can be seen by comparing Figures 6.2 and 6.3. These higher modes as well as the trends exhibited by these families of curves have been hitherto undocumented. All of the results presented in this section were computed using an incremental increase in the dimensionless flow velocity ΔU^* of 0.05 unless otherwise indicated.

In order for the fluid-tube system to be affected by compressibility both a nonzero value of the aspect ratio A^* and a finite sonic velocity c^* must be specified [see Eq. (4.41) or (5.3)]. A tube of infinite length does not respond to the compressibility of the fluid. Tables 6.7 and 6.8 contain critical velocities predicted by this theory for a tube having an aspect ratio of 0.1 over a range of sonic velocities for mass ratios β of 0.2 and 0.8. The aspect ratio has a tendency to increase the critical velocity while the fluid sonic velocity decreases it. The effects can cancel each other for some fluid-tube systems. Liquids correspond to values of c^* greater than roughly 100 while gases dominate the region below this value. The fluid velocity must become supersonic before instability occurs when the flowing medium is extremely compressible. Because the Mach numbers are near one these results for low values of c^* must be looked upon with some speculation since an inviscid linearized flow theory has been used. Predictions from it cannot be expected to accurately reflect behavior in the transonic flow regime since nonlinear terms have been neglected in the equations of fluid motion [132].

Table 6.7.
Critical Velocity Summary
for $A^* = 0.1$ and $\beta = 0.2$.

c^*	Second Mode Critical Velocity	Fourth Mode Critical Velocity
∞	5.70	14.96
1000*	5.70	14.96
100*	5.70	14.94
10	5.69	14.16
5**	5.66	5.35

*$\Delta U^* = 0.0625$.

**$\Delta U^* = 0.025$.

Tables 6.7 and 6.8 show that as c^* drops to ten and below that the system becomes unstable in its fourth mode rather than in its first or second mode. It is concluded that a reduction in sonic velocity can significantly affect the stability of cantilevered, fluid-conveying beams.

Figures 6.4 through 6.7 contain maps of the complex frequency as a function of the flow velocity for the two mass ratios being investigated. The first four modes are presented for a finite length tube ($A^*=0.1$) conveying an incompressible fluid and a compressible fluid ($c^*=10$). Comparison of Figure 6.4 with Figure 6.2 reveals that the region of the fourth mode over which stability was reattained with an increase in flow velocity has been eliminated

Table 6.8.
Critical Velocity Summary
for $A^* = 0.1$ and $\beta = 0.8$.

Sonic Velocity c^*	Mode Number of Critical Velocity			
	1	2	3	4
∞	15.63	--	--	--
1000	15.63	26.46	--	--
100	15.59	26.14	--	--
10	14.19	--	19.93	11.38

by inclusion of the finite value of the aspect ratio in the theory. Figure 6.5 illustrates the strong dependency of the mode shapes on c^* when the sonic velocity is deceased. Although it appears that the fourth mode passes through the origin a closer examination of the results reveals that the $\mathrm{Im}(\omega^*)$ never really reaches zero (although it does become quite small). Flutter occurs in the fourth mode at a value of U^* of 14.16. As c^* is decreased below 10 to a value of 5 for the lower value of β instability actually occurs in the fourth mode rather than in the second mode (see Table 6.7). Similar trends are exhibited in Figures 6.6 and 6.7 for the higher mass ratio β of 0.8.

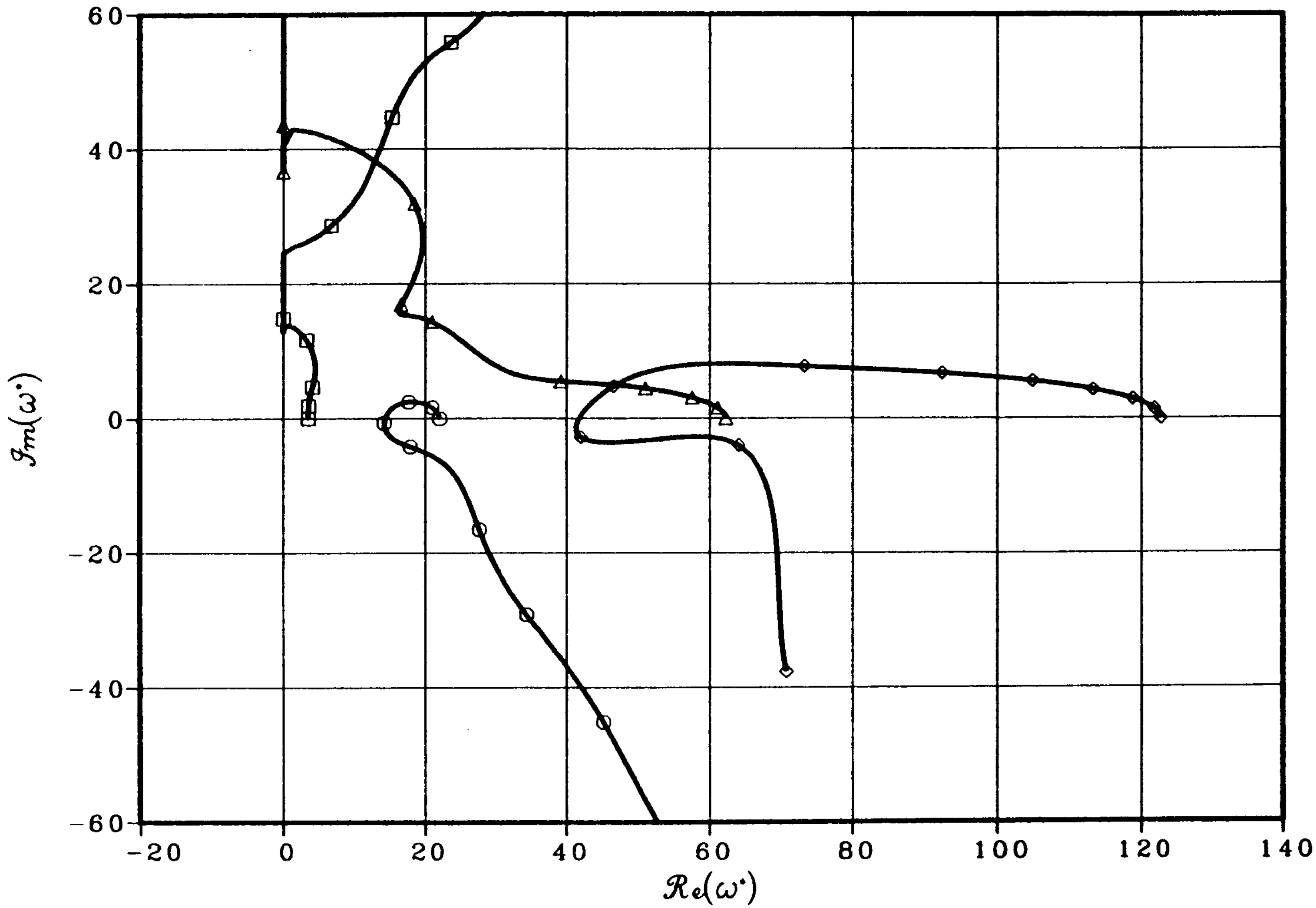

Figure 6.4. Complex Frequency Map for $A^* = 0.1$, $c^* \to \infty$, and $\beta = 0.2$.

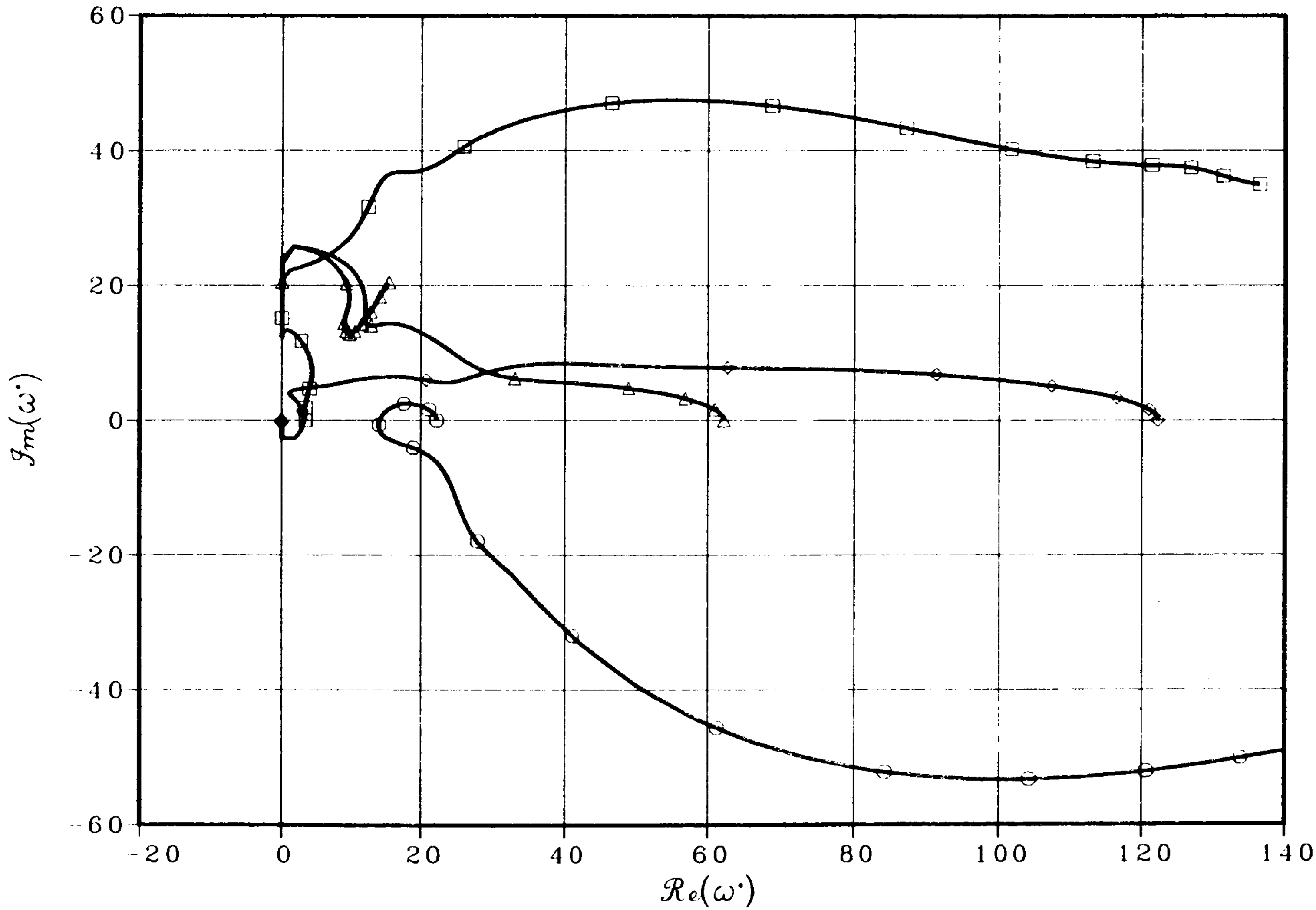

Figure 6.5. Complex Frequency Map for $A^* = 0.1$, $c^* = 10$, and $\beta = 0.2$.

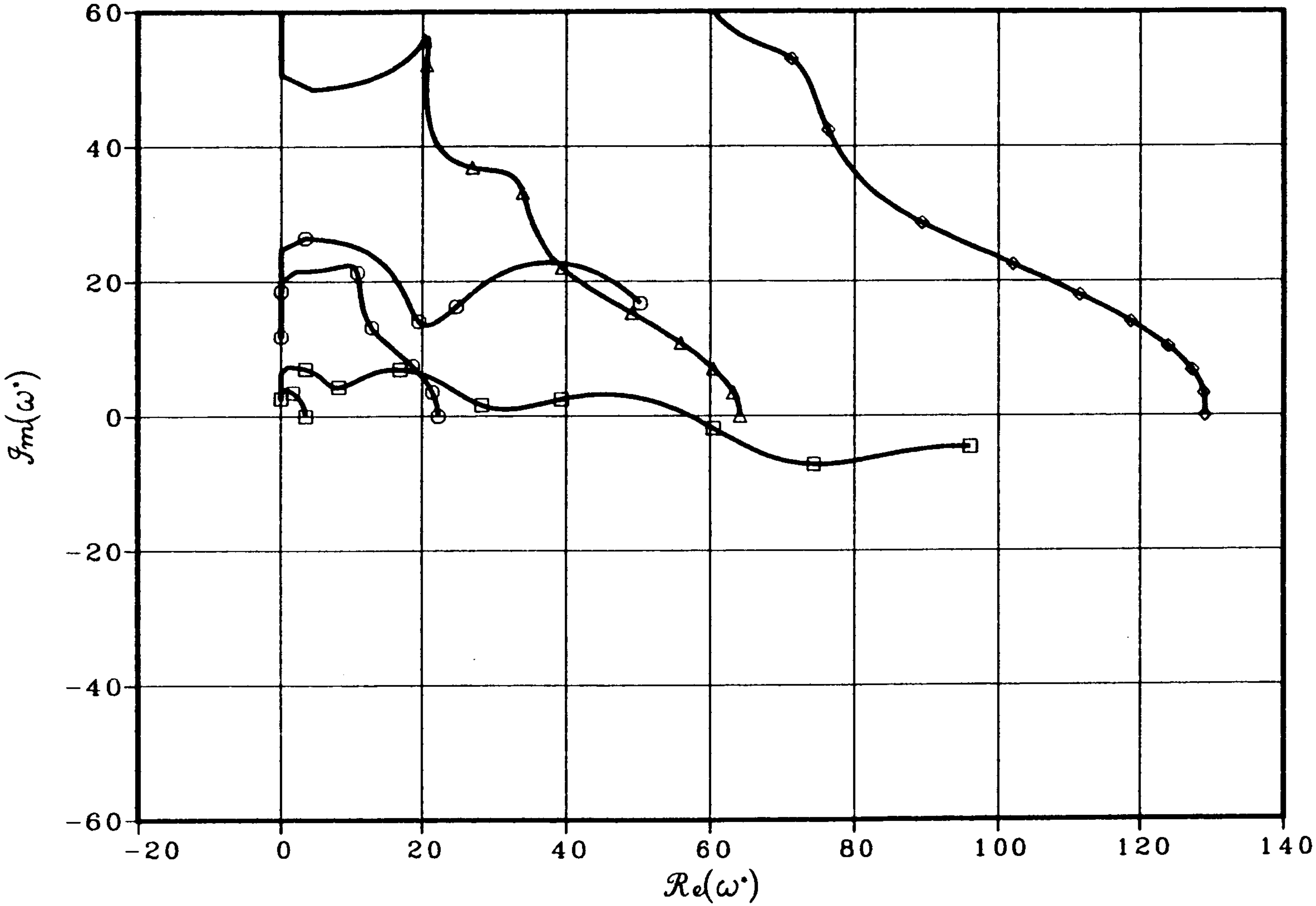

Figure 6.6. Complex Frequency Map for $A^* = 0.1$, $c^* \rightarrow \infty$, and $\beta = 0.8$.

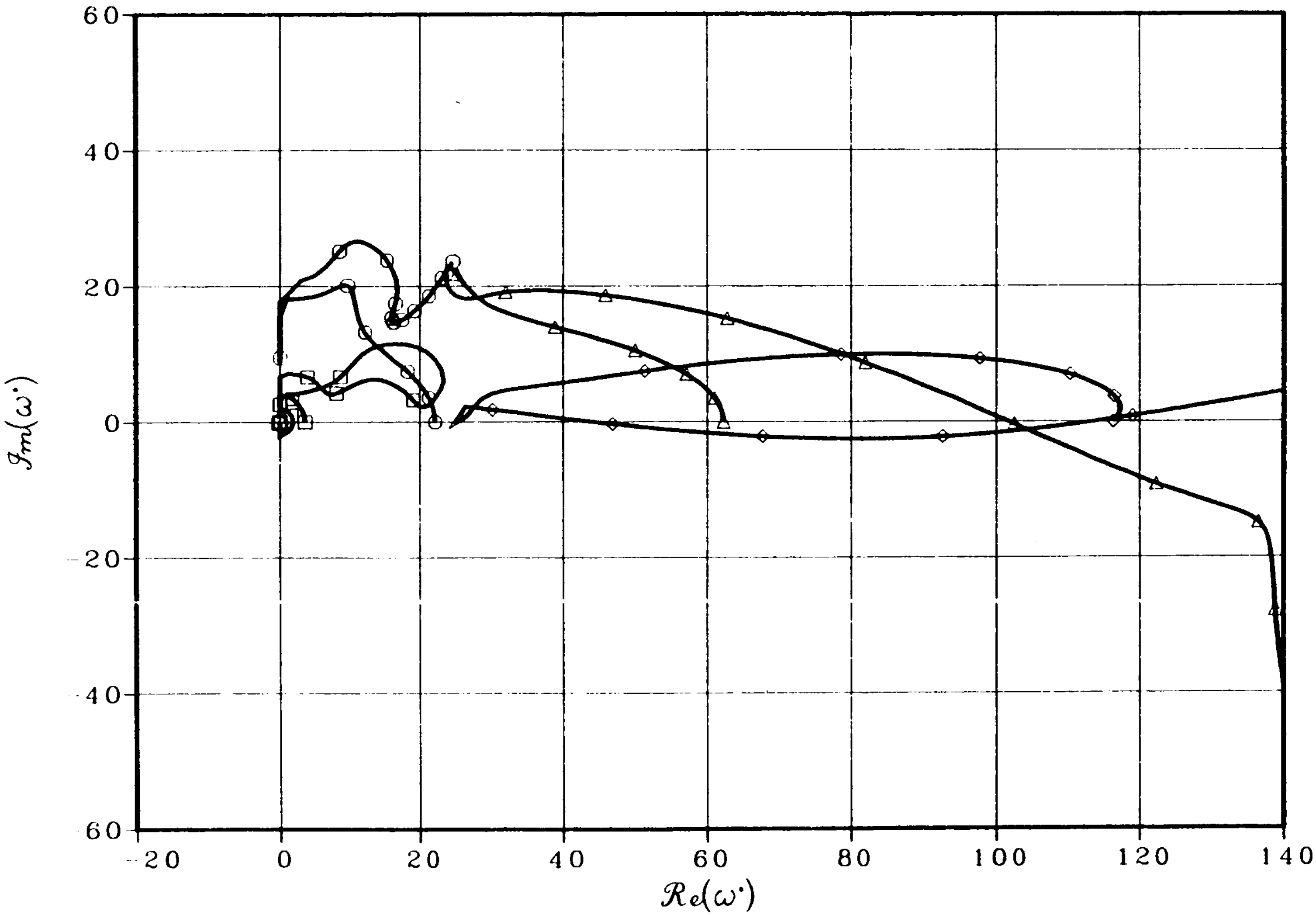

Figure 6.7. Complex Frequency Map for $A^* = 0.1$, $c^* = 10$, and $\beta = 0.8$.

6.4 Parameter Studies for a Cantilevered Timoshenko Tube

Comparison of the results presented in the preceding section with those published by Paidoussis and Laithier [59] indicate an inconsistency with regard to the dependency on aspect ratio. They measured a decrease in critical velocity as the tube length was shortened; however, their experiments utilized a silicon rubber tube having a finite shear modulus and nonzero hysteretic dissipation coefficient. The Bernoulli-Euler theory used to produce the results presented in the previous section cannot be expected to accurately predict the critical velocities of tubes made from such materials.

Using the Timoshenko theory a series of numerical experiments were performed with the physical parameters which defined the Silastic type E (pipe II) tube system used by Paidoussis and Laither [59] in their experiments. Table 6.9 lists these parameters. The fluid was water at room temperature and pressure whose properties are listed in Table 6.2. In order to get a measure of when compressibility might influence the results these same experiments were performed with air also at room temperature and pressure having the properties shown in Table 6.2. The value of the mass parameter β for this situation was 0.000213. The values of c^*, R^*, and S^* as a function of the aspect ratio A^* for these two systems are shown in Figures 6.8 through 6.10, respectively. A single curve appears in Figure 6.10 since the shear parameter S^* does not contain the fluid density ρ_0. Equation (3.21) was employed to calculate the required shear coefficient k from the tube diameters d_o and d_i as well as Poisson's ratio $\bar{\nu}$.

Table 6.9.
Physical Parameters Defining
System Used by Paidoussis
and Laither [59] in Their
Experiments.

Tube Material	:	Silastic Type E Silicon Rubber
Fluid	:	Water
d_o	:	0.0155 m
d_i	:	0.00635 m
Length Range	:	0.0635 m to 0.1631 m
β	:	0.153
μ and ν	:	0.04
Poisson's Ratio $\bar{\nu}$	:	0.5
Flexural Rigidity EI	:	0.00520 N-m^2

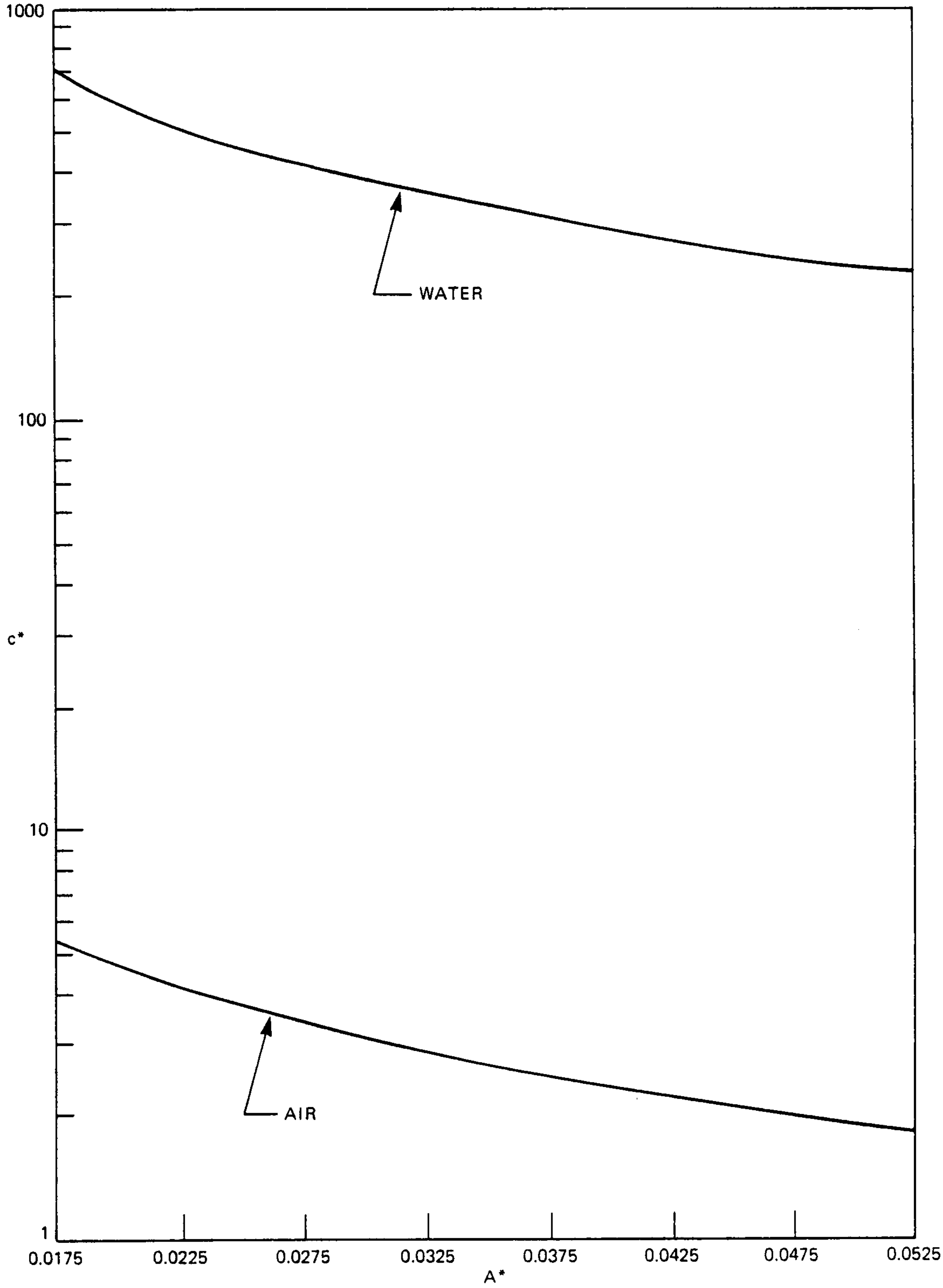

Figure 6.8. Dimensionless Sonic Velocity Versus Aspect Ratio.

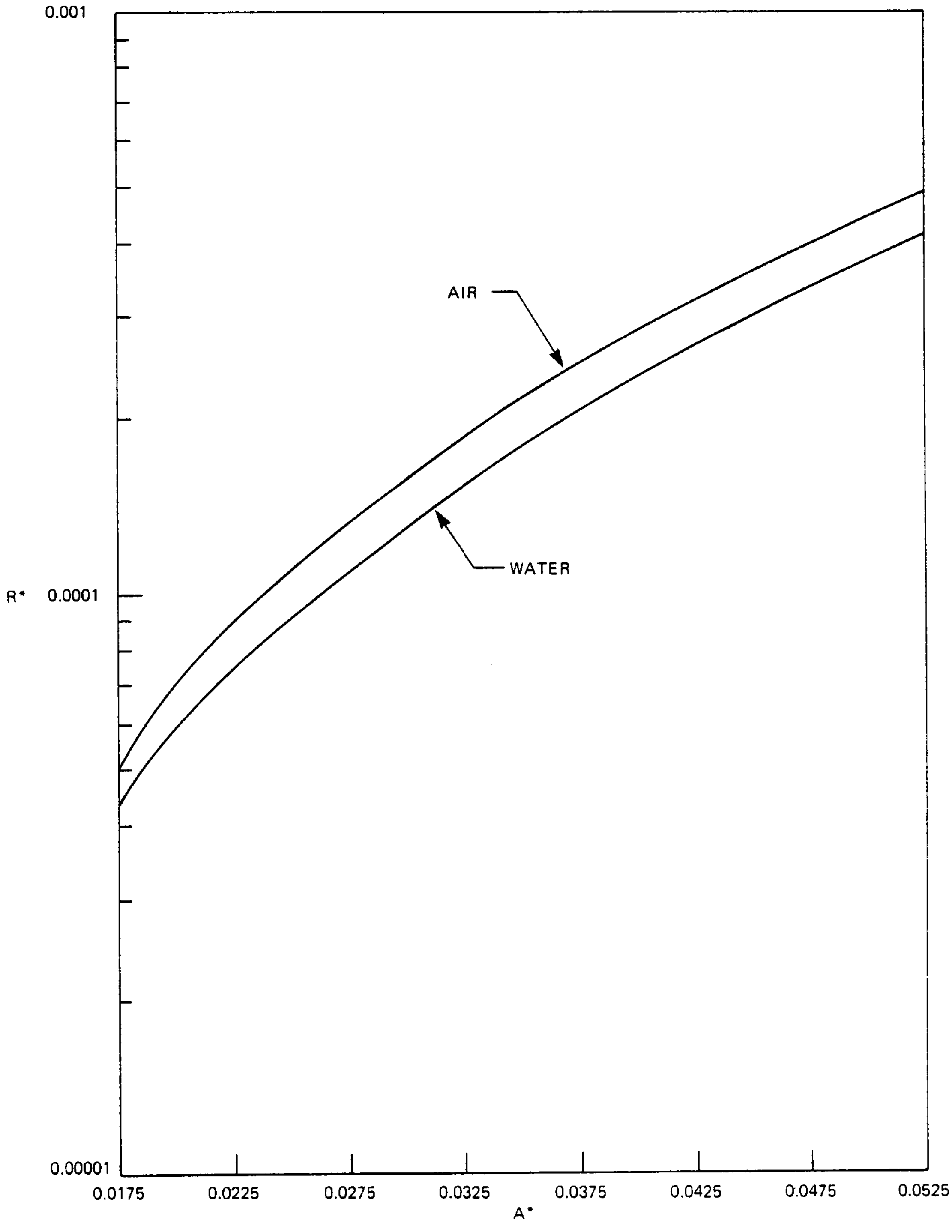

Figure 6.9. Dimensionless Rotary Inertia Parameter Versus Aspect Ratio.

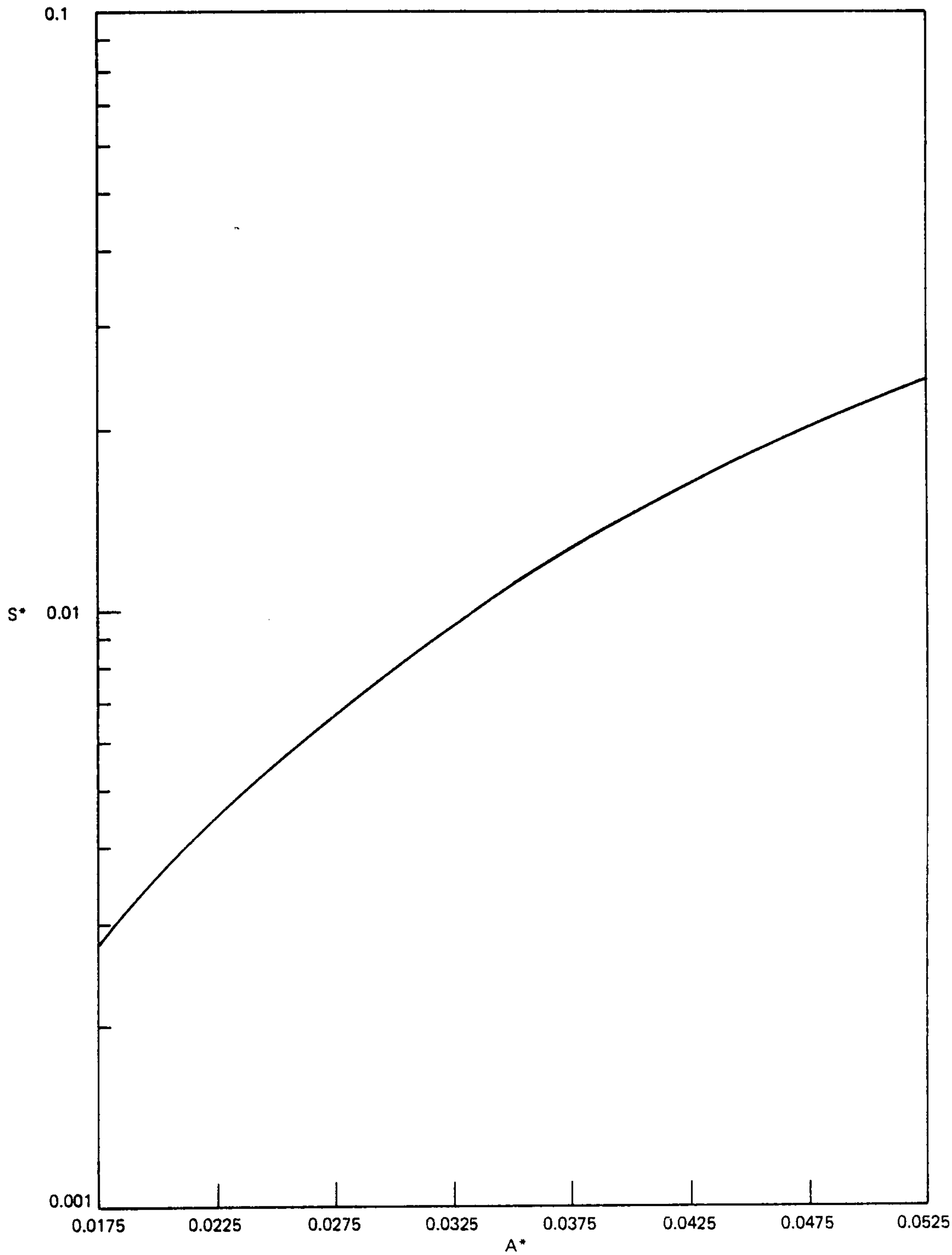

Figure 6.10. Dimensionless Shear Parameter Versus Aspect Ratio.

The experiments performed by Paidoussis and Laithier [59] used a vertical tube hanging downward perpendicular to the earth's surface. Moreover, their analysis accounted for the dead weight of the tube on a per unit length basis; the analysis performed in this study neglects this additional effect. As the tube becomes shorter the effects of dead weight do of course, decrease substantially. Paidoussis and Laithier used two different tubes in their experiments. Pipe II was selected for these simulations because it had a significantly higher flexural rigidity than Pipe I. This should minimize the effects of neglecting dead weight in the final results.

Figures 6.11 and 6.12 present a comparison between the results for the second mode critical velocity and frequency both calculated and measured by Paidoussis and Laithier [59] and the results computed in this study. The results are presented as a function of the dead weight parameter $(\rho_0 A + \rho_s A_s)L^3 g/EI$ which can be interpreted as a dimensionless length. As expected, the theory somewhat underpredicts the results for the longer tube lengths. The theories and experimental measurements agree quite well for the shorter tube lengths. The Timoshenko theory obviously is superior to the Bernoulli-Euler theory for the shorter tube lengths involved in the comparison. The results presented in Figures 6.11 and 6.12 are extremely important since they increase the confidence level that can be attached to the results predicted by the theory that has been presented.

The effects of compressibility are of a second order when the flowing fluid is water. Figures 6.13 through 6.16 present predictions as a function of the tube aspect ratio for the system summarized in Table 6.9 assuming the

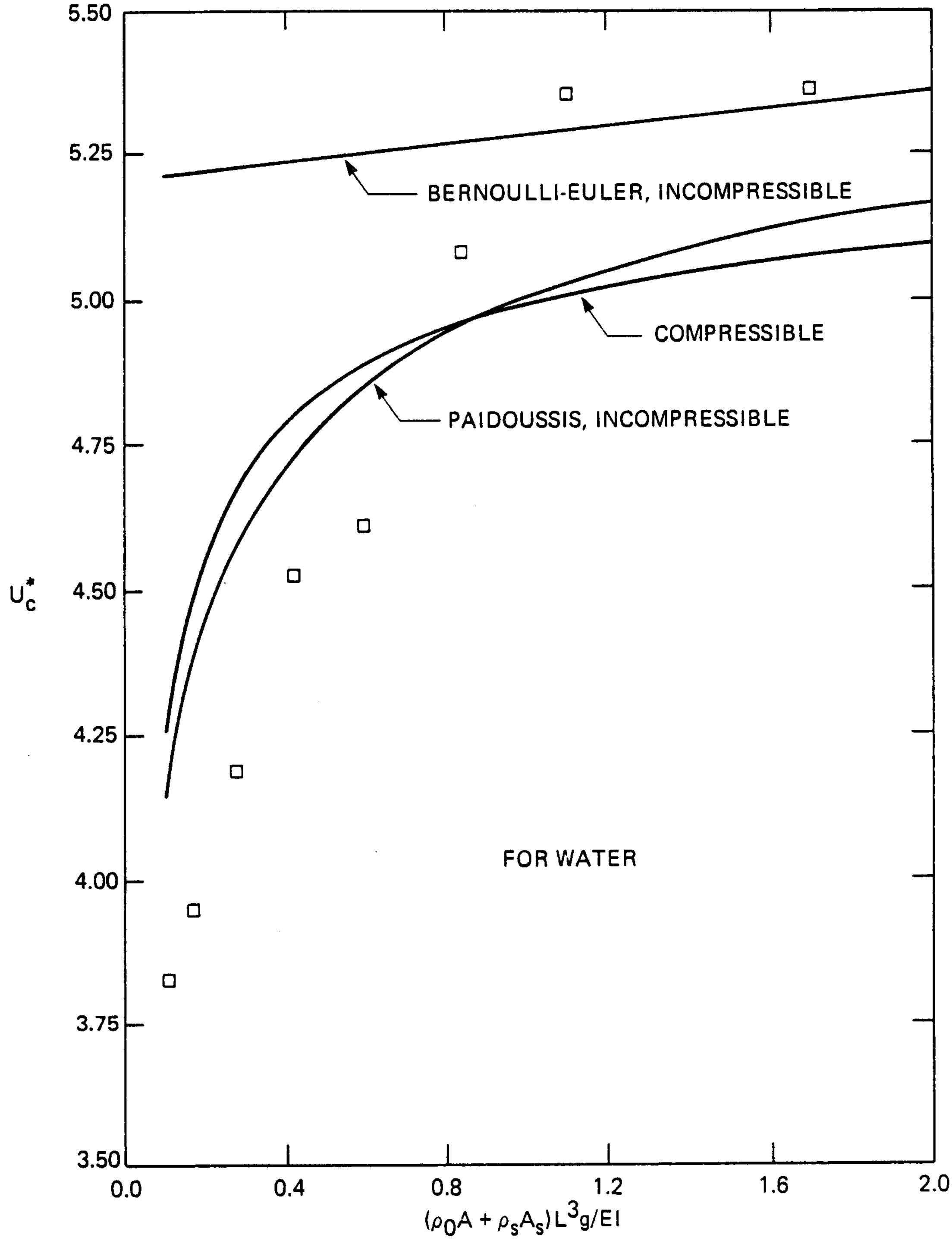

Figure 6.11. Comparison Between Predicted and Measured Dimensionless Critical Velocities for a Silastic Type E Tube With Water Flowing Through It.

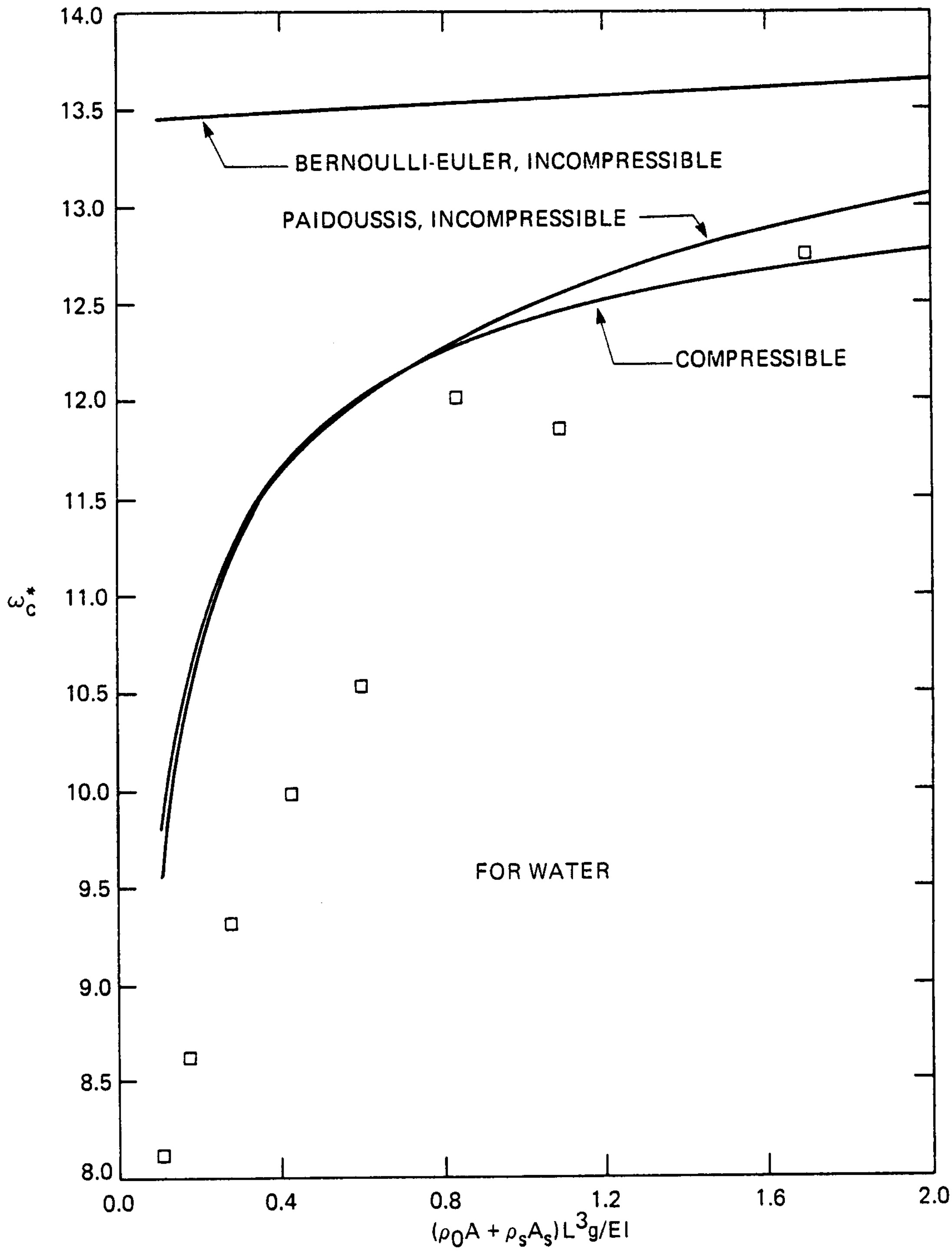

Figure 6.12. Comparison Between Predicted and Measured Dimensionless Critical Frequencies for a Silastic Type E Tube With Water Flowing Through It.

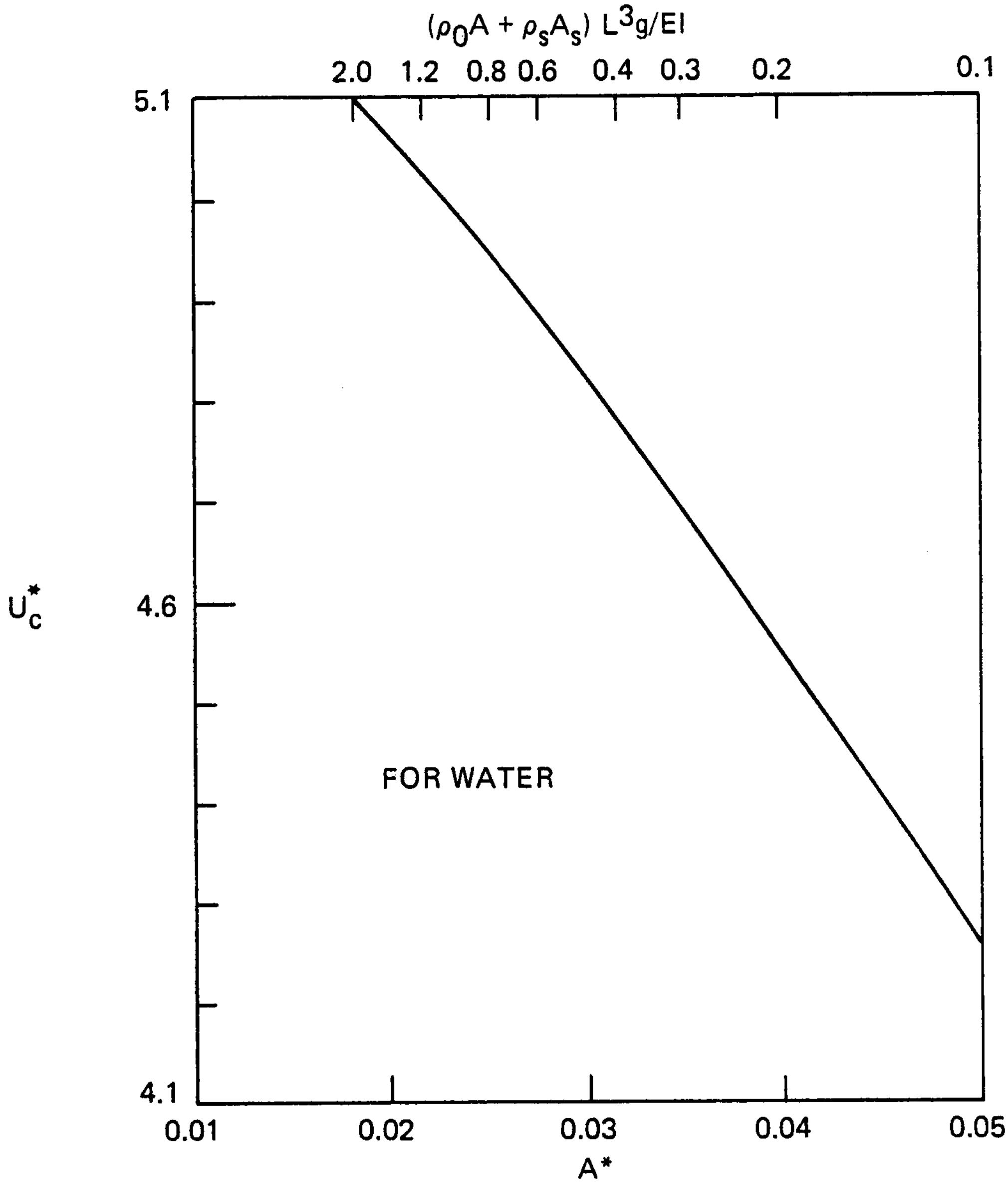

Figure 6.13. Dimensionless Critical Velocity Versus Aspect Ratio for a Silastic Type E Tube With Water Flowing Through It.

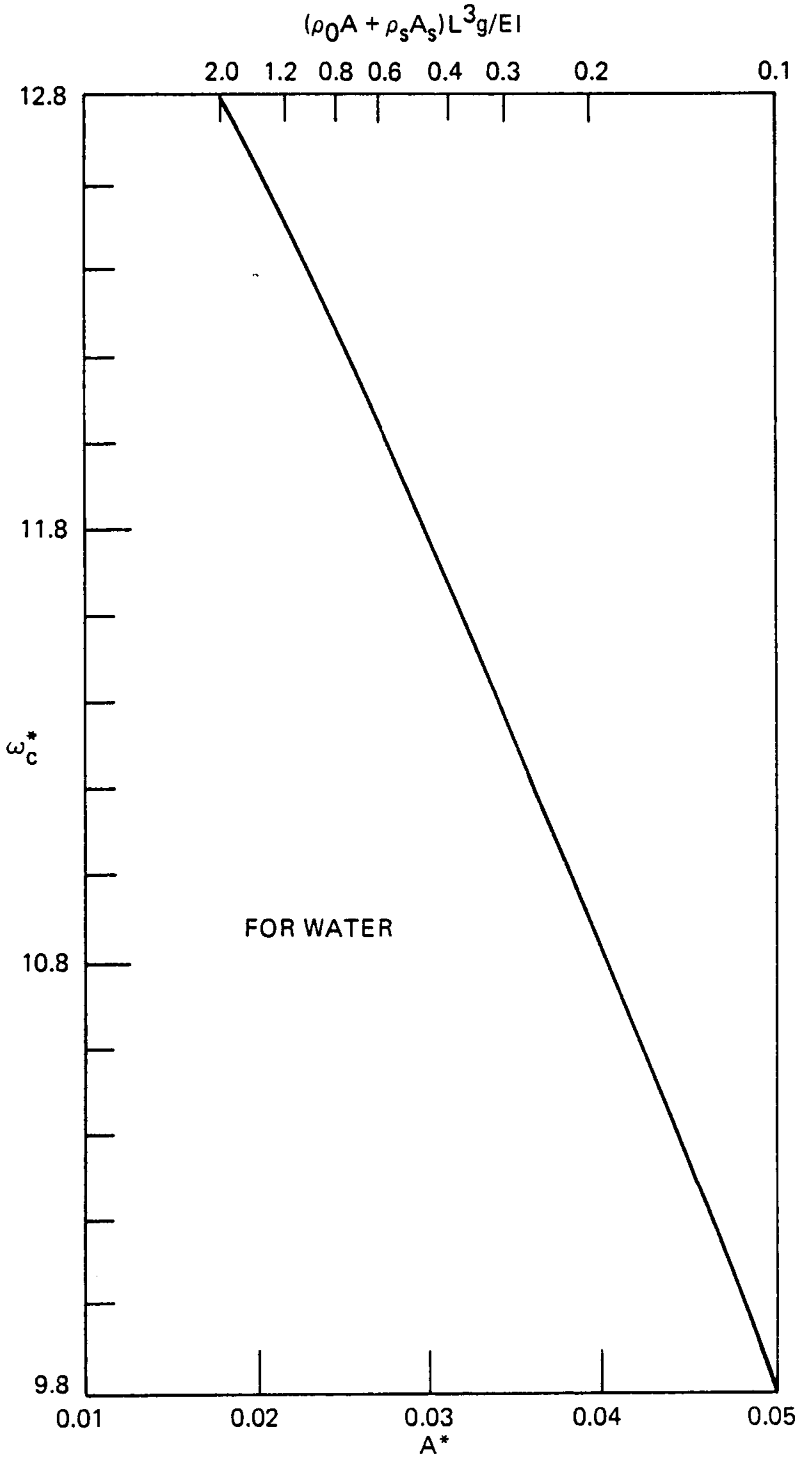

Figure 6.14. Dimensionless Critical Frequency Versus Aspect Ratio for a Silastic Type E Tube With Water Flowing Through It.

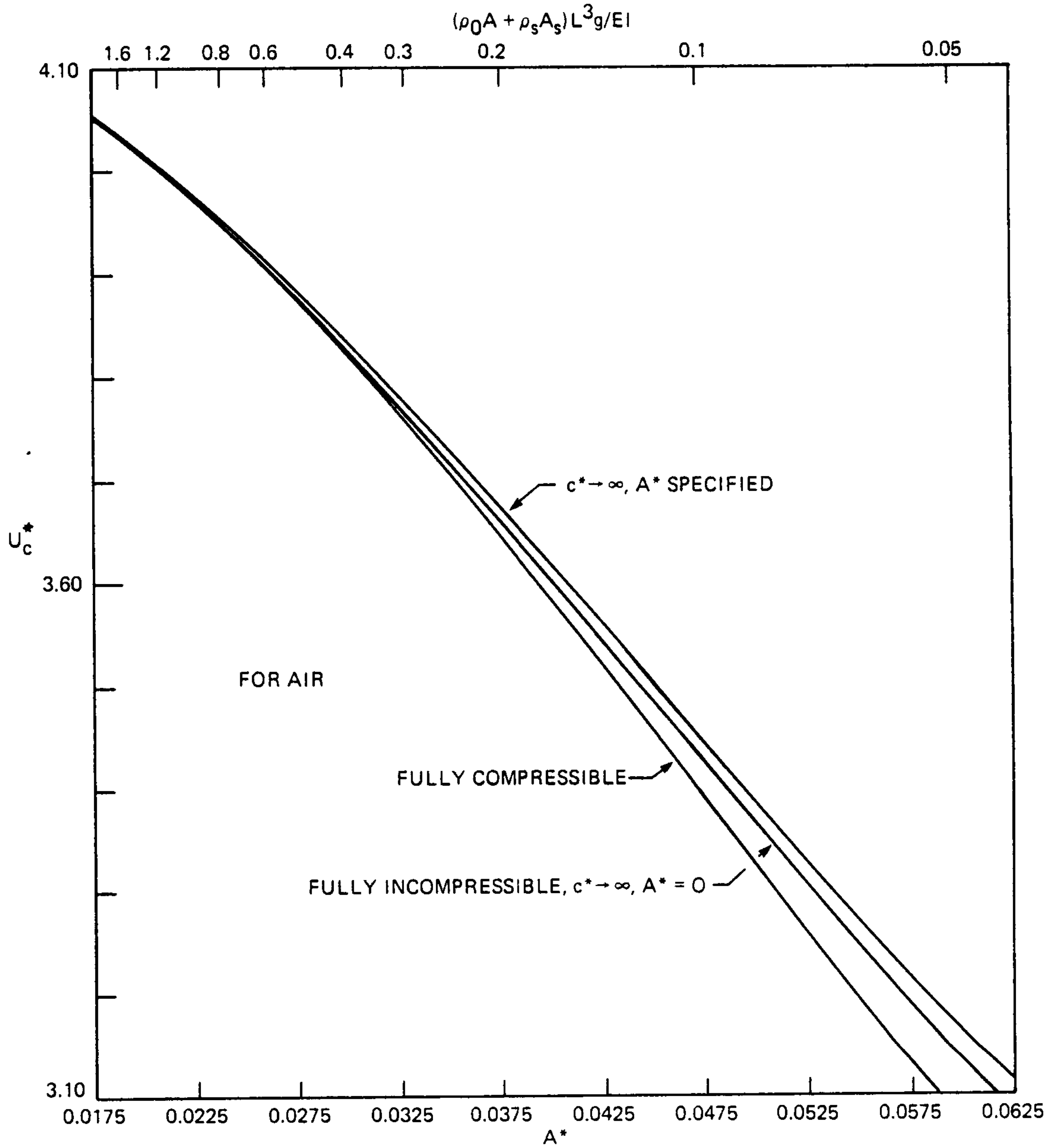

Figure 6.15. Dimensionless Critical Velocity Versus Aspect Ratio for a Silastic Type E Tube With Air Flowing Through It.

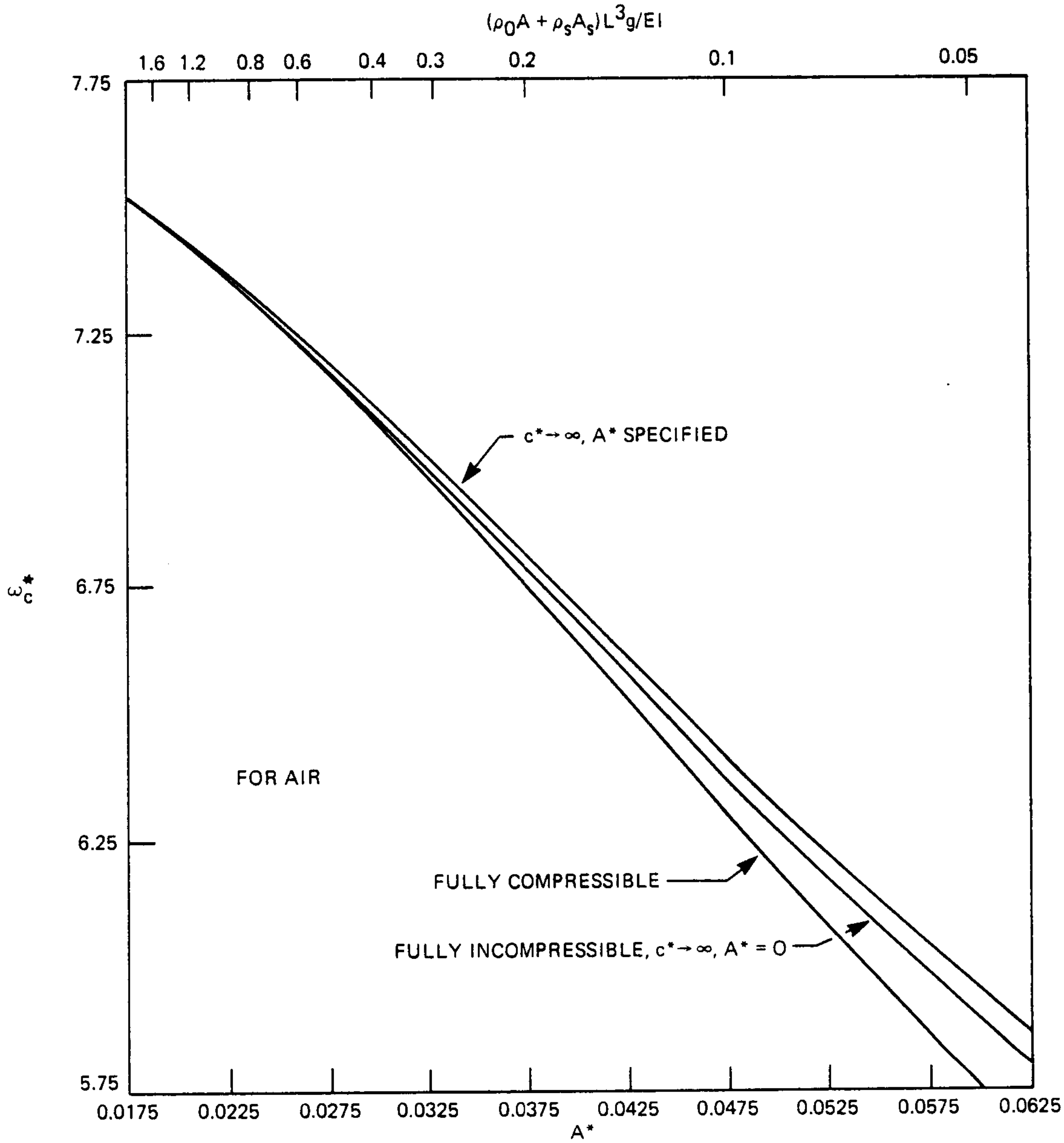

Figure 6.16. Dimensionless Critical Frequency Versus Aspect Ratio for a Silastic Type E Tube With Air Flowing Through It.

fluid to be both water and air. The aspect ratio does not change when the fluid is altered like the weight parameter does although the weight parameter is shown on the top horizontal axis for reference. The system loses stability in the first mode when the fluid is air. It is apparent from the figures that the critical velocity and frequency undergo a significant decrease when the fluid is changed from water to air. This is attributable to the lower mass parameter for air. Figures 6.15 and 6.16 also contain the results when the air is assumed to be compressible. Inclusion of a nonzero aspect ratio increases the critical velocity and corresponding frequency when the fluid is incompressible. The additional constraint of a relatively low sonic velocity then causes a decrease in the critical velocity and frequency relative to those predicted when the fluid is incompressible. These results corroborate those quoted in the preceding section for the Bernoulli-Euler tubes. It is obvious that the tube must be quite short ($A^* > 0.05$) before the effects of compressibility significantly alter the predictions.

Figures 6.17 and 6.18 display the critical Mach number (defined as the ratio U_c^*/c^*) for the two fluid-tube systems under investigation. As expected, instability occurs when the flow is subsonic if the fluid is a relatively incompressible one like water. However, when the fluid is a compressible one similar to air and the tube is short ($A^* > 0.02$), the isentropic flow must become supersonic before instability occurs.

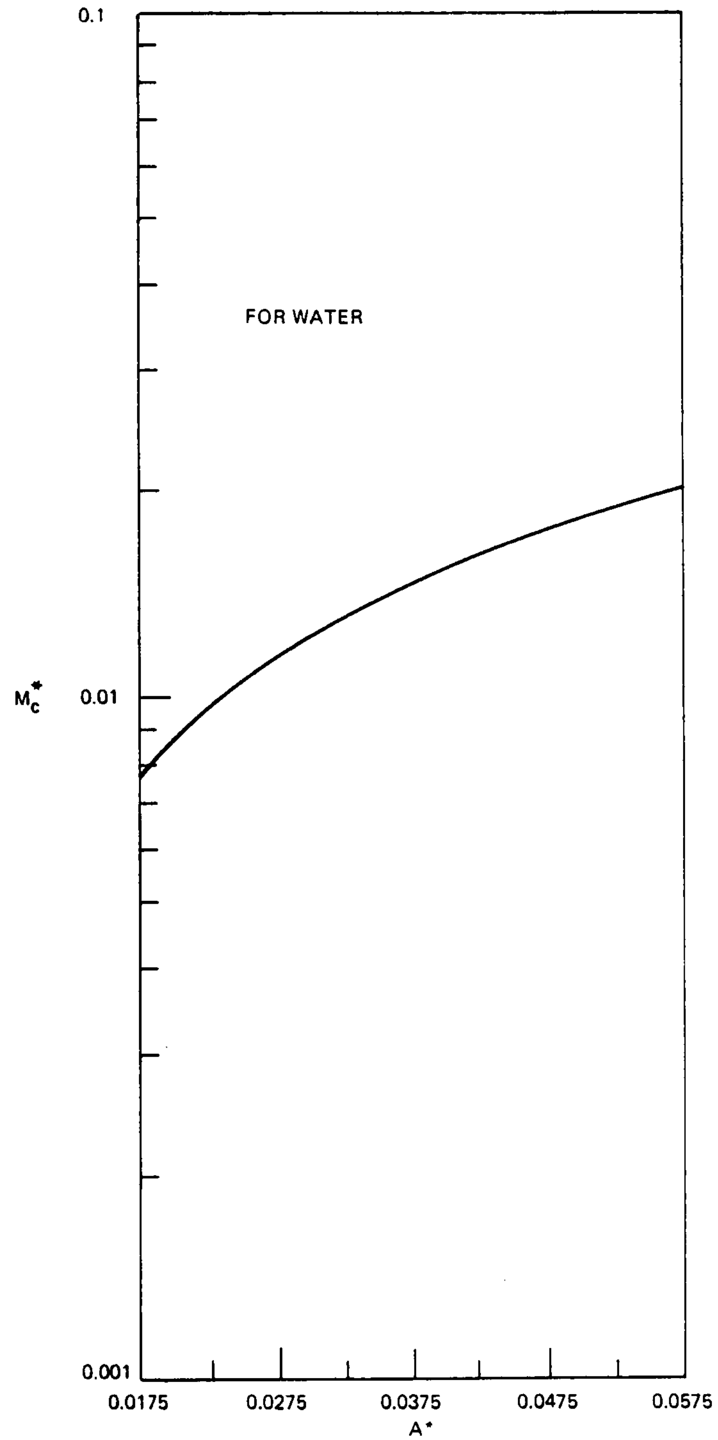

Figure 6.17. Critical Mach Number Versus Aspect Ratio for a Silastic Type E Tube With Water Flowing Through It.

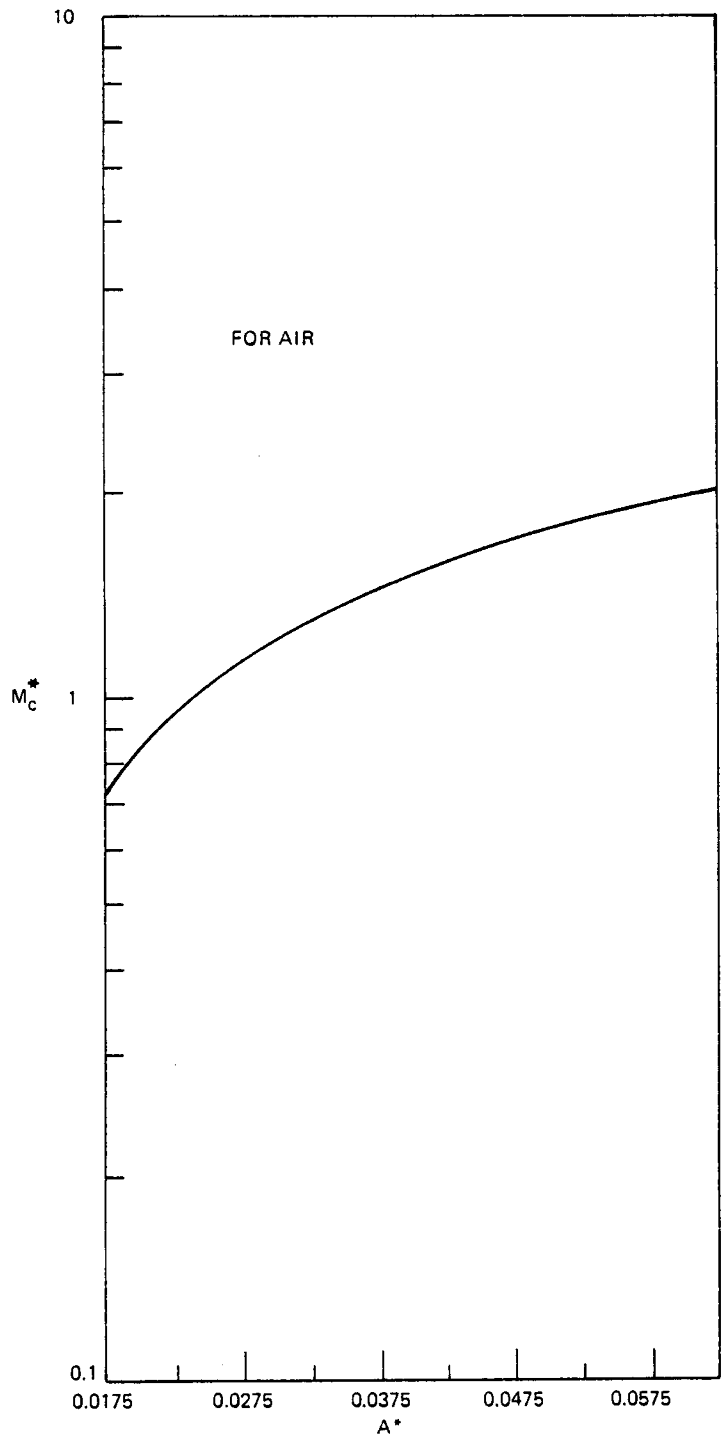

Figure 6.18. Critical Mach Number Versus Aspect Ratio for a Silastic Type E Tube With Air Flowing Through It.

6.5 Euler Stability Maps for a Simply Supported Tube

Euler's method of equilibrium is now applied to the case of a simply supported, fluid-conveying tube. This method is used to predict the critical flow velocity at which the tube buckles (divergence instability) in the axial direction. The required equation system is derived from Eqs. (4.13) and (4.23) by setting equal to zero terms containing partial derivatives with respect to the dimensionless time coordinate τ. The resultant equation pair can be written as follows:

$$[1 - fS^*U^{*2}]\eta_{\xi\xi\xi\xi} + fU^{*2}\eta_{\xi\xi} = 0 \tag{6.3}$$

$$[\Lambda_{\delta\delta} + \delta^{-1}\Lambda_\delta - \delta^{-2}\Lambda]\eta_\xi + A^{*2}[1 - M^{*2}]\Lambda\,\eta_{\xi\xi\xi} = 0 \tag{6.4}$$

The hysteretic damping coefficients have been set equal to zero since their usage implies time dependent harmonic motion. The necessary boundary conditions are given by Eqs. (4.27).

When a solution of the form

$$\eta(\xi) = \sum_{j=1}^{4} \gamma_j^* \, e^{\alpha_j^* \xi} \tag{6.5}$$

is substituted into Eq. (6.3) a quadratic polynomial equation in terms of the complex unknown α_j^* results. Only two distinct values of α_j^* are available. The solution $\eta(\xi)$ must then be written as follows since two of the four α_j^* are zero and nontrivial solutions are being sought:

$$\eta(\xi) = \gamma_1^* e^{\alpha_1^* \xi} + \gamma_2^* e^{\alpha_2^* \xi} + \gamma_3^* \xi + \gamma_4^* \tag{6.6a}$$

$$\alpha_3^* = \alpha_4^* = 0 \tag{6.6b}$$

Substitution of Eq. (6.5) into Eq. (6.4) yields an expression for κ_j analogous to Eq. (5.3). The result is

$$\kappa_j^2 = A^{*2} \alpha_j^{*2} \left[1 - \left(\frac{U^*}{c^*} \right)^2 \right] \quad , \; j = 1,2 \tag{6.7a}$$

$$\kappa_3 = \kappa_4 = 0 \tag{6.7b}$$

The compressibility factor f_j is given by Eq. (5.2) with the subscript n dropped. The appropriate equation is

$$f_j = \left[1 - \kappa_j \frac{J_2(\kappa_j)}{J_1(\kappa_j)} \right]^{-1} \quad , \; j = 1,2 \tag{6.8}$$

It is clear from Eq. (5.4) that $f_3 = f_4 = 1$ since $\kappa_3 = \kappa_4 = 0$.

Use of the boundary condition Eqs. (4.27) in conjunction with the solution form Eqs. (6.6) results in the frequency equation

$$\det \begin{bmatrix} 1 & 1 & 0 & 1 \\ e^{\alpha_1^*} & e^{\alpha_2^*} & 1 & 1 \\ \alpha_1^{*2} & \alpha_2^{*2} & 0 & 0 \\ \alpha_1^{*2} e^{\alpha_1^*} & \alpha_2^{*2} e^{\alpha_2^*} & 0 & 0 \end{bmatrix} = 0 \tag{6.9}$$

This determinant reduces to the equation, $e^{\alpha_1^*} - e^{\alpha_2^*} = 0$, which cannot be further reduced since α_1^* and α_2^* are complex unknowns.

The Euler stability problem for the simply supported Timoshenko beam conveying a compressible fluid can be summarized as follows:

$$\alpha_j^{*2} + \frac{f_j U^{*2}}{[1 - f_j S^* U^{*2}]} = 0 \quad , \quad j = 1,2 \tag{6.10}$$

$$e^{\alpha_1^*} - e^{\alpha_2^*} = 0 \tag{6.11}$$

The auxiliary equations for κ_j and f_j are given by Eqs. (6.7) and (6.8), respectively. Real values of U^* are sought which satisfy simultaneously Eqs. (6.7), (6.8), (6.10), and (6.11).

The computer code described in the previous chapter was used initially to calculate numerical solutions to this problem. The curves of ω_n^* had one endpoint on the real axis in accordance with Eq. (5.12) which corresponded to the $U^* = 0$ condition. As U^* was sequentially increased these curves would transverse the real axis in the direction of the origin. The actual value of U^* at which ω_n^* became precisely zero ($0 + 0 \cdot i$) could be obtained by executing the program in an iterative manner. It was noted during these preliminary calculations that a precise relationship existed between α_1^* and α_2^*. The results of these observations are

$$\alpha_1^* = in\pi \tag{6.12a}$$

$$\alpha_2^* = -in\pi \tag{6.12b}$$

$$\kappa_1 = \kappa_2 \equiv \kappa \tag{6.12c}$$

$$f_1 = f_2 \equiv f \tag{6.12d}$$

$$\alpha_1^{*2} = \alpha_2^{*2} = -n^2\pi^2 \tag{6.12e}$$

The stability problem in Eqs. (6.10) and (6.11) can be reformulated as follows:

$$U_{nc}^* = \frac{n\pi}{\sqrt{f}\sqrt{1 + n^2\pi^2 S^*}} \tag{6.13a}$$

$$f_n = \left[1 - \kappa_n \frac{J_2(\kappa_n)}{J_1(\kappa_n)}\right]^{-1} \tag{6.13b}$$

$$\kappa_n = n\pi A^* \sqrt{(U_{nc}^*/c^*)^2 - 1}\ , \tag{6.13c}$$

$$\text{for } n = 1,2, \ldots, \infty$$

The subscript c has been appended to U^* because the roots correspond to $\omega_n^* = 0 + 0 \cdot i$, for $n = 1,2, \ldots, \infty$, which by definition are the Euler buckling modes. There are an infinite number of these solutions. Therefore, the subscript n must be placed on U^*, κ, and f to denote this situation.

This problem can be handled using standard root finding techniques (single compilation of the Muller algorithm) since only the one unknown U^*_{nc}, $n = 1,2, \ldots, \infty$, is present once c^*, A^*, and S^* are specified. Only the first or lowest critical velocity is of interest. This root is denoted here as U^*_c while the corresponding value of the compressibility factor is simply f. An initial guess is provided by the solution [24] for a Bernoulli-Euler tube ($S^* = 0$) conveying an incompressible fluid ($A^* = 0$ and $c^* \rightarrow \infty$) which is $U^*_{nc} = n\pi$, $n = 1,2, \ldots, \infty$.

A computer program was developed in which A^* was sequentially increased in equal step sizes starting from zero. The solution for U^*_c was initialized at π. A step size in A^* of 0.1 was utilized while covering the range of A^* from zero to one. As c^* became smaller (less than two) many interations (2000 to 3000) of the Muller algorithm were required before convergence occurred indicating that the compressible form of this eigenvalue problem was somewhat ill-conditioned.

Figures 6.19, 6.20, and 6.21 are predictions from this theory for U^*_c, f, and M^*_c, respectively, for a Bernoulli-Euler tube ($S^* = 0$). It is evident from Figure 6.19 that fluid compressibility, through specification of the tube aspect ratio and the dimensionless fluid sonic velocity, dramatically affects the critical velocity of a simply supported tube. The straight line for $c^* = \pi$ in Figures 6.19, 6.20, and 6.21 is the transonic line since the critical Mach number is precisely one along it. The critical velocity increases with aspect ratio and decreases with sonic velocity in the subsonic region in a manner analogous to the predictions for the cantilevered, fluid-conveying beam. Instability in the

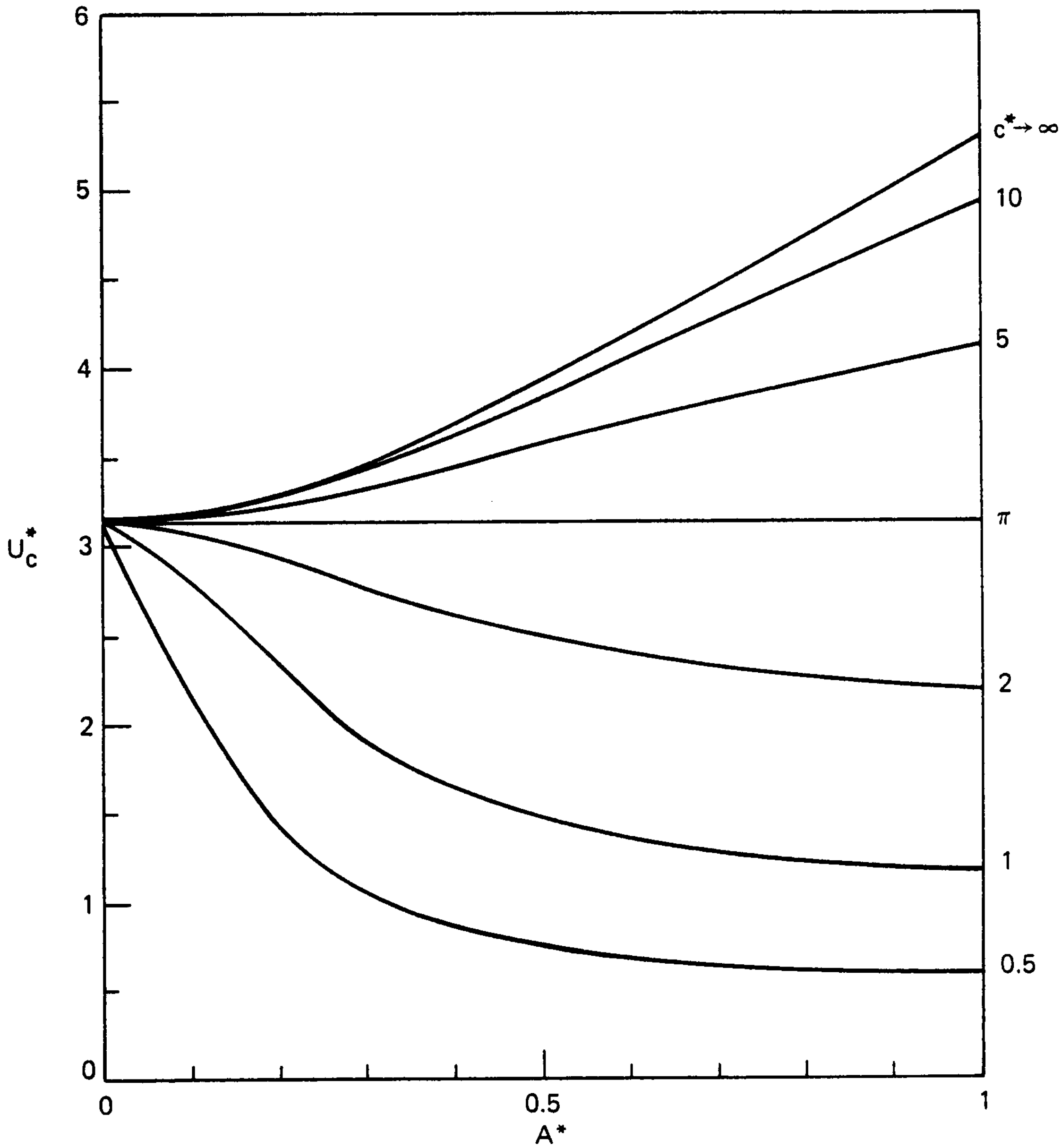

Figure 6.19. Dimensionless Critical Velocity Versus Aspect Ratio for a Simply Supported Beroulli-Euler ($S^* = 0$) Tube Conveying a Compressible Fluid.

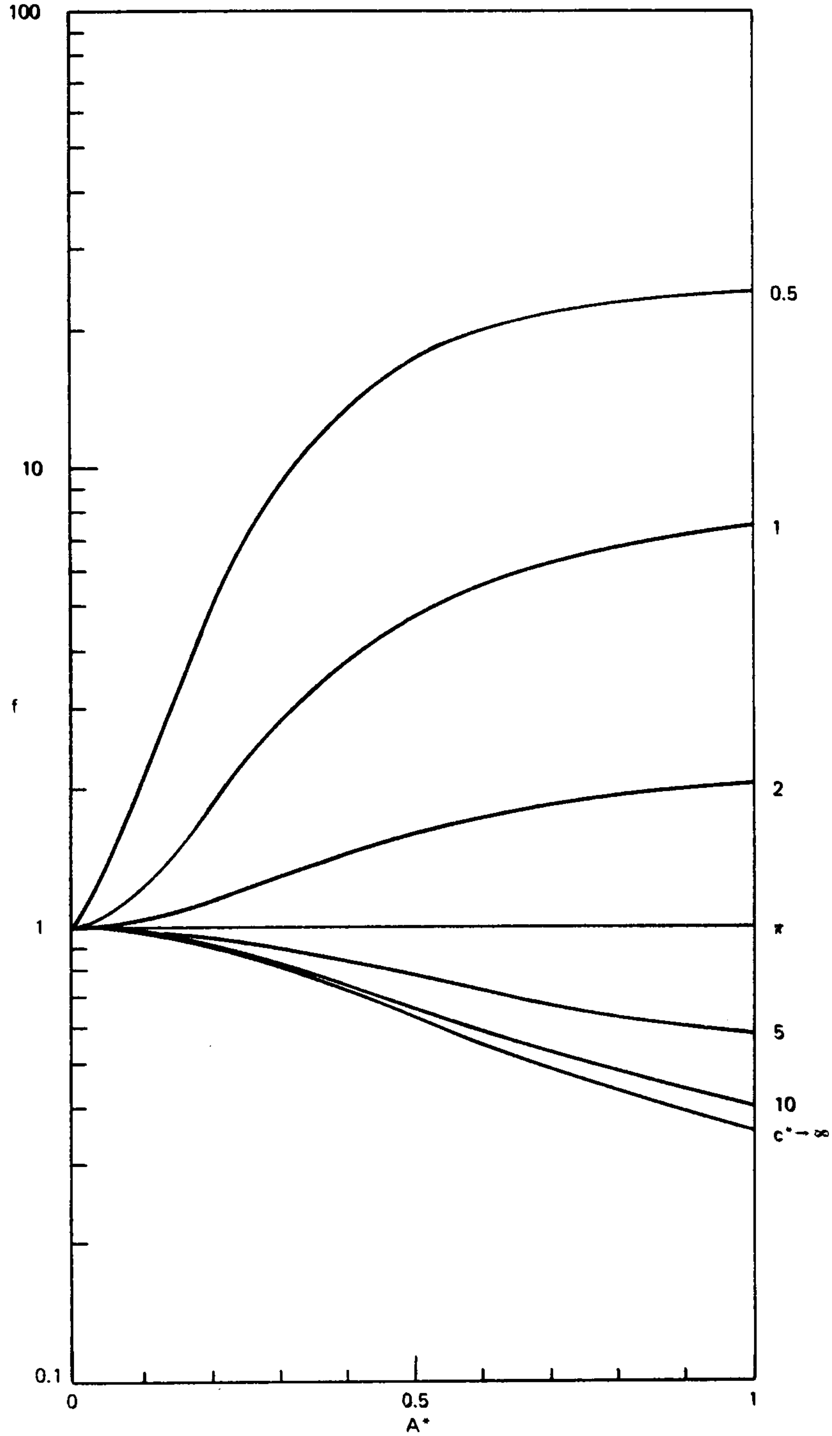

Figure 6.20. Compressibility Factor Versus Aspect Ratio for a Simply Supported Bernoulli-Euler ($S^* = 0$) Tube Conveying a Compressible Fluid.

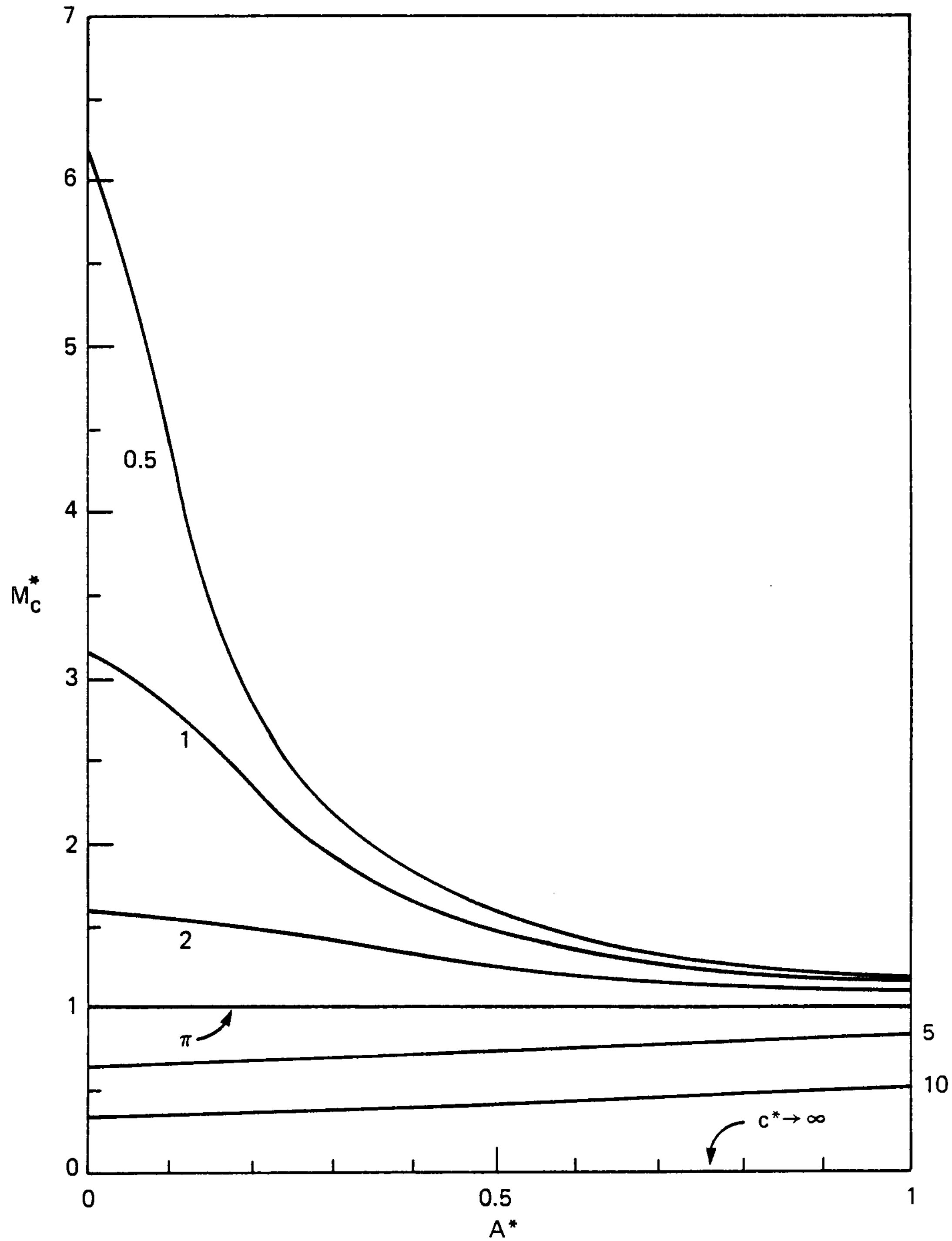

Figure 6.21. Critical Mach Number Versus Aspect Ratio for a Simply Supported Bernoulli-Euler ($S^* = 0$) Tube Conveying a Compressible Fluid.

supersonic flow regime shows a completely opposite trend with respect to aspect ratio. A shortened tube has a lower critical velocity when the critical flow speed is supersonic. This phenomenon is indicative of the mathematical classification of the equations of fluid motion. They are a parabolic system in the subsonic region while being hyperbolic when the flow speed is supersonic. It is apparent from Figure 6.21 that the critical flow speeds extend well into the hypersonic region when the sonic speed is quite low.

The compressibility factor f is a real quantity in this Euler stability problem. From Figure 6.20 it is seen to increase with reduced sonic velocity. Values of f are less than one when the flow is subsonic while they are greater than one for supersonic speeds.

Figures 6.22 through 6.24 present similar calculations for a simply supported Timoshenko tube having a relatively low shear modulus ($S^* = 0.1$). The trends are the same as before except that the relative level of the curves has been shifted downward. The critical velocities are expected to be somewhat lower since the Bernoulli-Euler beam theory neglects the effects of shear.

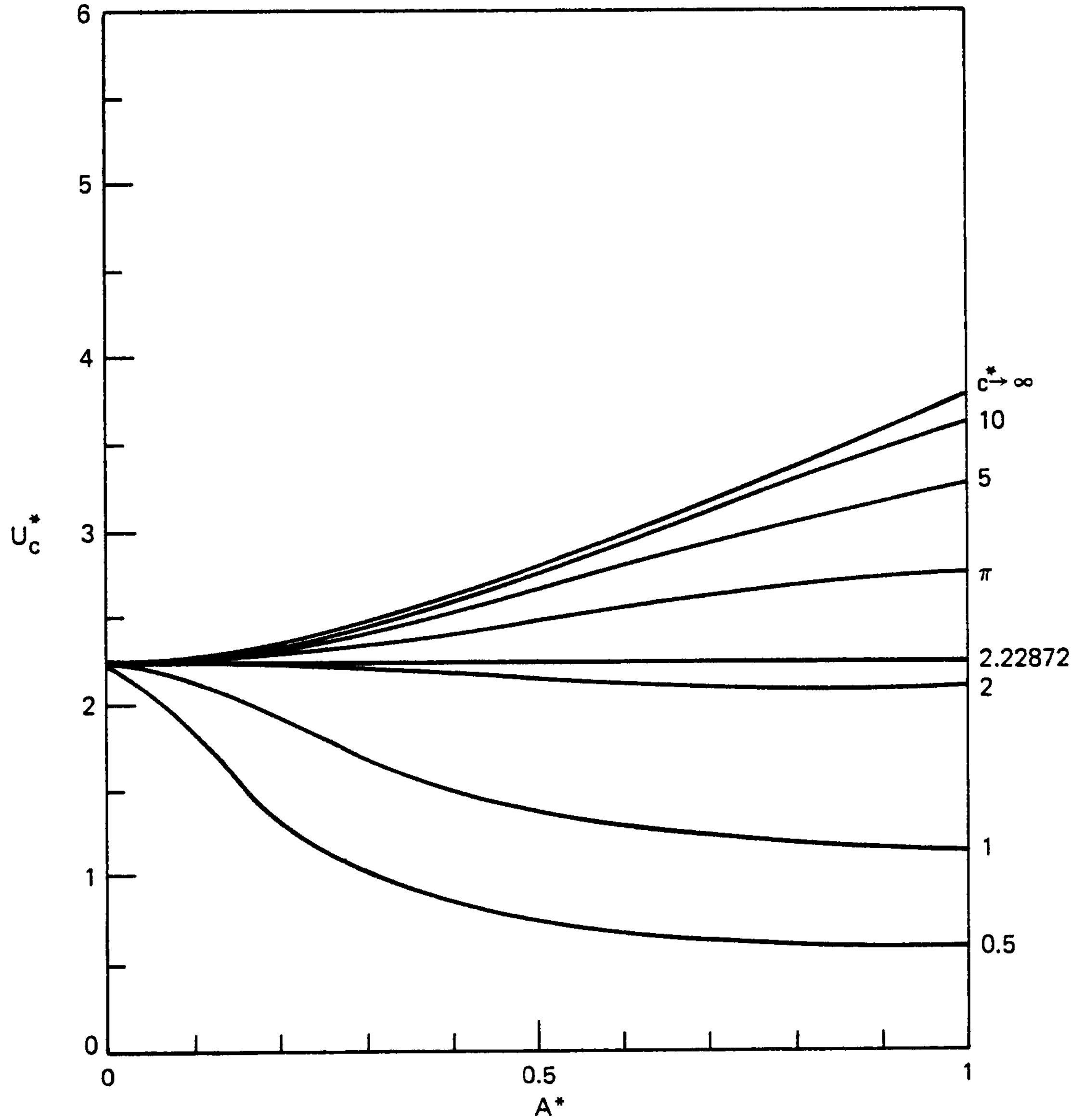

Figure 6.22. Dimensionless Critical Velocity Versus Aspect Ratio for a Simply Supported Timoshenko ($S^* = 0.1$) Tube Conveying a Compressible Fluid.

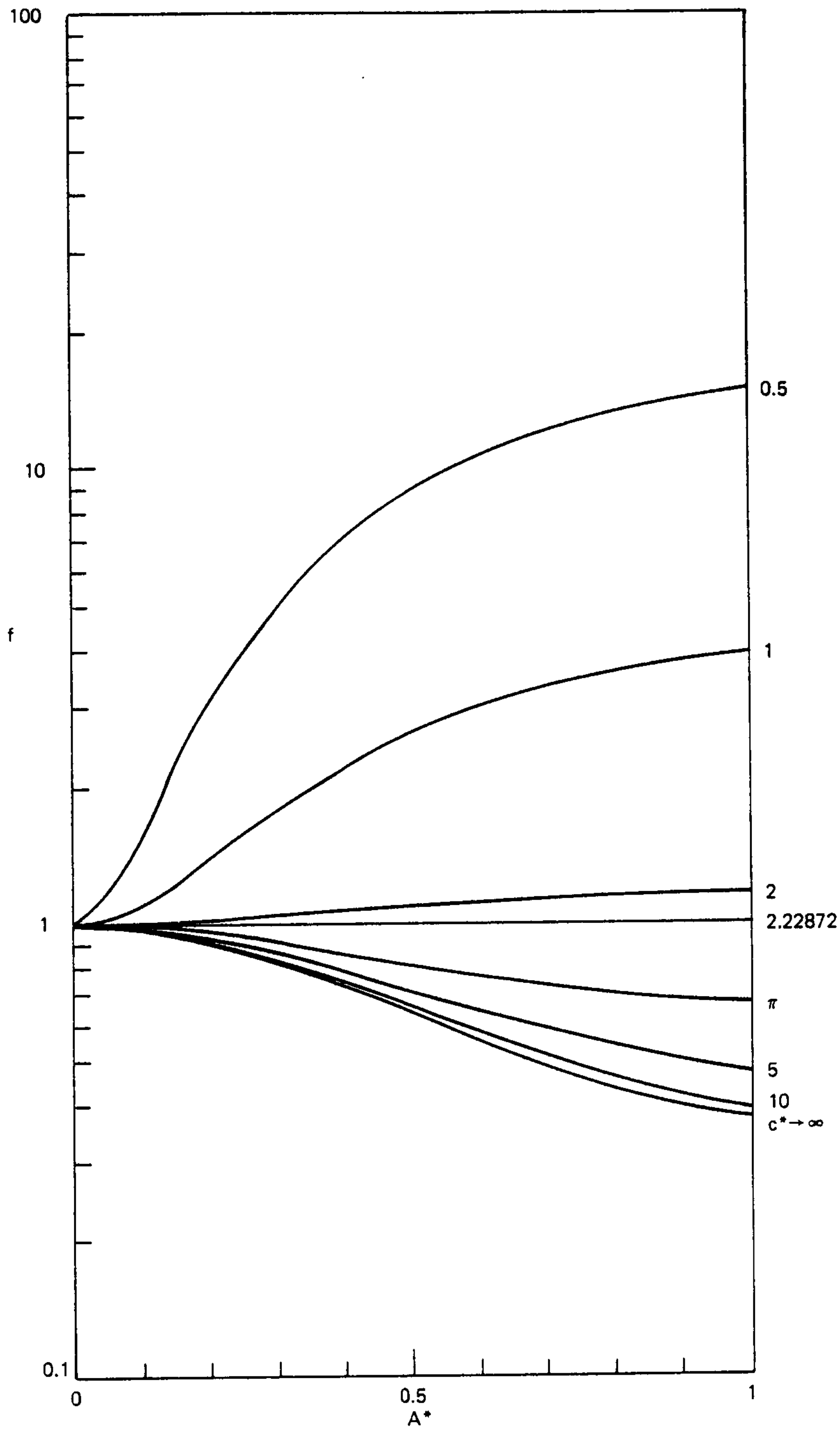

Figure 6.23. Compressibility Factor Versus Aspect Ratio for a Simply Supported Timoshenko ($S^* = 0.1$) Tube Conveying a Compressible Fluid.

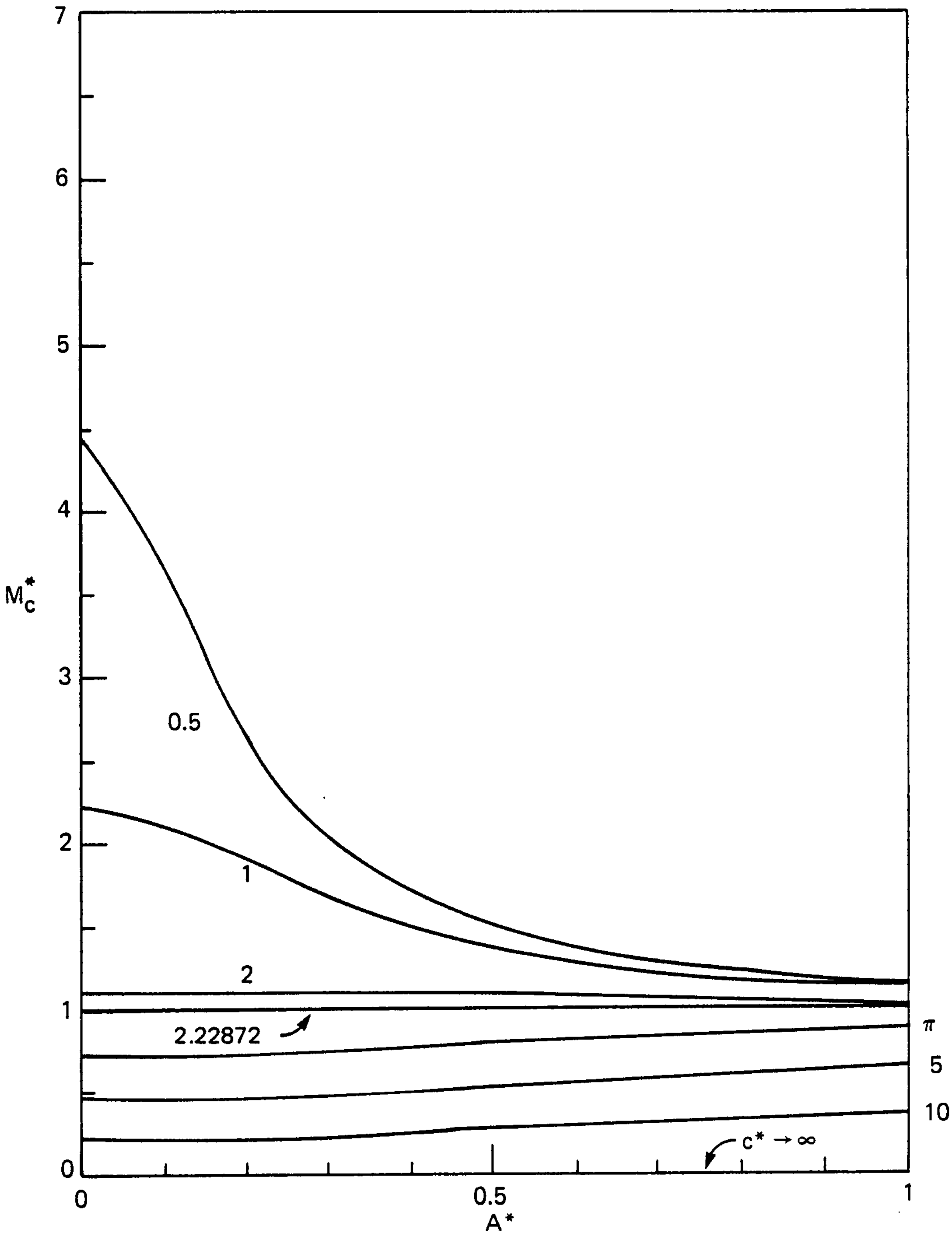

Figure 6.24. Critical Mach Number Versus Aspect Ratio for a Simply Supported Timoshenko ($S^* = 0.1$) Tube Conveying a Compressible Fluid.

7. CONCLUSIONS AND RECOMMENDATIONS

The purpose of this study was to predict the onset of unstable motion of cantilevered and simply supported Timoshenko beams conveying a compressible fluid. No calculations have appeared in the open literature which consider these two physical systems. The analysis is general enough to allow for viscous damping external to the tube and material damping either of the strain rate or hysteretic type. Interactions between shear deformation, rotary inertia, and the three damping mechanisms are accounted for. The compressible flow through the tube is isentropic. The motion of the beam and the fluid are coupled together by a compatibility condition which ensures that they vibrate together. The following conclusions were obtained from the results that were computed in this study:

1. In the case of cantilevered beams, increased aspect ratios raise critical velocities while sonic velocity reductions decrease them. This is true for both Bernoulli-Euler and Timoshenko beams conveying compressible fluids.

2. The critical value for aspect ratio occurs at 0.025 in the cantilevered case. Below this value the Bernoulli-Euler theory can be utilized to predict the stability of fluid-conveying beams while above it the Timoshenko theory should be used. This statement is applicable to both compressible and incompressible fluid-conveying tubes. The isentropic flow through the tube becomes supersonic before instability occurs if the tube is extremely short.

3. The critical value for dimensionless sonic velocity in the cantilevered case is approximately 10 to 100. Below this range fluid compressibility must be accounted for in a stability analysis. The range between 10 and 100 is strongly dependent on the thermodynamic state of the fluid. The lower value applies to liquids while the higher value should be used when the fluid is a gas.

4. A crossover range exists where the effects of increased aspect ratio and reduced dimensionless sonic velocity cancel each other.

5. Cantilevered tubes of either the Bernoulli-Euler or Timoshenko type conveying a compressible fluid that are parallel to the earth's surface (i.e., horizontal) lose stability in a flutter mode.

6. The effects of fluid compressibility can significantly excite the higher modes of beam vibration such that instability occurs in one of them before it occurs in a lower mode. In some cases it can remove any return-to-stability associated with an increase in flow velocity after instability has already taken place.

7. Fluid compressibility affects the Euler critical velocity at which buckling or divergence instability in the axial direction occurs when the tube is simply supported. Items one through four above generally apply to this situation although increased aspect ratio causes a decrease in critical velocity when the critical speeds are supersonic.

8. Muller's method is superior to Newton's method in nested root solver applications.

It has been shown that fluid compressibility can affect the dynamic stability of fluid-conveying tubes. Some of the assumptions employed in the analysis oversimplify the problem; moreover, the numerical scheme is cumbersome and limited in scope. Many problem areas still remain. It is recommended that the following work be performed:

1. The gravitational body force term should be added to the equation of motion of the beam.

2. A more efficient numerical technique for solving this problem must be found. The methodology utilized in this study is both time consuming and costly thus making the overall computer code of somewhat limited usefulness

3. The computer code designed in this study successfully predicted the first nine modes for the Bernoulli-Euler tube conveying an incompressible fluid; likewise, the plot routine produced graphs of these families of curves with extremely high resolution. A study should be undertaken to document these families of curves over the entire range of the mass parameter.

4. A method must be found to handle the singularity occurring at the origin. This problem severly limits the parameter range over which the computer code developed in this study can be deployed.

5. A numerical study should be performed to investigate the behavior of the solution at Mach one. Such calculations would be of interest to those involved in the transonic flow problem since the motion of the solid has been coupled to that of the fluid.

6. A set of experiments should be carried out to verify the supersonic instability that has been predicted for short tubes.

7. The supersonic speeds predicted in this study may not be achievable in practice because such real effects as choking or shock wave formation occur because of fluid friction and heat transfer along the tube wall. Isentropic flow addresses neither of these two effects. The basic theory should be extended to account for these phenomena.

8. The variation of axial tensile or compressive stress in the tube has been neglected. It is expected that this effect will become increasingly important as the flow speeds are increased. Its inclusion in the theory should be considered.

9. The theory should be extended so that the tube is treated as a thin shell rather than a beam.

10. Many different homogeneous boundary conditions are compatible with the beam analysis employed in this study (clamped-clamped for instance—see Bishop and Johnson [130, p. 285]). They should be incorporated into the computer code so that it can be applied to a larger class of problems.

LIST OF REFERENCES

LIST OF REFERENCES

1. Blevins, R. D., *Flow-Induced Vibration,* Van Nostrand Reinhold Co., New York, 1977.

2. Shin, Y. S., and Wambsganss, M. W. "Flow-Induced Vibration in LMFBR Steam Generators: A State-Of-The-Art Review," Nuclear Engrg. and Design **40,** 235–284 (1977).

3. Hetsroni, G., and Steininger, D. A., Preparers, "Workshop Proceeding: Flow-Induced Vibrations," Electric Power Research Institute Workshop Report No. WS-78-125, Palo Alto, California, November, 1978.

4. Wambsganss, M. W. "Vibration of Reactor Core Components," Reactor and Fuel-Processing Technology **10** (3), 208–219 (1967).

5. Nelms, H. A., and Segaser, C. L., "Survey of Nuclear Reactor System Primary Circuit Heat Exchangers," Oak Ridge National Laboratory Report No. ORNL-4399, UC-38-Engineering and Equipment, April, 1969.

6. Coit, R. L., Peake, C. C., and Lohmeier, A., "Design and Manufacture of Large Surface Condensers--Problems and Solutions," Proc. American Power Conf. **28,** 469–483 (1969).

7. Hartlen, R. T., "Recent Field Experience With Flow-Induced Vibration of Heat Exchanger Tubes," Proc. International Symposium on Vibration Problems in Industry, U. K. Atomic Energy Authority, Keswick, England, April, 1973, Paper No. 611.

8. Hartlen, R. T., and Jaster, W., "Pickering GS Steam Generators: Detection of Tube Impacting in Unit 3, Boiler 2, and Proposed Further Monitoring," Ontario Hydro Research Div. Report No. 75-314-K, August 7, 1975.

9. Swanson, W. M., "The Magnus Effect: A Summary of Investigations to Date," Trans. ASME, J. Basic Engrg. **83**, 461–470 (1961).

10. Hirschfeld, F., "Wind Power--Pipe Dream or Reality?" Mech. Engrg. **99** (9), 20–28 (1977).

11. Anmann, O. H., von Karman, T., and Woodruff, G. B., "The Failure of the Tacoma Narrows Bridge," a Report to the Honorable J. M. Carmody, Administrator, Federal Works Agency, 1940.

12. Hannah, I. W., "Resume of the Report on the Failures," Proc. Conf. on Natural Draught Cooling Towers--Ferrybridge and After, The Institution of Civil Engineers, London, 1967, pp. 1–7.

13. Thomann, H., "Wind Effects on Buildings and Structures," American Scientist **63**, 278–287 (1975).

14. Khan, F. R., and Parmelee, R. A., "Service Criteria for Tall Buildings for Wind Loading," Proc. Third International Conf. on Wind Effects on Buildings and Structures, Tokyo, 1971.

15. Li, T., and DiMaggio, D. D., "Vibration of a Propellant Line Containing Flowing Fluid," Proc. AIAA Fifth Annual Structures and Materials Conference CP-8, AIAA, New York, April, 1964, pp. 194–199.

16. Diaz, J. M., and Jain, R. K., "Vibration Analysis of Pump Discharge Lines," Proc. ASCE, J. Hydraulics Div. **96** (HY11), 2279–2296 (1970).

17. Weaver, D. S., Adubi, F. A., and Kouwen, N., "Flow-Induced Vibrations of a Hydraulic Valve and Their Elimination," Trans. ASME, J. Fluids Engrg. **100**, 239–245 (1978).

18. Weaver, D. S., Kouwen, N., and Mansour, W. M., "On the Hydroelastic Vibration of a Swing Check Valve," Proc. IUTAM-IAHR Symposium on Flow-Induced Structural Vibrations, Springer-Verlag, Berlin/Heidelberg, 1974, pp. 333–338.

19. Hogben, N., "Fluid Loading on Offshore Structures, A State-of-Art Appraisal: Wave Loads," Maritime Technology Monograph No. 1, The Royal Institution of Naval Architects, London, 1974.

20. Plate, E., "Marine Structures," Proc. IUTAM-IAHR Symposium on Flow-Induced Structural Vibrations, Springer-Verlag, Berlin/Heidelberg, 1974, pp. 528–530.

21. Hara, F., Shigeta, T., and Shibata, H., "Two-Phase Flow by Induced Random Vibrations," Proc. IUTAM-IAHR Symposium on Flow-Induced Structural Vibrations, Springer-Verlag, Berlin/Heidelberg, 1974, pp. 691–700.

22. Brodov, Y. M., Savelyev, R. Z., Permyakov, V. A., Kuptsov, V. K., and Galperin, A. G., "The Effect of Vibration on Heat Transfer and Flow of Condensing Steam on a Single Tube," Heat Transfer--Soviet Research **9** (1), 152–156 (1977).

23. Streeter, V., and Wylie, E. B., *Hydraulic Transients,* McGraw-Hill Book Co., Inc., New York, 1967.

24. Paidoussis, M. P., and Issid, N. T., "Dynamic Stability of Pipes Conveying Fluid," J. Sound Vib. **33** (3), 267–294 (1974).

25. Ashley, H., and Haviland, G., "Bending Vibrations of a Pipe Line Containing Flowing Fluid," Trans. ASME, J. Applied Mechanics **72** 229–232 (1950).

26. Burgreen, D., Byrenes, J. J., and Benforado, D. M., "Vibrations of Rods Induced by Water in Parallel Flow," Trans. ASME **80**, 991–1003 (1958).

27. Hawthorne, W. R., "The Early Development of the Dracone Flexible Barge," Proc. Institution Mech. Engrs. **175**, 52–83 (1961).

28. Taylor, G. I., "Analysis of the Swimming of Long and Narrow Animals," Series A, Proc. Royal Soc. London **214**, 158–183 (1952).

29. Lighthill, M. J., "Note on the Swimming of Slender Fish," J. Fluid Mech. **9**, 305–317 (1960).

30. Cesari, F., and Curioni, S., "Buckling Instability in Tubes Subject to Internal and External Axial Fluid Flow," Proc. Fourth Conference on Dimensioning and Strength Calculations, Akadémiai Kiadó, Budapest, Hungary, 1973, pp. 301–311.

31. Shilling III, R. B., and Lou, Y. K., "The Effect of Internal-Flow on the Dynamic Responses of a Cantilever Pipe," ASME Paper No. 78-Pet-57, ASME, New York, 1978.

32. McDonald, D. A., *Blood Flow in Arteries,* Second Edition, The Williams & Wilkins Co., Baltimore, 1974.

33. Anliker, M., and Raman, K. R., "Korotkoff Sounds at Diastole--a Phenomenon of Dynamic Instability of Fluid-Filled Shells," Int. J. Solids Structures **2** (3), 467–491 (1966).

34. Chen, S. S., "Flow-Induced Vibrations of Circular Cylindrical Structures. Part II: Cross-Flow Considerations," U.S. Naval Research Laboratory Shock and Vib. Digest **9** (11) 21–27 (1977).

35. Chen, S. S., "Flow-Induced Vibrations of Circular Cylindrical Structures. Part I: Stationary Fluids and Parallel Flow," U.S. Naval Research Laboratory Shock and Vib. Digest **9** (10), 25–38 (1977).

36. Naudascher, E., Editor, *Proc. IUTAM-IAHR Symposium on Flow-Induced Structural Vibrations,* Springer-Verlag, Berlin/Heidelberg, 1974.

37. Weightman, P., Editor, *Proc. International Symposium on Vibration Problems in Industry,* U.K. Atomic Energy Authority, Keswick, England, April, 1973.

38. Au-Yang, M. K., and Brown, S. J., Editors, *Fluid Structure Interaction Phenomena in Pressure Vessel and Piping Systems,* ASME Document No. PVP-PB-026, ASME, New York, 1977.

39. Chen, S. S., and Bernstein, M. D., Editors, *Flow Induced Vibrations,* ASME Document No. H00154, ASME, New York, 1979.

40. Mulcahy, T. M., and Chen, S. S., "Annotated Bibliography on Flow-Induced Vibrations," Argonne National Laboratory Technical Memorandum No. ANL-CT-74-05, January, 1974.

41. Feodos'yev, V. P., "Vibrations and Stability of a Pipe When Liquid Flows Through it," Inzenernyi Sbornik **10,** 169–170 (1951).

42. Housner, G. W., "Bending Vibrations of a Pipe Line Containing Flowing Fluid," Trans. ASME, J. Applied Mechanics **19,** 205–208 (1952).

43. Niordson, F. I. N., "Vibrations of a Cylindrical Tube Containing Flowing Fluid," Kungliga Tekniska Högskolans Handlingar (Stockholm) **73,** 1–27 (1953).

44. Niordson, F. I. N., "Vibrations of a Cylindrical Waterfilled Tube," Proc. of the Eighth International Congress on Theoretical and Applied Mechanics, University of Istanbul, 1953, pp. 348–350.

45. Long, R. H., "Experimental and Theoretical Study of Transverse Vibration of a Tube Containing Flowing Fluid," Trans. ASME, J. Applied Mechanics **22**, 65–68 (1955).

46. Handelman, G. H., "A Note on the Transverse Vibration of a Tube Containing Flowing Fluid," Quarterly of Applied Mathematics **13** (3), 326–330 (1955).

47. Bolotin, V. V., *Nonconservative Problems of the Theory of Elastic Stability,* Pergamon Press Ltd., Oxford, England, 1963.

48. Bisplinghoff, R., Ashley, H., and Halfman, R., *Aeroelasticity,* Addison-Wesley Publishing Co., Inc., Reading, Massachusetts, 1955.

49. Benjamin, T. B., "Dynamics of a System of Articulated Pipes Conveying Fluid. I. Theory, and II. Experiments," Series A, Proc. Royal Soc. London **261,** 457–499 (1961).

50. Nemat-Nasser, S., Prasad, S. N., and Herrmann, G., "Destabilizing Effect of Velocity-Dependent Forces in Nonconservative Continuous Systems," AIAA J. **4** (7), 1276–1280 (1966).

51. Nemat-Nasser, S., and Herrmann, G., "Torsional Instability of Cantilevered Bars Subjected to Nonconservative Loading," Trans. ASME, J. Applied Mechanics **33,** 102–104 (1966).

52. Nemat-Nasser, S., and Herrmann, G., "Adjoint Systems in Nonconservative Problems of Elastic Stability," AIAA J. **4** (12), 2221–2222 (1966).

53. Gregory, R. W., and Paidoussis, M. P., "Unstable Oscillation of Tubular Cantilevers Conveying Fluid. I. Theory, and II. Experiments," Series A, Proc. Royal Soc. London **293,** 512–542 (1966).

54. Hermann, G., and Nemat-Nasser, S., "Instability Modes of Cantilevered Bars Induced by Fluid Flow Through Attached Pipes," Int. J. Solids Structures **3,** 39–52 (1967).

55. Naguleswaran, S., and Williams, C. J. H., "Lateral Vibration of a Pipe Conveying a Fluid," J. Mech. Engrg. Sci. **10** (3), 228–238 (1968).

56. Paidoussis, M. P., and Deksnis, E. B., "Articulated Models of Cantilevers Conveying Fluid: The Study of a Paradox," J. Mech. Engrg. Sci. **12** (4), 288–300 (1970).

57. Paidoussis, M. P., "Dynamics of Tubular Cantilevers Conveying Fluid," J. Mech. Engrg. Sci. **12** (2), 85–103 (1970).

58. Hill, J. L., and Swanson, C. P., "Effects of Lumped Masses on the Stability of Fluid Conveying Tubes," Trans. ASME, J. Applied Mechanics **37**, 494–497 (1970).

59. Paidoussis, M. P., and Laithier, B. E., "Dynamics of Timoshenko Beams Conveying Fluid," J. Mech. Engrg. Sci. **18** (4), 210–220 (1976).

60. Chen, S. S., "Forced Vibration of a Cantilevered Tube Conveying Fluid," J. Acoustical Society of America **48** (3), 773–775 (1970).

61. Srinivasan, P., and Lakshminarayanan, V., "Vibration of Pipe Carrying Flowing Fluid," Proc. ASCE, Transportation Engrg. J. **96** (TE2), 165–174 (1970).

62. Kornecki, A., "On Application of Galerkin's Method to Non-Self-Adjoint Equations," Israel J. of Technology **9** (1–2), 189–194 (1971).

63. Jones, L. H., and Goodwin, B. E., "The Transverse Vibrations of a Pipe Containing Flowing Fluid: Methods of Integral Equations," Quarterly of Applied Mathematics **29**, 363–374 (1971).

64. Satter, M. A. and Yaghoubi, M. A., "Free and Forced Vibrations of a Simply Supported Pipe Carrying Flowing Fluid," J. Industrial Mathematics Society **25** (2), 53–66 (1975).

65. Armenakas, A. E., "On the Accuracy of Some Dynamic Shell Theories," Proc. ASCE, J. Engrg. Mechanics Div. **93** (EM5), 95–109 (1967).

66. Paidoussis, M. P., and Denise, J. P., "Flutter of Thin Cylindrical Shells Conveying Fluid," J. Sound Vib. **20** (1), 9–26 (1972).

67. Paidoussis, M. P., "Stability of Tubular Cylinders Conveying Fluid," Proc. IUTAM-IAHR Symposium on Flow-Induced Structural Vibrations, Springer-Verlag, Berlin/Heidelberg, 1974, pp. 676–683.

68. Weaver, D. S., and Unny, T. E., "Hydroelastic Behavior of a Cylindrical Shell," Proc. IUTAM-IAHR Symposium on Flow-Induced Structural Vibrations, Springer-Verlag, Berlin/Heidelberg, 1974, pp. 684–690.

69. Kempner, J., "Remarks on Donnell's Equations," Trans. ASME, J. Applied Mechanics **22**, 117–118 (1955).

70. Weaver, D. S., and Unny, T. E., "On the Dynamic Stability of Fluid-Conveying Pipes," Trans. ASME, J. Applied Mechanics **40**, 48–52 (1973).

71. Thurman, A. L., and Mote, C. D., Jr., "Nonlinear Oscillation of a Cylinder Containing a Flowing Fluid," Trans. ASME, J. Engrg. Industry **91**, 1147–1155 (1969).

72. Liu, H. S., and Mote, C. D., Jr., "Dynamic Response of Pipes Transporting Fluids," Trans. ASME, J. Engrg. Industry **96**, 591–596 (1974).

73. Chen, S. S., "Dynamic Stability of Tube Conveying Fluid," Proc. ASCE, J. Engrg. Mechanics Div. **97** (EM5), 1469–1485 (1971).

74. Clinch, J. M., "Prediction and Measurement of the Vibrations Induced in Thin-Walled Pipes by the Passage of Internal Turbulent Water Flow," J. Sound Vib. **12** (4), 429–451 (1970).

75. Lakis, A. A., and Paidoussis, M. P., "Prediction of the Response of a Cylindrical Shell to Arbitrary or Boundary-Layer-Induced Random Pressure Fields," J. Sound Vib. **25** (1), 1–27 (1972).

76. Satter, M. A., and Ahmadi, G., "Mean-Square Response of a Pipe Carrying Flowing Fluid to Non-Stationary Random Excitations," J. Sound Vib. **51** (4), 577–581 (1977).

77. Widnall, S. E., and Dowell, E. H., "Aerodynamic Forces on an Oscillating Cylindrical Duct With an Internal Flow," J. Sound Vib. **6** (1), 71–85 (1967).

78. Hannoyer, M. J., and Paidoussis, M. P., "Instabilities of Tubular Beams Simultaneously Subjected to Internal and External Axial Flows," ASME Paper No. 77-DET-95, ASME, New York, 1977.

79. Hannoyer, M. J., and Paidoussis, M. P., "Dynamics of Slender Tapered Beams With Internal or External Axial Flow. Part 1: Theory, and Part 2: Experiments," Trans. ASME, J. Applied Mechanics **46** (1), 45–57 (1979).

80. Benjamin, T. B., "The Threefold Classification of Unstable Disturbances in Flexible Surfaces Bounding Inviscid Flows," J. Fluid Mech. **16** (3), 436–450 (1963).

81. Clough, R. W., and Penzien, J., *Dynamics of Structures,* McGraw-Hill Book Co., Inc., New York, 1975.

82. Borg, S. F., *Fundamentals of Engineering Elasticity,* D. Van Nostrand Co., Inc., Princeton, New Jersey, 1962.

83. Lazan, B. J., "Damping Studies in Materials Science and Materials Engineering," in *Internal Friction, Damping, and Cyclic Plasticity,* ASTM Special Technical Publication No. 378, ASTM, Philadelphia, 1965, pp. 1–20.

84. Ruzicka, J. E., and Derby, T. F., *Influence of Damping in Vibration Isolation,* Edited and Produced by the Technical Information Div., Naval Research Laboratory, SVM-7, 1971.

85. Daily, J. W., and Harleman, D. R. F., *Fluid Dynamics,* Addison-Wesley Publishing Co., Inc., Reading, Massachusetts, 1966.

86. Sartory, W. K., Personal Communication, Martin Marietta Energy Systems, Inc., Oak Ridge Gaseous Diffusion Plant, Oak Ridge, Tennessee, April, 1983.

87. Snowdon, J. C., "Representation of the Mechanical Damping Possessed by Rubberlike Materials and Structures," J. Acoustical Society of America **35** (6), 821–829 (1963).

88. Scanlan, R. H., and Mendelson, A., "Structural Damping," AIAA J. **1** (4), 938–939 (1963).

89. Timoshenko, S. P., "On the Correction for Shear of the Differential Equation for Transverse Vibrations of Prismatic Bars," Series 6, Philosophical Magazine **41,** 744–746 (1921).

90. Timoshenko, S. P., "On the Transverse Vibrations of Bars of Uniform Cross-Section," Series 6, Philosophical Magazine **43,** 125–131 (1922).

91. Aalami, B., and Atzori, B., "Flexural Vibrations and Timoshenko's Beam Theory," AIAA J. **12** (5), 679–685 (1974).

92. Cowper, G. R., "The Sear Coefficient in Timoshenko's Beam Theory," Trans. ASME, J. Applied Mechanics **33** (2), 335–340 (1966).

93. Bird, B. B., Stewart, W. E., and Lightfoot, E. N., *Transport Phenomena,* John Wiley & Sons, Inc., New York, 1960.

94. Babarsky, R. J., and Wood III, H. G., "An Analysis From First Principles of the Source/Sink Terms in the Pancake Equation," University of Virginia, School of Engrg. and Applied Science, Charlottesville, Virginia, Internal Report No. UVA-ER-795-82, July, 1982.

95. Liepmann, H. W., and Roshko, A., *Elements of Gasdynamics,* John Wiley & Sons, Inc., New York, 1957.

96. John, J. E. A., *Gas Dynamics,* Allyn and Bacon, Inc., Boston, 1969.

97. Roache, P. J., *Computational Fluid Dynamics,* Revised Printing, Hermosa Publishers, Albuquerque, New Mexico, 1976.

98. Arfken, G., *Mathematical Methods for Physicists,* Second Edition, Academic Press, Inc., New York, 1970.

99. Watson, G. N., *A Treatise on the Theory of Bessel Functions,* Second Edition, Cambridge University Press, London, 1952.

100. Onoe, Morio, *Tables of Modified Quotients of Bessel Functions of the First Kind for Real and Imaginary Arguments,* Columbia University Press, New York, 1958.

101. Abramowitz, M. and Stegun, I. A., Editors, *Handbook of Mathematical Functions with Formulas, Graphs, and Mathematical Tables,* Dover Publications, Inc., New York, 1965.

102. Knopp, K., *Theory and Applcation of Infinite Series,* Blackie & Son Ltd., London, 1928.

103. Traub, J. F., *Iterative Methods for the Solution of Equations,* Prentice-Hall, Inc., Englewood Cliffs, New Jersey, 1964.

104. Rabinowitz, P., Editor, *Numerical Methods for Nonlinear Algebraic Equations,* Gordon and Beach Science Publishers, Inc., New York, 1970.

105. Ortega, J. M. and Rheinboldt, W. C., *Solution of Nonlinear Equations in Several Variables,* Academic Press, Inc., New York, 1970.

106. Moré, J. J. and Cosnard, M. Y., "Numerical Solution of Nonlinear Equations," ACM Transactions on Mathematical Software **5** (1), 64–85, March, 1979.

107. Carnahan, B., Luther, H. A., and Wilkes, J. O., *Applied Numerical Methods,* John Wiley & Sons, Inc., New York (1969).

108. Lin, S., "A Method for Finding Roots of Algebraic Equations," J. Math. and Phys. **22,** 60–77 (1943).

109. Jenkins, M. A. and Traub, J. F., "Zeros of a Complex Polynomial," Algorithm 419, Communications of the A.C.M. **15** (2), 97–99, February, 1972.

110. Conte, S. D. and de Boor, C., *Elementary Numerical Analysis: An Algorithmic Approach,* Second Edition, McGraw-Hill Book Co., Inc., New York, 1972.

111. Ward, J. A., "The Down-Hill Method of Solving f(z) = 0," J. Assoc. Comput. Mach. **4,** 148–150 (1957).

112. Brent, R. P., "Some Efficient Algorithms for Solving Systems of Nonlinear Equations," SIAM J. Numer. Anal. **10** (2), 327–344, April, 1973.

113. Gaffney, P. W., "Information and Advice on Numerical Software," Oak Ridge National Laboratory Report No. ORNL/CSD/TM-147, May, 1981.

114. Muller, D. E., "A Method for Solving Algebraic Equations Using an Automatic Computer," Mathematical Tables and Other Aids to Computation (MTAC) **10** (53–56), 208–215 (1956).

115. Frank, W. L., "Finding Zeros of Arbitrary Functions," J. Assoc. Comput. Mach. **5**, 154–160 (1958).

116. Lance, G. N., *Numerical Methods for High Speed Computers,* Iliffe & Sons Ltd., London, 1960.

117. Conte, S. D., *Elementary Numerical Analysis an Algorithmic Approach,* McGraw-Hill Book Co., Inc., New York, 1965.

118. Sookne, D. J., "Bessel Functions I and J of Complex Argument and Integer Order," J. Research National Bureau Standards **77B** (3 & 4), 111–114, July–December, 1973.

119. Sookne, D. J., "Certification of an Algorithm for Bessel Functions of Real Argument," J. Research National Bureau Standards **77B** (3 & 4), 115–124, July–December, 1973.

120. Sookne, D. J., "Bessel Functions of Real Argument and Integer Order," J. Research National Bureau Standards **77B** (3 & 4), 125–132, July–December, 1973.

121. Sookne, D. J., "Certification of an Algorithm for Bessel Functions of Complex Argument," J. Research National Bureau Standards **77B** (3 & 4), 133–136, July–December, 1973.

122. Graham, N., *Introduction to Computer Science a Structured Approach,* West Publishing Co., St. Paul, Minnesota, 1979.

123. Young, D., and Felgar, R. P., "Tables of Characteristic Functions Representing Normal Modes of Vibration of a Beam," University of Texas Publication No. 4913, Bureau of Engrg. Research of Texas University, University of Texas, Austin, July, 1949.

124. Bolz, R. E., and Tuve, G. L., Editors, *CRC Handbook of Tables for Applied Engineering Science,* The Chemical Rubber Co., Cleveland, Ohio, 1970.

125. Van Vlack, L. H., *Elements of Materials Science an Introductory Text for Engineering Students,* Second Edition, Addison-Wesley Publishing Co., Inc., Reading, Massachusetts, 1964.

126. Clauser, H. R., Editor, "Data Section--Fibers, Felts, Wood & Paper," in *Materials Engineering* (Materials Selector Issue), Reinhold Publishing Corp., New York, Vol. 68, No. 5, p. 331, Mid-October, 1968.

127. Anderson, K. E., Editor, *Water Well Handbook,* Fourth Edition (Fifth Printing), Missouri Water Well & Pump Contractors Association, Inc., Belle, Missouri, 1971.

128. Resnick, R. and Halliday, D., *Physics Part I,* Third Printing, John Wiley & Sons, Inc., New York, 1966.

129. Johnson, R. O., Stoneking, J. E., and Carley, T. G., "Dynamics of Bernoulli-Euler Beams Conveying Compressible Fluid," Proc. of the Twelfth Southeastern Conference on Theoretical and Applied Mechanics, Auburn University, Vol. I, 1984, pp. 461–465.

130. Bishop, R. E. D., and Johnson, D. C., *The Mechanics of Vibration,* Cambridge University Press, London, 1960.

131. Ziegler, H., *Principles of Structural Stability,* Blaisdell Publishing Co., Waltham, Massachusetts, 1968.

132. Gunzburger, M. D., Personal Communication, Department of Mathematics, Carnegie-Mellon University, Pittsburgh, Pennsylvania, July, 1983.

APPENDICES

APPENDIX A

Frequency Equation Forms

The notation used in this appendix is discussed in Section 4.7.

A.1 Simply Supported Case

1. $p \neq q \neq r \neq s$

See Eqs. (4.56) and (4.59).

2. $p = q \neq r \neq s$

$$E_n^*(\xi) = (A + B\xi)\, e^{p\xi} + Ce^{r\xi} + De^{s\xi} \tag{A.1}$$

$$F(\omega_n^*) = \det\begin{bmatrix} 1 & 0 & 1 & 1 \\ e^p & e^p & e^r & e^s \\ p^2 & 2p & r^2 & s^2 \\ p^2e^p & (p^2 + 2p)e^p & r^2e^r & s^2e^s \end{bmatrix} = 0 \tag{A.2}$$

3. $p = q \neq r = s$

$$E_n^*(\xi) = (A + B\xi)e^{p\xi} + (C + D\xi)e^{r\xi} \tag{A.3}$$

$$F(\omega_n^*) = \det\begin{bmatrix} 1 & 0 & 1 & 0 \\ e^p & e^p & e^r & e^r \\ p^2 & 2p & r^2 & 2r \\ p^2e^p & (p^2+2p)e^p & r^2e^r & (r^2+2r)e^r \end{bmatrix} = 0 \qquad (A.4)$$

4. $p = q = r \neq s$

$$E_n^*(\xi) = (A + B\xi + C\xi^2)e^{p\xi} + De^{s\xi} \qquad (A.5)$$

$$F(\omega_n^*) = \det\begin{bmatrix} 1 & 0 & 0 & 1 \\ e^p & e^p & e^p & e^s \\ p^2 & 2p & 2 & s^2 \\ p^2e^p & (p^2+2p)e^p & (p^2+4p+2)e^P & s^2e^s \end{bmatrix} = 0 \qquad (A.6)$$

5. $p = q = r = s$

$$E_n^*(\xi) = (A + B\xi + C\xi^2 + D\xi^3)e^{p\xi} \qquad (A.7)$$

$$F(\omega_n^*) = \det\begin{bmatrix} 1 & 0 & 0 & 0 \\ e^p & e^p & e^p & e^p \\ p^2 & 2p & 2 & 0 \\ p^2e^p & (p^2+2p)e^p & (p^2+4p+2)e^p & (p^2+6p+6)e^p \end{bmatrix} = 0$$

(A.8)

A.2 Cantilevered Case

Equations (4.56), (A.1), (A.3), (A.5), and (A.7) apply in this section for each of the five separate cases. Refer to the preceding section of this appendix for these equational forms.

1. $p \neq q \neq r \neq s$

$$F(\omega_n^*) = \det\begin{bmatrix} 1 & 1 & 1 & 1 \\ p & q & r & s \\ p^2e^p & q^2e^q & r^2e^r & s^2e^s \\ p^3e^p & q^3e^q & r^3e^r & s^3e^s \end{bmatrix} = 0 \qquad (A.9)$$

2. $p = q \neq r \neq s$

$$F(\omega_n^*) = \det\begin{bmatrix} 1 & 0 & 1 & 1 \\ p & 1 & r & s \\ p^2e^p & (p^2 + 2p)e^p & r^2e^r & s^2e^s \\ p^3e^p & (p^3 + 3p^2)e^p & r^3e^r & s^3e^s \end{bmatrix} = 0 \qquad (A.10)$$

3. $p = q \neq r = s$

$$F(\omega_n^*) = \det\begin{bmatrix} 1 & 0 & 1 & 0 \\ p & 1 & r & 1 \\ p^2e^p & (p^2 + 2p)e^p & r^2e^r & (r^2 + 2r)e^r \\ p^3e^p & (p^3 + 3p^2)e^p & r^3e^r & (r^3 + 3r^2)e^r \end{bmatrix} = 0 \qquad (A.11)$$

4. $p = q = r \neq s$

$$F(\omega_n^*) = \det\begin{bmatrix} 1 & 0 & 0 & 1 \\ p & 1 & 0 & s \\ p^2e^p & (p^2 + 2p)e^p & (p^2 + 4p + 2)e^p & s^2e^s \\ p^3e^p & (p^3 + 3p^2)e^p & (p^3 + 6p^2 + 6p)e^p & s^3e^s \end{bmatrix} = 0 \qquad \text{(A.12)}$$

5. $p = q = r = s$

$$F(\omega_n^*)$$

$$= \det\begin{bmatrix} 1 & 0 & 0 & 0 \\ p & 1 & 0 & 0 \\ p^2e^p & (p^2 + 2p)e^p & (p^2 + 4p + 2)e^p & (p^2 + 6p + 6)e^p \\ p^3e^p & (p^3 + 3p^2)e^p & (p^3 + 6p^2 + 6p)e^p & (p^3 + 9p^2 + 18p + 6)e^p \end{bmatrix}$$

$$= 0 \qquad \text{(A.13)}$$

APPENDIX B

Series Expansion of the Compressibility Factor

Equation (5.2) contains a quantity which often appears in problems of mathematical physics and engineering. This quantity is the quotient function of the first kind [100] which is usually represented by the symbol $\tilde{\mathfrak{F}}_\nu(z)$ where z is a complex variable and ν is a real number. More specifically, $\tilde{\mathfrak{F}}_\nu(z)$ is defined by the equation

$$\tilde{\mathfrak{F}}_\nu(z) = \frac{zJ_{\nu+1}(z)}{J_\nu(z)} \tag{B.1}$$

If ν is set equal to the integer one and z equal to κ_{jn} then Eq. (B.1) represents the quantity appearing in Eq. (5.2).

The quantity $\tilde{\mathfrak{F}}_\nu(z)$ can be expanded into a power series near the origin [100, p. 5]. The result is

$$\tilde{\mathfrak{F}}_\nu(z) = \sum_{s=1}^{\infty} a_{2s} z^{2s} \tag{B.2}$$

where

$$a_2 = \frac{1}{2(\nu + 1)} \tag{B.3}$$

$$a_{2s} = \frac{1}{2(\nu + s)} \{a_2 a_{2s-2} + a_4 a_{2s-4} + \cdots + a_{2s-2} a_2\} \tag{B.4}$$

and the radius of convergence reaches to the first zero of $J_\nu(z)$. Table B.1 lists the first seven series coefficients for the case when ν is equal to the integer one. By using these coefficients $\tilde{\mathcal{J}}_1(z)$ can be written in the usual series form of a Bessel function as

$$\begin{aligned} \tilde{\mathcal{J}}_1(z) = & \frac{2}{2!1!}\left(\frac{z}{2}\right)^2 + \frac{2}{3!2!}\left(\frac{z}{2}\right)^4 \\ & + \frac{6}{4!3!}\left(\frac{z}{2}\right)^6 + \frac{32}{5!4!}\left(\frac{z}{2}\right)^8 \\ & + \frac{260}{6!5!}\left(\frac{z}{2}\right)^{10} + \frac{2970}{7!6!}\left(\frac{z}{2}\right)^{12} \\ & + \frac{45290}{8!7!}\left(\frac{z}{2}\right)^{14} + \cdots \end{aligned} \tag{B.5}$$

which is generally valid as z approaches zero. Equation (B.5) is particularly suited for machine calculation for small z since $J_2(z)$ and $J_1(z)$ both approach zero as $z \rightarrow 0$ [101].

Following the series manipulation methods suggested by Knopp [102, pp. 180–184] a similar series representation may be constructed for

Table B.1.
Coefficients of the Power
Series Expansion of $\tilde{\mathfrak{F}}_\nu(z)$
with $\nu = 1$.

s = 1:	$a_2 = 1/4$
s = 2:	$a_4 = 1/96$
s = 3:	$a_6 = 1/1536$
s = 4:	$a_8 = 1/23040$
s = 5:	$a_{10} = 13/4423680$
s = 6:	$a_{12} = 11/55050240$
s = 7:	$a_{14} = 647/47563407360$

determining the compressibility factor for small z. The following equation may be written for $\nu = 1$:

$$f = [1 - \tilde{\mathfrak{F}}_\nu(z)]^{-1} = \sum_{s=0}^{\infty} b_{2s} z^{2s} \quad , \quad \text{for } \nu = 1 \tag{B.6}$$

The function $\tilde{\mathfrak{F}}_\nu(z)$ is defined in Eqs. (B.2) through (B.4). The coefficients b_{2s} must now be formally determined.

Manipulation of Eq. (B.6) yields the equation

$$\left[1 - \sum_{s=1}^{\infty} a_{2s} z^{2s}\right]\left[b_0 + \sum_{s=1}^{\infty} b_{2s} z^{2s}\right] = 1 \tag{B.7}$$

It is clear that $b_o = 1$. The remaining b_{2s} can be found by expanding the series and equating the coefficients of like powers of z to zero. The result is

$$f = 1 + \sum_{s=1}^{\infty} b_{2s} z^{2s} \tag{B.8}$$

where

$$b_{2s} = a_{2s} + b_2 a_{2s-2} + \cdots + b_{2s-2} a_2 \tag{B.9}$$

The a_{2s} are determined using Eqs. (B.3) and (B.4). The parameter ν is understood to be equal to one. Table B.2 lists the first seven coefficients of the series in Eq. (B.8). It should be remarked that the coefficients listed in Tables

Table B.2.
Coefficients of the Power
Series Expansion of f
Expressed in Eq. (B.8).

$s = 1$:	$b_2 = 1/4$
$s = 2$:	$b_4 = 7/96$
$s = 3$:	$b_6 = 11/512$
$s = 4$:	$b_8 = 73/11520$
$s = 5$:	$b_{10} = 8269/4423680$
$s = 6$:	$b_{12} = 273197/495452160$
$s = 7$:	$b_{14} = 7736647/47563407360$

B.1 and B.2 have been calculated using the methods just described as well as by using the basic series definitions of $J_1(z)$ and $J_2(z)$ and then performing the series divisions using standard longhand methods. Both procedures produced identical results.

An equation similar to Eq. (B.5) can be written for the compressibility factor. The results is Eq. (5.4).

VITA

Robert Ost Johnson, the second son of Rex M. and Mildred O. Johnson, was born in Evansville, Indiana, on June 15, 1949. After graduation in 1967 from Benjamin Bosse High School in Evansville, Indiana, he attended the University of Evansville and received a B.S. degree in Engineering in 1972. He then accepted a graduate assistantship in the Heat Transfer Laboratory at Purdue University and graduated with a M.S. in Engineering in 1975. After accepting a position in the Mechanical Engineering Branch with the Tennessee Valley Authority in Knoxville, Tennessee, he began work towards the Ph.D. degree on a part-time basis in the Department of Engineering Science and Mechanics at the University of Tennessee, Knoxville. Mr. Johnson accepted a position as a development engineer in the Centrifuge Physics Department, Centrifuge Division, Oak Ridge Gaseous Diffusion Plant, Oak Ridge, Tennessee, operated by Union Carbide Corporation - Nuclear Division and subsequently by Martin Marietta Energy Systems, Incorporated, for the U.S. Department of Energy, in March, 1980. He has continued his work towards the Ph.D. degree since then. Mr. Johnson is a member of the Honor Society of Phi Kappa Phi and the American Society of Mechanical Engineers. He is a registered Professional Engineer in the state of Tennessee.

Mr. Johnson and the former Rexana L. Stephens of Newburgh, Indiana, were married on June 8, 1972. They presently reside in Knoxville, Tennessee.